FILE COPY
ESD ACCESSION LIST
DRI Call No. 87856
Copy No. 1 of 2 cys.
ESD-TR-77-252

MTP-170

MULTIPATH MEASUREMENTS OVER TROPOSCATTER PATHS

NOVEMBER 1977

Prepared for

DEPUTY FOR CONTROL AND COMMUNICATIONS SYSTEMS
ELECTRONIC SYSTEMS DIVISION
AIR FORCE SYSTEMS COMMAND
UNITED STATES AIR FORCE
Hanscom Air Force Base, Bedford, Massachusetts

Approved for public release;
distribution unlimited.

Project No. 6900
Prepared by
THE MITRE CORPORATION
Bedford, Massachusetts
Contract No. F19628-75-C-0001

ADA044611

When U.S. Government drawings, specifications, or other data are used for any purpose other than a definitely related government procurement operation, the government thereby incurs no responsibility nor any obligation whatsoever; and the fact that the government may have formulated, furnished, or in any way supplied the said drawings, specifications, or other data is not to be regarded by implication or otherwise, as in any manner licensing the holder or any other person or corporation, or conveying any rights or permission to manufacture, use, or sell any patented invention that may in any way be related thereto.

Do not return this copy. Retain or destroy.

REVIEW AND APPROVAL

This technical report has been reviewed and is approved for publication.

KENNETH E. RHODES, Major, USAF
Project Engineer
AN/TRC-170 Program

FOR THE COMMANDER

CHARLES E. MILLER, Lt Col, USAF
Ass't Director, 478T System Program Office
Deputy for Control
and Communications Systems

REPORT DOCUMENTATION PAGE		READ INSTRUCTIONS BEFORE COMPLETING FORM
1. REPORT NUMBER ESD-TR-77-252	2. GOVT ACCESSION NO.	3. RECIPIENT'S CATALOG NUMBER
4. TITLE (and Subtitle) MULTIPATH MEASUREMENTS OVER TROPOSCATTER PATHS		5. TYPE OF REPORT & PERIOD COVERED 6. PERFORMING ORG. REPORT NUMBER MTP-170
7. AUTHOR(s) A. Sherwood L. Suyemoto		8. CONTRACT OR GRANT NUMBER(s) F19628-75-C-0001
9. PERFORMING ORGANIZATION NAME AND ADDRESS The MITRE Corporation Box 208 Bedford, MA 01730		10. PROGRAM ELEMENT, PROJECT, TASK AREA & WORK UNIT NUMBERS Project No. 6900
11. CONTROLLING OFFICE NAME AND ADDRESS Deputy for Control and Communications Systems Electronic Systems Division, AFSC Hanscom Air Force Base, MA 01731		12. REPORT DATE NOVEMBER 1977 13. NUMBER OF PAGES 153
14. MONITORING AGENCY NAME & ADDRESS(if different from Controlling Office)		15. SECURITY CLASS. (of this report) UNCLASSIFIED 15a. DECLASSIFICATION/DOWNGRADING SCHEDULE

16. DISTRIBUTION STATEMENT (of this Report)

Approved for public release; distribution unlimited.

17. DISTRIBUTION STATEMENT (of the abstract entered in Block 20, if different from Report)

18. SUPPLEMENTARY NOTES

19. KEY WORDS (Continue on reverse side if necessary and identify by block number)

DIGITAL TROPOSCATTER COMMUNICATION
FADING DISPERSIVE CHANNEL
MULTIPATH
TROPOSCATTER CHANNEL

20. ABSTRACT (Continue on reverse side if necessary and identify by block number)

In support of a program to develop a new family of digital troposcatter radio terminals for tactical application, The MITRE Corporation and Rome Air Development Center jointly conducted an extended series of multipath measurements over two troposcatter paths of 86 and 168 miles at 4.7 GHz. The results of these tests include long-term statistics for and correlation among RMS multipath spread, path loss, fade rate, surface refractivity, and effective earth radius. The data obtained on these

20. ABSTRACT (concluded)

parameters is currently being used in the evaluation of various high-speed digital modulation/detection techniques and in the specification of radio terminal performance. This paper describes the test program, reports test results, and discusses related test programs, troposcatter multipath prediction, and the impact of dispersion on digital communication.

ACKNOWLEDGMENTS

This report has been prepared by The MITRE Corporation under Project 6900. The contract is sponsored by the Electronic Systems Division, Air Force Systems Command, Hanscom Air Force Base, Massachusetts. Capt. J. Payne of ESD acted as program coordinator.

The program was successfully completed because of the valuable contributions of many civilian and military personnel. We especially acknowledge the dedication and thoroughness with which K. Griebsch of the Republic of West Germany performed the on-site data reduction and assisted in data collection.

I. Fantera of Rome Air Development Center (RADC) co-managed the planning and conduct of the test program. In addition, numerous RADC site personnel operated and maintained the radio systems and much of the instrumentation; however, the efforts of P. Bradley, D. Mangold, J. Pritchard, and especially W. Schneider warrant special recognition. Capt. G. Eller provided assistance in setting up the on-line data processing system.

We also acknowledge the guidance of Dr. L. Ehrman of Signatron who assisted in structuring and implementing the data collection program; and Dr. P. A. Bello of CNR, Inc., and Dr. F. Unkauf of Raytheon, Inc., who provided several helpful suggestions.

The 108th Air National Guard Tactical Communication Squadron and the Air Force Communication Service 3rd Mobile Communication Group assisted in the initial setting up of the radio systems. The USAF Environmental Technical Application Center preprocessed and provided selected meteorological data.

Of the MITRE personnel working on the program, E. DeMichael was responsible for operating and maintaining the on-site data collection/processing subsystem, and D. Erwin assisted in the correlation of meteorological data with channel measurement data.

TABLE OF CONTENTS

TABLE OF CONTENTS (concluded)

LIST OF ILLUSTRATIONS

LIST OF ILLUSTRATIONS (Continued)

LIST OF ILLUSTRATIONS (Continued)

LIST OF ILLUSTRATIONS (Continued)

LIST OF ILLUSTRATIONS (Continued)

LIST OF ILLUSTRATIONS (Concluded)

LIST OF TABLES

LIST OF TABLES (Concluded)

SECTION I

SUMMARY

From October 1974 through August 1975 personnel from the Rome Air Development Center (RADC) and The MITRE Corporation were jointly involved in a field test program to measure the multipath characteristics of troposcatter paths. The purpose of the measurement program was to collect multipath profile statistics and other data in support of a program to develop a family of digital troposcatter radio terminals for tactical application.

The RADC test range in northwestern New York was the site of the two paths over which the measurements were made. This range has been in existence for more than 18 years; therefore, considerable equipment and the resources of experienced personnel were available for the test program. The majority of tests were conducted over an 86-statute-mile path from Ontario Center to Verona using AN/TRC-97D radios at 4780 MHz using standard 8-foot parabolic reflectors as well as 15-foot antennas. Site personnel conducted a more limited number of tests at 4690 MHz over a 168-mile path from Youngstown to Verona using AN/TRC-132A radios and their standard 28-foot parabolic reflectors.

The channel data attained from the tests includes measurements of multipath power profiles, path loss, and fade rate for five combinations of path length and antenna aperture. The USAF Environmental Technical Applications Center made available to the project meterological data, including surface refractivity (N_s), upper air refractivity profiles and wind shear, based on observations made at normal reporting stations in the area.

The observed values of two-sided RMS multipath spread (Δ) ranged from a high of 0.37 μs down to 0.05 μs. For the primary test configuration (86-mile path with 8-foot reflectors), the values of Δ which were exceeded 1, 10, 50, 90 and 99% of the time were 0.37, 0.27, 0.18, 0.12 and 0.08 μs respectively. These results are consistent with earlier measurements of correlation bandwidth over similar paths and are considerably wider than that predicted by application of the Bello channel model when standard input parameter assumptions are made. When considered relative to a required data rate of about 2 Mbps, the observed dispersion could result in a significant intersymbol interference (ISI) penalty for wideband data transmission systems such as binary FSK. The observations suggest that specialized signal processing techniques be considered that can reduce or eliminate ISI penalty and realize an implicit multipath diversity advantage.

By calculating normalized correlation coefficients, test personnel looked at the observed data for possible correlations. In general, the correlation between multipath spread Δ and other variables such as path loss, surface refractivity and effective earth radius, was not significant over long observation periods. For shorter observation periods, moderate correlations (-0.5 to -0.6 range) existed between Δ and received signal level (RSL). It is possible that this correlation is due, in part, to a correlation between multipath spread and aperture-to-medium coupling loss. As expected, a high correlation (> 0.9) was observed between surface refractivity N_s and path loss.

Seasonal and diurnal variations in path loss followed expected patterns: path loss was much higher in winter than in summer; during summer a diurnal trend was observed whereby the path loss decreased from early morning through mid-day and then increased through the afternoon; during the winter, diurnal variations did not have a significant pattern.

Seasonal variations in multipath spread were not significant. There was an interesting diurnal trend over the short path with standard 8-foot reflectors; observed values of Δ were wider during winter mornings than during winter afternoons and, during the summer, the converse was observed.

At present there exist a large volume of empirical data relative to troposcatter path loss and reliable path loss prediction techniques are available for a wide range of conditions. Such is not the case for multipath spread and fade rate, both of which can significantly affect the design and performance of high-speed digital troposcatter systems. During the next ten years it is expected that most military troposcatter systems will change over from analog to digital transmission, which suggests the need for development of reliable techniques for predicting multipath spread and fade rate. Such development would require a systematic collection and analysis of channel and meteorological data on a large-scale basis. Because of the prohibitive expense of such an undertaking, data collection efforts will probably remain restricted to the rather specialized and limited test programs such as the one reported herein.

SECTION II

TEST PROGRAM

2.1 BACKGROUND AND OBJECTIVES

The Air Force has engineering responsibility for a new generation of all-digital troposcatter radio terminals for Tri-Service tactical application. The family of radio terminals, designated as AN/TRC-170 ( ) (V), includes a small radio terminal similar in size to the existing AN/TRC-97. The small terminal is expected to operate in the frequency range of 4.4 - 5.0 GHz with antenna reflectors about the same size as the 8-foot TRC-97 antennas. These terminals are to provide a multi-channel trunking capability of up to 64 channels at 32 Kbps per channel at ranges of up to 100 miles. The large terminals in the family may have antenna reflectors up to 28 feet and are to provide a 64-channel trunking capability at ranges up to 200 miles. In any case, there is the usual desire to obtain reliable performance at minimum cost, complexity, size, weight, set-up time, etc. The tactical nature of the intended application will place even more severe constraints on size, weight, set-up time and prime power. This, in turn, will restrict transmitter power and antenna gain, thereby placing additional emphasis on development of efficient signal processing techniques.

It has long been appreciated that short-to-medium range troposcatter channels are mildly dispersive. Using twice the RMS multipath spread ($\Delta = 2\sigma$) as a measure of dispersion, expected values of Δ are in the order of tens to hundreds of nanoseconds depending upon path geometry, antenna beamwidth, etc. Dispersion is usually thought of on a relative basis. Using one of the more recent channel models developed by Bello [1], it was expected that for TRC-97 links in the 80-100 mile range, Δ would be of

the order of 20 to 100 ns. If relatively low speed digital transmission were considered, say 100 Kbps, then symbol intervals T might be in the order of 10,000 ns or longer. In such a case, the relative pulse spreading caused by the channel would be insignificant. One would consider the channel to be non-dispersive or non-distorting. In the frequency domain, the signal bandwidth would be narrow relative to the correlation bandwidth, and fading would be flat (non-frequency selective). Conventional modem techniques, say QPSK modulation with fixed matched filter demodulators, could be used without any significant penalty.

As the ratio of multipath spread to symbol width (Δ/T) becomes larger, conventional matched filter signal processing will result in two related types of penalty. First, the channel pulse spreading results in intersymbol interference (ISI) which degrades performance and leads to an irreducible error rate effect. As signal-to-noise ratio (SNR) is increased, a point is reached where no further reduction in error rate is achievable. For even modest values of Δ/T, say 0.1, a significant performance degradation may be observed relative to flat fading performance. Secondly, the channel pulse spreading is due to propagation over physically independent paths; hence, the signal components received at different delays fade with near total independence. This effect serves to offer an implicit multipath diversity which, given the necessary signal processing, could be used profitably to improve performance relative to flat fading performance. Failure to exploit this available signal energy results in a penalty relative to what could be achieved. As the ratio of Δ/T ranges from zero up to the range unity or greater, the total multipath-related penalty expressed in dB SNR necessary to achieve a given error rate increases. The penalty can range from 0 to tens of dB to, in some

cases, infinity. It is essential to know the expected range of Δ/T. The ISI penalty could be too large for a conventional receiver; on the other hand, a complex receiver could be employed when the potential advantage is actually marginal or non-existent.

Within the context of the TRC-170 development, a nominal data rate of about 2 Mbps is of interest. Making the reasonable assumption that QPSK modulation would be employed, a symbol width would be of the order of 1000 ns. If the expected dispersion were in the range of 20 ns, then Δ/T would be only 0.02. A complex receiver would have only marginal advantage over a conventional fixed matched filter. That this expectation was common early in the TRC-170 development was not necessarily unreasonable, for the Bello channel model had general acceptance as a useful tool for predicting expected dispersion. The model and certain empirical factors (see Section 5.3) within it had been verified on a longer path at L Band ($\sim$ 900 MHz).

There did exist other empirical data which indicated that the dispersion over such tactical links would be considerably wider than predicted by the Bello model when the standard model empirical factors were employed. The data were in the form of correlation bandwidth measurements made by Martin-Marietta [2, 3] and Signatron [4]. These measurements were indirect measurements of dispersion; however, the results were not, in general, well known or integrated with direct multipath measurements or channel models. The results, upon examination, indicated that TRC-97-type paths in the 80-to-120 mile range may have an average Δ of 120 ns or more and that a wide variation can be expected over any given path. The data indicated that Δ may be expected to range from about 50 to more than 300 ns for such a path. If this were true, then Δ/T could be expected to range from 0.05 to more than 0.3 even for relatively short paths.

Conceptual formulations, and in some cases hardware prototypes of ideal, or near-ideal receiver structures for fading dispersive channels are not new [5,6,7,8]. It is only in the past few years, however, that the available component and fabrication technology and government sponsorship have led to practical physical realizations that might be appropriate for field application. Several past and current projects sponsored by USAF/RADC and ARMY/ECOM have led to at least four competing digital modem techniques that are now in various stages of hardware development. Each offers reduction of ISI penalty and realization of an implicit in-band diversity. Some may offer these advantages at a level of complexity which is only a modest increase over the conventional receiver.

At a time when specialized signal processing techniques were becoming practical, evidence became available that the expected dispersion may be in the range for which these techniques could significantly improve efficiency. Because of this fact and the availability of instrumentation and experience resources at the RADC tropo test range, MITRE and RADC undertook a joint effort to obtain channel measurement data and to evaluate the performance of the various digital tropo modem techniques.

2.2 TEST PATHS AND FACILITIES

2.2.1 Test Paths

The location of the test sites is shown in Figure 2-1. Also shown as dashed lines are other test paths which have been used in earlier test programs. While partial terrain profiles of the two test paths are presented in Figure 2-2, it should be noted that they do not accurately define the radio horizon on these links at 5 GHz.

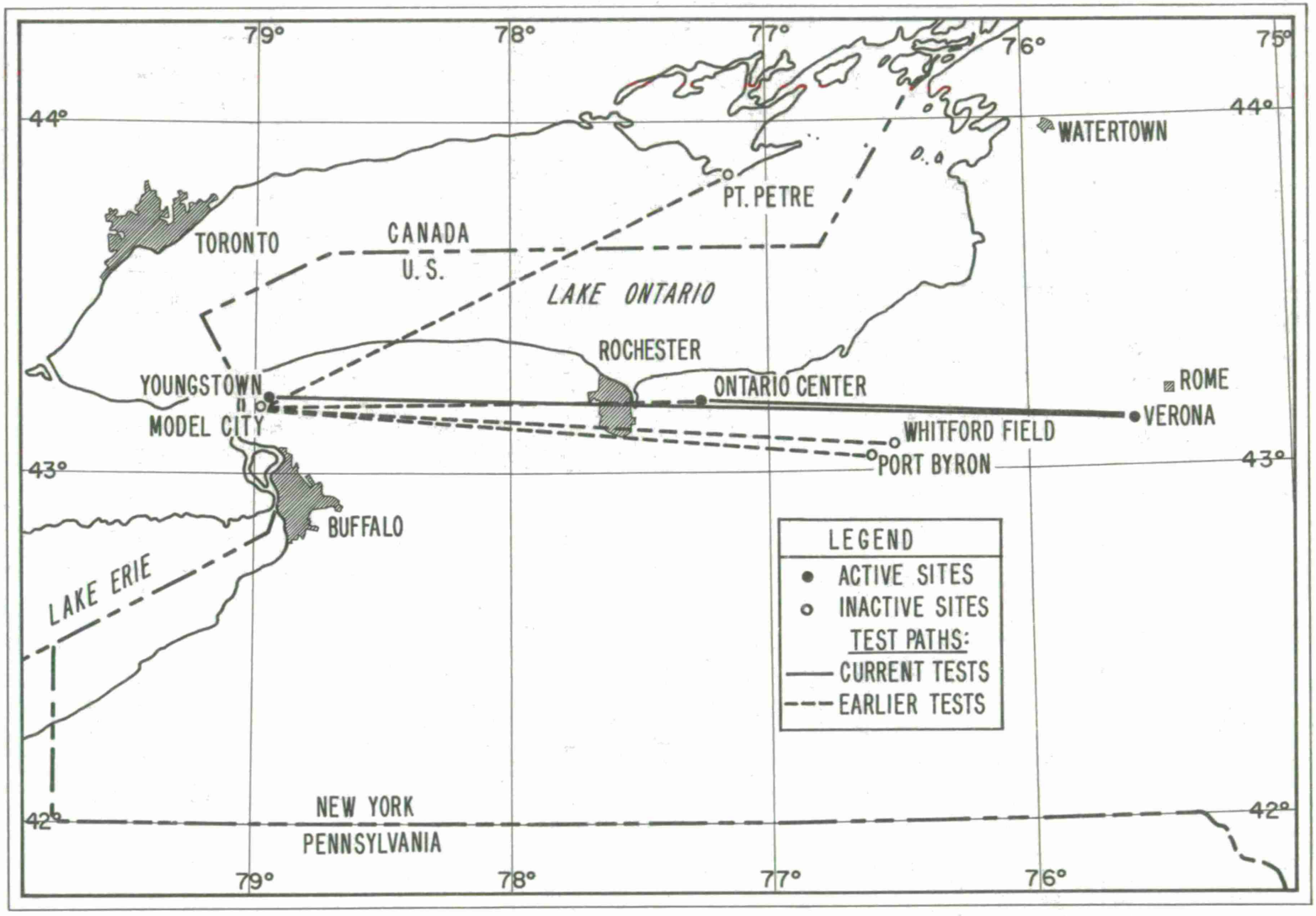

Figure 2-1. RADC Test Range

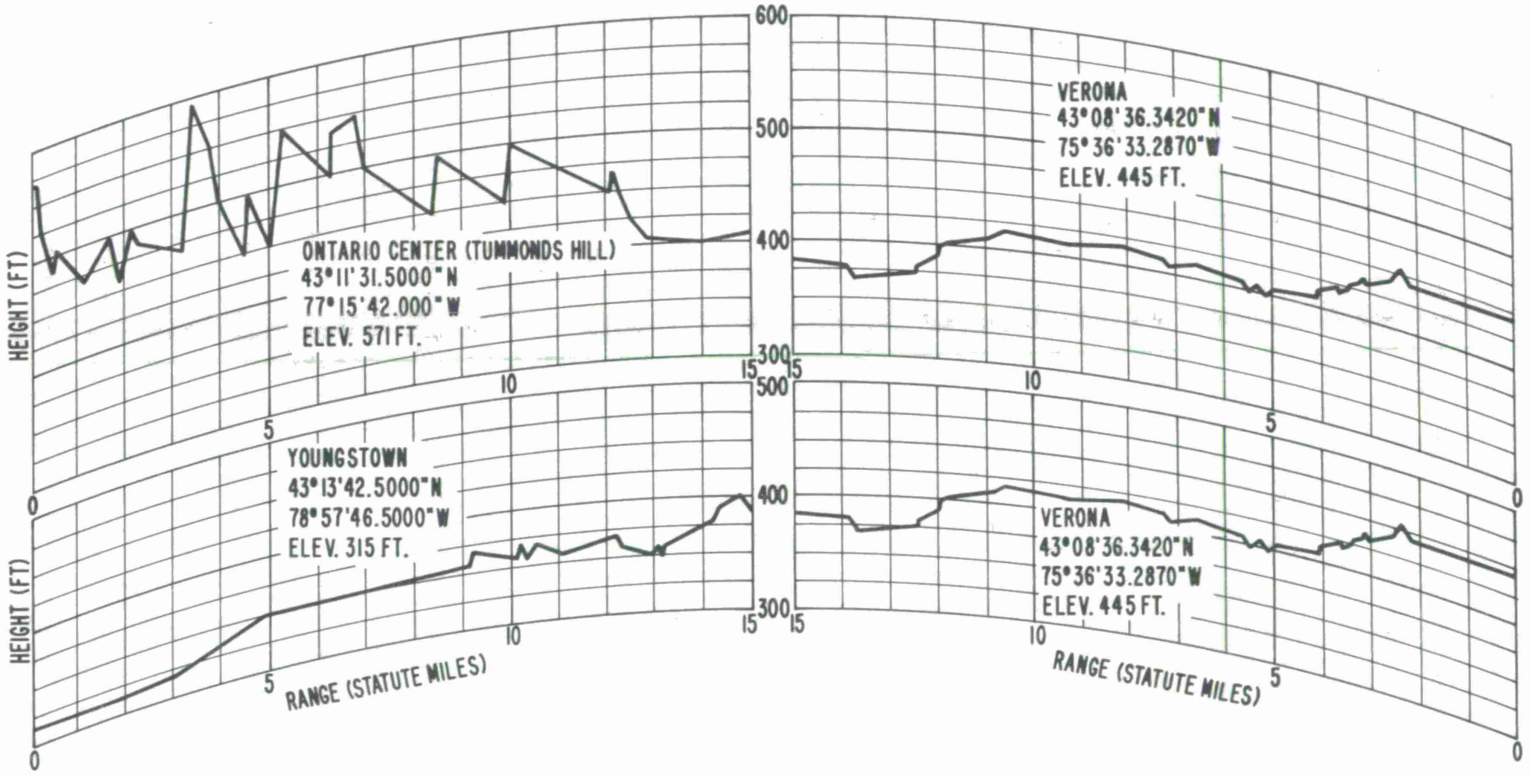

Figure 2-2. Partial Terrain Analysis

Comparison of measured path loss values with predicted values indicate that the tree lines at both the Youngstown and Verona sites effectively establish the radio horizon. The terrain east of the Youngstown site is slightly elevated with a tree line 4,000 feet from the transmit site. The approximate take-off angle for this site is one degree. The terrain west of the Verona receive site is flat with a tree line 8,000 feet west of the site. The approximate take-off angle for this site is 0.5 degree. The profile given for the vicinity of the Ontario Center transmit site does not accurately reflect the topography along the path. Visual measurement of the horizon yields a take-off angle of one-third degree.

Both paths are overland and are near, and parallel to, Lake Ontario. The lake often influences the meterological conditions along these paths and this influence may make the data gathered on these paths somewhat atypical of inland troposcatter paths.

2.2.2 Radio Systems

The radio terminals employed in the test program were obtained and set up specifically in support of the TRC-170 development program. The TRC-97 radios used on the short path were provided by and set up by the 108th Air National Guard (ANG) TAC COMM Squadron located at Hancock Field, New York. The TRC-132 A radios were provided by the US Army and were set up by AFCS 3rd MOBILE COMM Group.

2.2.2.1 TRC-97 D Radio Terminal

The TRC-97 can operate in the frequency range of 4.4 to 5.0 GHz on any of 1200 frequencies spaced in 500 KHz increments. These tests were run at 4780 MHz. The single power amplifier (PA) is a four-cavity

air-cooled Kystron (Varian #VA-888E) rated at a nominal 1 KW output. Up to about 1.4 KW may be realized with high efficiency tuning for narrow bandwidth signals; broadband tuning may reduce output to about 0.9 KW. The standard antenna group includes two 8-foot parabolic reflectors per terminal for dual space diversity operation. For these tests, an additional 15-foot reflector was set up at each radio terminal. The receivers use two-stage tunnel diode amplifiers (TDA) for pre-RF amplification with an effective receiver noise figure in the 5 to 6 dB range.

Because the radio/instrumentation interface was at 70 MHz IF, all FDM/FM-related portions of the radio terminal were bypassed. The only other changes made to the basic radio configuration were to broadband tune the power amplifier and to replace the built-in frequency synthesizer used to derive the up and down conversion local oscillators (LO) with an external, highly stable unit.

2.2.2.2 TRC-132 A Radio Terminal

The TRC-132 radio terminal can operate in the 4.5 to 5.0 GHz range in 100 KHz increments. Each terminal has dual 10 KW rated power amplifiers for dual frequency diversity capability; however, channel measurements were made on only one frequency, 4690 MHz. (The other PA was operational at 4500 MHz and was used in other modem testing.) The PAs are four-cavity liquid-cooled Klystrons (Varion #VA-1908B). Broadband tuning may reduce output to about 5 KW at the recommended drive power level. The standard antenna group includes two 28-foot parabolic reflectors per terminal for dual space diversity operation. The receivers use a single-stage TDA pre-RF amplifier with an effective receiver noise figure in the 7 to 8 dB range.

All FDM/FM portions of the radio terminal were bypassed with the instrumentation interface at 70 MHz IF. As with the TRC-97, the PA was broadbanded and the built-in frequency synthesizer was replaced by a highly stable unit. In addition, the entire LO chain was replaced with frequency multiplier chains from TRC-97 terminals; the transmit pre-selection filter was replaced with a wider band unit from TRC-97; and narrowband filters in the receiver pre-IF amplifier were eliminated.

2.2.2.3 Test Path Parameters

A summary of the parameters for each test path configuration is given in Table 2-1. Values of antenna gain and antenna beamwidth are calculated using a standard antenna efficiency of 55 percent. Values of aperture-to-medium coupling loss are calculated using the C. C. I. R. approach (see Section 5.4). The given antenna elevation angles were measured and represent the values for which minimum path loss was observed.

2.3 TEST INSTRUMENTATION

Because the test configuration was the same for both test paths, only the TRC-97 short path setup is described.

2.3.1 Basic Test Configuration

Figure 2-3 is an overall block diagram of the basic test setup. The RAKE "multipath analyzer" transmitter and receiver interface with the radio system at 70 MHz IF. At each site all timing and frequency references were derived from a 5 MHz GR-1115-B standard oscillator with a frequency stability in the order of 1 part in 10^{10}. This included all RAKE timing signals and unmodulated 70 MHz carrier and the radio local oscillator (LO).

Table 2-1

Path Parameters

Transmitter Location	Ontario Center			Youngstown
Transmitter Power (watts)	1,000	1,000	1,000	3,000
Antennas: (Transmitter, Receiver)				
Size (ft)	8,8	8,15 (or 15,8)	15,15	28,28
Gain (dB)	39.1,39.1	39.1,44.5	44.5,44.5	49.8,49.8
3dB Beamwidth (deg)	1.9,1.9	1.9,1.0	1.0,1.0	0.54,0.54
Elevation Angle (deg)	3/4,3/4	3/4,3/4	3/4,3/4	1/2,0
Aperture-to-Medium Coupling Loss (dB)	5.2	6.9	9.4	16.8
Distance (St. mi)	86	86	86	168
Frequency (MHz)	4,780	4,780	4,780	4,690

OVER-AIR PROPAGATION TESTS

VG-38,454

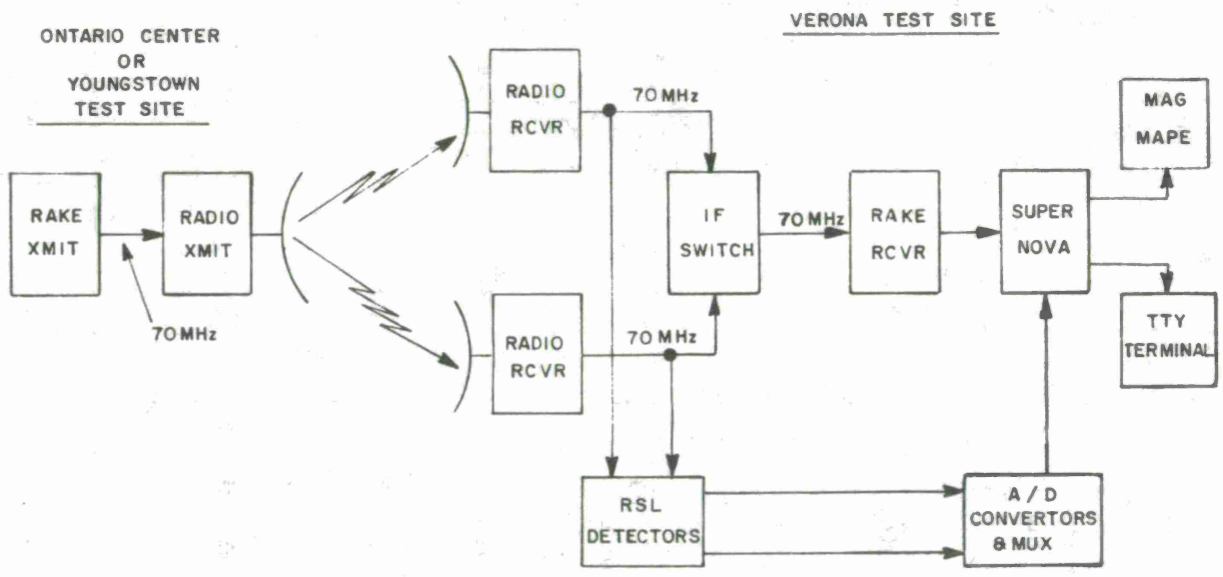

Figure 2-3. Basic Test Configuration

The radio LO was derived by locking a HP frequency synthesizer to the 5 MHz reference and generating a 49.0625 MHz reference frequency, which was then input to the TRC-97/X96 multiplier chain for the desired 4710 MHz LO. The fine adjustment of the 5 MHz standard oscillator reduced the overall frequency translation error to less than 1 Hz.

The Verona test lab, which was about 300 feet from the radio terminal, contained all receiver-site instrumentation.

2.3.2 Multipath Measurements

These measurements were made with a "multipath analyzer" [9] built for RADC by Sylvania, Inc. Since the system uses a concept from the original RAKE communication system [5] for fading dispersive channels, the term RAKE is usually used in place of multipath analyzer. In the original RAKE system, destructive multipath interference was eliminated by isolating signal energy received at different delays and then realigning and combining the signals. Only isolation of signal energy as a function of delay is of interest for channel measurement. The RAKE channel measurement technique [10] consists of using a maximal-length binary sequence as a probe signal and, at the receiver, cross correlating locally generated sequences with the received signal (Figure 2-4). The auto-correlation function of such a sequence has a sharp peak at zero shift (relative delay) and then drops to near zero until the shift is equal to the sequence length (Figure 2-5). A cross-correlation at the receiver, using an identical sequence, is then responsive to signal energy received in a specific delay interval, the interval being the width of the sequence correlation peak. A bank of such cross-correlators, each operating over different delay intervals, can be used to estimate channel impulse response as a function of delay. If the overall bandwidth of the radio system is sufficiently wide, the delayed response will be primarily due to multipath propagation.

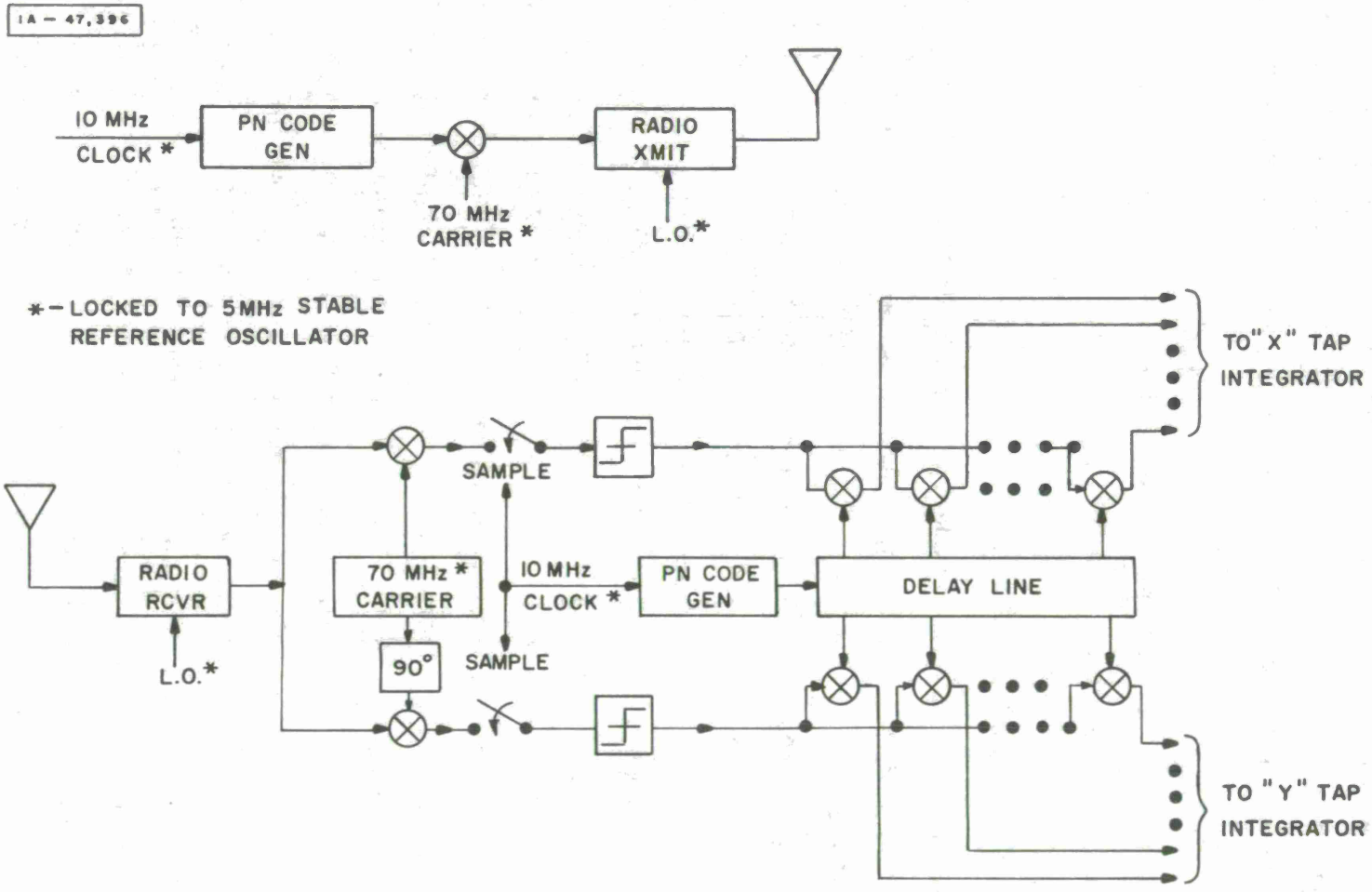

Figure 2-4. RAKE System Functional Diagram

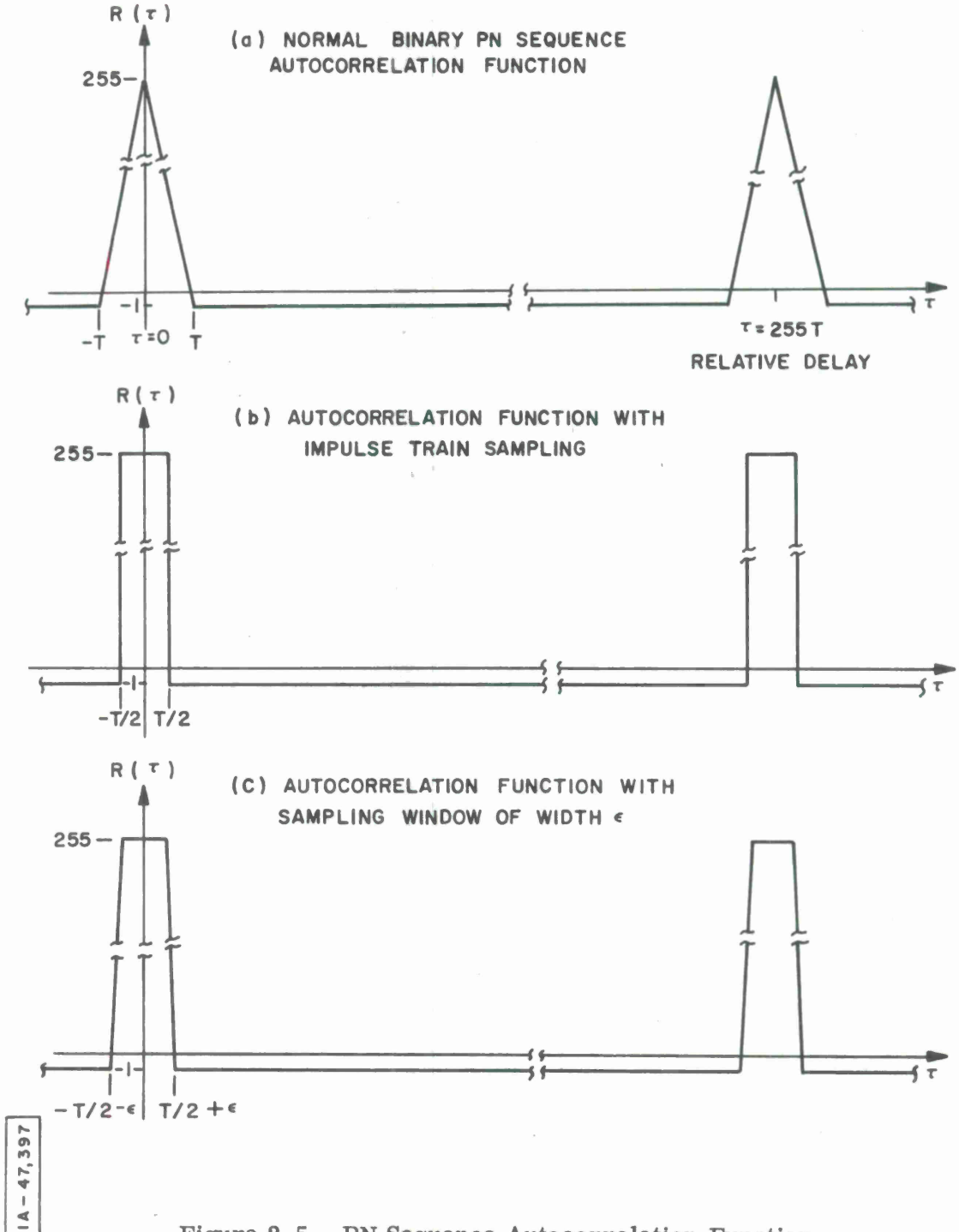

Figure 2-5. PN Sequence Autocorrelation Function

For these measurements, the binary probe sequence was converted to 70 MHz IF using binary PSK modulation at a 10 MHz rate. The RAKE transmit data clock and 70 MHz carrier were derived from the stable master oscillator. At the RAKE receiver, a second stable oscillator was used to generate receiver timing and two 70 MHz reference carriers with 90^{o} relative phase shift. The received IF signal is mixed with each of these references to recover "inphase" and "quadrature" baseband sequences. Even though the modulation is binary PSK, the channel introduces random time variable phase shift. The received signal, at a given delay, is a vector of random phase and amplitude. In order to measure the channel response, both components of the vector must be observed. This is consistent with the concept that, for a bandpass process, the equivalent low pass (baseband) impulse response is in general a complex function.

The two recovered sequences are then sampled with a narrow window polarity sensor at the data rate, an approximation to impulse train sampling. Impulse train sampling results in a rectangular auto-correlation peak the width of one bit interval T (Figure 2-5b) as opposed to the usual triangular peak of base width 2T (Figure 2-5a). The width of the sampling window, which is about 10 ns wide, results in a trapezoidal shape peak as shown in Figure 2-5c.

The remaining processing is all-digital and consists of cross-correlating ten locally generated sequences with each of the two recovered sequences and integrating over several thousand bits. The ten local sequences differ from each other only in delay, each being delayed one bit interval T from the previous. This is equivalent to a tapped delay line receiver with cross-correlators at discrete delay values. At the end of each integration period, an estimate is formed of the channel's equivalent low pass complex impulse response at each of 10 discrete delays.

Denoting the time variable impulse response by h (t, τ) where τ is the delay variable, an estimate is formed of

$$\hat{h}(t_j, \tau_k) = \hat{x}_{jk} + i\,\hat{y}_{jk}, \quad k = 1, 2, \ldots, 10$$

at times t_j. These channel snapshots are then used to form the time average estimate of the multipath power profile:

$$\hat{Q}(\tau_k) = \langle (\hat{x}_k^2 + \hat{y}_k^2) \rangle, \quad k = 1, 2, \ldots, 10. \tag{2-1}$$

This is proportional to the average power received from paths having delays in the interval $(\tau_k - T/2, \tau_k + T/2)$ where T is the width of one bit interval.

Assuming a complex Gaussian wide-sense stationary uncorrelated scattering model (WSSUS), Bello [11] has defined the delay power spectrum Q (ξ) as

$$E\left\{h^*(\xi)\, h(\eta)\right\} = Q(\xi)\, \delta(\eta - \xi) \tag{2-2}$$

where $Q(\xi)\,d\xi$ is proportional to power received in the delay interval $(\xi, \xi + d\xi)$. The measured $\hat{Q}(\tau_k)$ is used as a discrete time average estimate of the continuous ensemble average $Q(\xi)$. In particular, twice the standard deviation of $\hat{Q}(\tau_k)$, $\Delta = 2\sigma$, is used here as an estimate of the width of $Q(\xi)$.

The specific RAKE parameters that were employed are:

(a) Data Rate - A 10 MHz rate was chosen from among choices of 10, 5, 2.5 and 1.25 MHz. This resulted in a $(\sin x/x)^2$ shape spectrum at IF with the distance between the first spectral nulls being 20 MHz. The multipath resolution (delay between adjacent taps) was 100 ns.

(b) Integration Period - A 10 ms (9.792 ms) integration period was chosen from among 1.25, 10 and 80 ms. The 10-ms mode results in 100 complex samples per second which tracks channel fade rates of up to 100 Hz for single-channel operation. Actual operation consisted of dual channel probing using a coaxial switch to alternate sampling between the two channels. This resulted in 50 samples per second per channel or a capability to track fade rates up to 50 Hz. Since all tests that included aircraft reflection effects were eliminated or aborted, the 50 Hz capability was more than adequate to follow "natural" fading.

(c) Observation Period - This is the length of time over which the channel samples, or snapshots, are time averaged to estimate a multipath power profile. The original data processing software, and RAKE receiver, were configured for a fixed number of integration periods per observation (experiment). For the 10 ms integration period mode, 11,264 samples are processed, which results in an observation period of 110.3 seconds. This time is long enough to provide a good profile estimate at typical fade rates (1-5 Hz) and usually short enough to avoid significant changes in channel fading statistics during the course of an observation. Since the 110-sec period was considered to be a good compromise, no attempt was made to change this preset parameter.

2.3.3 RSL Measurements

The RSL detectors shown in Figure 2-3 are usually referred to as log-linear envelope detectors. The particular units employed in these

tests had a nominal 3 dB input bandwidth of 10 MHz centered at 70 MHz; they perform a logarithmic compression of the input IF envelope which is followed by a several-stage (progressive saturating) envelope detector. Output is a dc voltage that is a linear function of $\log_{10}(P_{IF})$, P_{IF} = input power, over an 80 dB dynamic range.

The RSL instrumentation was calibrated over the range -110 to -70 dBm at least once every 24 hours, normally at about 0830 hours. The calibration was accomplished by injecting known signal levels into the receiver front end at 4,780 MHz using an HP-618 SHF signal generator; this was done for each of nine signal levels over the -110 to -70 dBm range in 5 dB increments. For each input signal level at RF, the output DC voltage was "saved" on a calibration console by adjusting reference DC voltage levels to null a meter which measured the difference between the sampled and reference voltages. The nine reference voltages were then available for A/D conversion and input to the on-line computer.

The on-line computer software includes a calibration routine during which the nine reference voltages are sampled and associated with the nine respective received signal levels. A linear interpolation is then performed between adjacent 5 dB reference levels, resulting in a calibration table in 1 dB increments over the -110 to -70 dBm range.

2.4 TESTING PROCEDURES AND DATA RECORDING

Standardized testing procedures were followed for most tests. Any variations are noted in the discussion of appropriate test results.

2.4.1 Standard Procedures

Most tests were conducted during normal working hours, 0800-1600 hours local time, five days a week. The normal early morning routine consisted of calibrating the RSL instrumentation at the Verona receive site and sweeping the transmitter frequency response and measurement of transmitter output power. Transmitter sweep was accomplished at very low drive power. The check consisted of observing the 1 dB bandwidth of the transmitter and, if necessary, fine tuning the 4-cavity Klystron PA to maintain a 1 dB bandwidth of at least 12 MHz centered at 70 MHz. This bandwidth had been determined experimentally as the minimum bandwidth for which bandlimiting constraints of the radio system would have negligible effect on multipath measurements (see Section 2.5).

Channel measurements were normally made once each hour, on-the-hour whenever possible, that is, when the instrumentation and on-line computer system were operational. This test schedule coincided with normal meterological observations, and was usually altered only if aircraft were present in the common volume. The scheduled test would be delayed or aborted and restarted at a time when the aircraft effect was no longer observable. Also, unscheduled tests were conducted when sudden changes in path loss or multipath spread occurred or when an unusual condition such as layering was observed. On a few occasions, the test schedule extended to late evening and/or around-the-clock.

Each observation normally consisted of a 3-minute measurement of RSL on each of two space-diversity receivers. Within this 3-minute interval, a 110-second RAKE experiment was conducted to determine the multipath power profile for each channel.

From 1 October 1974 to 17 December 1974, all tests were done with the AN/TRC-97 standard 8-foot reflectors. During the period 18 December 1974 through 22 April 1975, one TRC-97 receiver was connected to the standard 8-foot reflector while the other was connected to a 15-foot reflector. Most tests up to 24 February 1975 were conducted with the standard 8-foot reflector at the Ontario center transmit site. Starting on 24 February and through 4 March, the transmit antenna was a 15-foot reflector. From 5 March through 18 April, the transmit antenna was alternated between the 8-foot and 15-foot reflectors with changeover at 1200 hours local time each day. All short path tests made subsequent to 22 April 1975 were made with the standard 8-foot reflectors at the transmit and receive sites (both receivers).

During the period 28 April through 12 May 1975, tests were conducted over the TRC-132A long path link using the standard 28-foot reflectors. Starting in the afternoon of 12 May, a long period of over-the-air modem testing was conducted on the TRC-97D short path that continued through 10 July and included normal RAKE testing, which was alternated with modem error rate tests. In general, during this period, several RAKE tests were made per hour; however, only the nominal one-per-hour, on-the-hour tests have been selected for inclusion in the results presented herein.

The final segment of tests was conducted over the TRC-132A long path during the period 17 July through 7 August 1975.

2.4.2 On-Line Data Processing

A Super Nova computer was used for on-line processing of RSL and RAKE data.*

2.4.2.1 RSL Data Processing

The voltage out of the log-linear RSL detectors was sampled and A/D converted at a rate of 10 Hz for each of the two diversity channels. Thus, a normal 3-minute test resulted in 1800 RSL samples per channel. Each sample was compared with the stored calibration table and the accumulator for the appropriate RSL level incremented. At the end of a test, the Probability Density Function (PDF) and Cumulative Distribution Function (CDF) are printed out. The PDF is simply the number of counts at each RSL level and the CDF runs from zero to 100% (low RSL to high). The first RSL increment for which the CDF $\geq$ 50% is declared the median RSL.

The number of one-way crossings of the median per minute is also printed out and used as a measure of fade rate. This is a running calculation where the first-minute median is calculated and then, during the second minute, crossings relative to the first-minute median are noted. Crossings during the third minute are relative to the median for the first two minutes, and so forth.

2.4.2.2 RAKE Data Processing

Each RAKE output sample is an estimate of the equivalent low pass complex impulse response at time j;

$$\hat{h}\,(t_j, \tau_k) = \hat{x}_{jk} + i\,\hat{y}_{jk}\,, \quad k = 1, 2, \ldots, 10.$$

---

*Details of the software package for this processing are given by L. Suyemoto in "Software for Channel Characterization Test of the Joint ESD/MITRE/RADC Troposcatter Radio Test Program," MITRE Technical Report MTR-3016, which has not been approved for public release.

The nominal 50 samples per second per channel result in 5,632 samples over the 110-second observation period. The time average power for each tap is calculated as

$$\hat{Q}(\tau_k) = \frac{1}{K} \sum_{j=1}^{n} (\hat{x}_{jk}^2 + \hat{y}_{jk}^2) \qquad (2\text{-}3)$$

where K is a normalization constant such that the resulting $\hat{Q}(\tau_k)$, $k = 1, 2, \ldots, 10$ is of approximate unit area. The ten values of $Q(\tau_k)$ are then printed out as relative power values. In addition, the highest tap power is assigned a zero dB reference and the ten $\hat{Q}(\tau_k)$ are also printed out in dB relative to the reference.

The mean delay ($\bar{\tau}$) and also twice the standard deviation ($\Delta = 2\sigma$) are calculated and printed. They are based on the $\hat{Q}(\tau_k)$ for all k from 1 through 10 even though signal energy may not be presented in all taps. This may lead to errors in the calculation of Δ as all taps have a noise floor which can contribute to the calculation of Δ.

Denoting $\hat{Q}(\tau_k)$ by Q_k, $\bar{\tau}$ and Δ are calculated as

$$\bar{\tau} = \frac{\sum \tau_k Q_k}{\sum Q_k}$$

and

$$\Delta = 2\left[\frac{\sum \tau_k^2 Q_k}{\sum Q_k} - (\bar{\tau})^2 - \frac{1 \times 10^{-14}}{21}\right]^{1/2}, \quad k = 1,2,\ldots, 10 \qquad (2\text{-}4)$$

The factor $1 \times 10^{-14}/21$ is a carry-over from an original software package developed by Sylvania and its exact purpose is not known. The intent may have been to compensate for the finite noise floor of the RAKE receiver.

The original printed values of $\bar{\tau}$ and Δ were in all cases recalculated selecting only those taps for which a recognizable signal was present, a subjective judgement. The recalculated values are based on

$$\bar{\tau} = \frac{\sum \tau_k Q_k}{\sum Q_k} \tag{2-5}$$

and

$$\Delta = 2 \left[\frac{\sum \tau_k^2 Q_k}{\sum Q_k - 1} - (\bar{\tau})^2 \right]^{1/2} \tag{2-6}$$

where k is the index for only those taps having recognizable signal energy. The choice involved both magnitude above the noise floor (in general $>$ 0.5dB) and the shape of the power profile.

2.5 INTEGRATION TESTS

During August and September 1974 a series of back-to-back tests were conducted to verify the measurement system and radio interfaces.

2.5.1 RAKE Back-to-Back

Initial checks were made with the RAKE in a digital loop-back test where the locally generated sequence is delayed to coincide with Tap 5. The results are presented in Table 2-2. There is no spreading of signal energy into adjacent taps and the ratio of peak correlation to "off" correlation is 35.3 dB.

Table 2-2

Results of RAKE Loop-Back Tests

	RAKE Output Power Profiles in dB			
Tap No.	Digital Loop Back	IF Loop Back	Initial Radio Loop Back	Radio Loop Back With 13 MHz 1 dB Bandwidth
1	-35.3	-31.4	-15.2	-23.3
2	-35.3	-24.7	0	0
3	-35.3	0	-18.9	-24
4	-35.3	-22.2	-26.2	-25.2
5	0	-30.2	-27.1	-25.6
6	-35.3	-30.9	-27.4	-25.6
7	-35.3	-31.1	-31.7	-28.7
8	-35.3	-31.1	-33.6	-30.1
9	-35.3	-31.6	-32.0	-29.9
10	-35.3	-31.4	-33.6	-29.9

Table 2-2 also shows the results of RAKE back-to-back testing at IF. This test was conducted in the normal operate mode with the receiver timing adjusted so as to center the correlation peak in RAKE Tap 3. The signal-to-noise ratio (SNR) at the receiver was adjusted to -15 dB (in 10 MHz bandwidth), a standard operating mode to linearize the digital cross-correlation [12]. As can be seen in this table, adjacent taps are down by 24.7 and 22.2 dB. In theory, the correlation shape shown in Figure 2-5 should result in adjacent taps being down by 26 dB. That does not, however, include the effect of the additive noise which leads to a reduction in the peak value.

2.5.2 RAKE/Radio Tests

A series of back-to-back RAKE tests were conducted through the TRC-97 radio. Two radios were used, one located in the laboratory facility as a transmitter and the second the receiver terminal employed in subsequent over-the-air tests. The test configuration is shown in Figure 2-6. The objective of this series of tests was to tune the radio filters and power amplifier so that the RAKE performance would essentially be the same as observed during the RAKE back-to-back IF test. Table 2-2 shows one of the test runs conducted after an initial tuning of the radio. Adjacent taps are down only 15.2 and 18.9 dB. Also shown are the results after tuning the Klystron power amplifier for a 1 dB bandwidth of approximately 13 MHz. (This bandwidth actually included all filtering from IF to IF.) Adjacent taps are down by 23.3 and 24 dB which is similar to the RAKE back-to-back results; here, however, subsequent taps also appear to reflect a slight spreading effect.

2.5.3 RAKE/Channel Simulator Tests

A troposcatter channel simulator [13] was used to verify the capability of the RAKE system to estimate multipath profiles as shown in Figure 2-7. The simulator is a tapped delay line model with 0.1μs tap spacings. Multipath profiles are "programmed" by attenuators that establish relative average power for each Rayleigh fading tap. Fade rate (2 σ Doppler) is adjustable from 0.1 to 10 Hz and built-in additive white noise sources allow adjustment of output SNR over a wide range. Table 2-3 presents typical results of these tests; for each test, the simulator programmed profile is shown on the left and the RAKE estimate on the right. Fade rate and equivalent RSL are also given. The RSL number is

that short term median RSL for a TRC-97 receiver (N. F. ≈ 5 dB) for which the SNR would be the same as that set at the output of the channel simulator. The results indicate that the RAKE system accurately estimates multipath profiles over a range of SNR and fade rates. The noise floor of the RAKE receiver precludes accurate estimates of multipath profile tails where the fall off is in the order of 22 dB down from the dominant central portion. This has only minor impact on the estimation of RMS multipath spread.

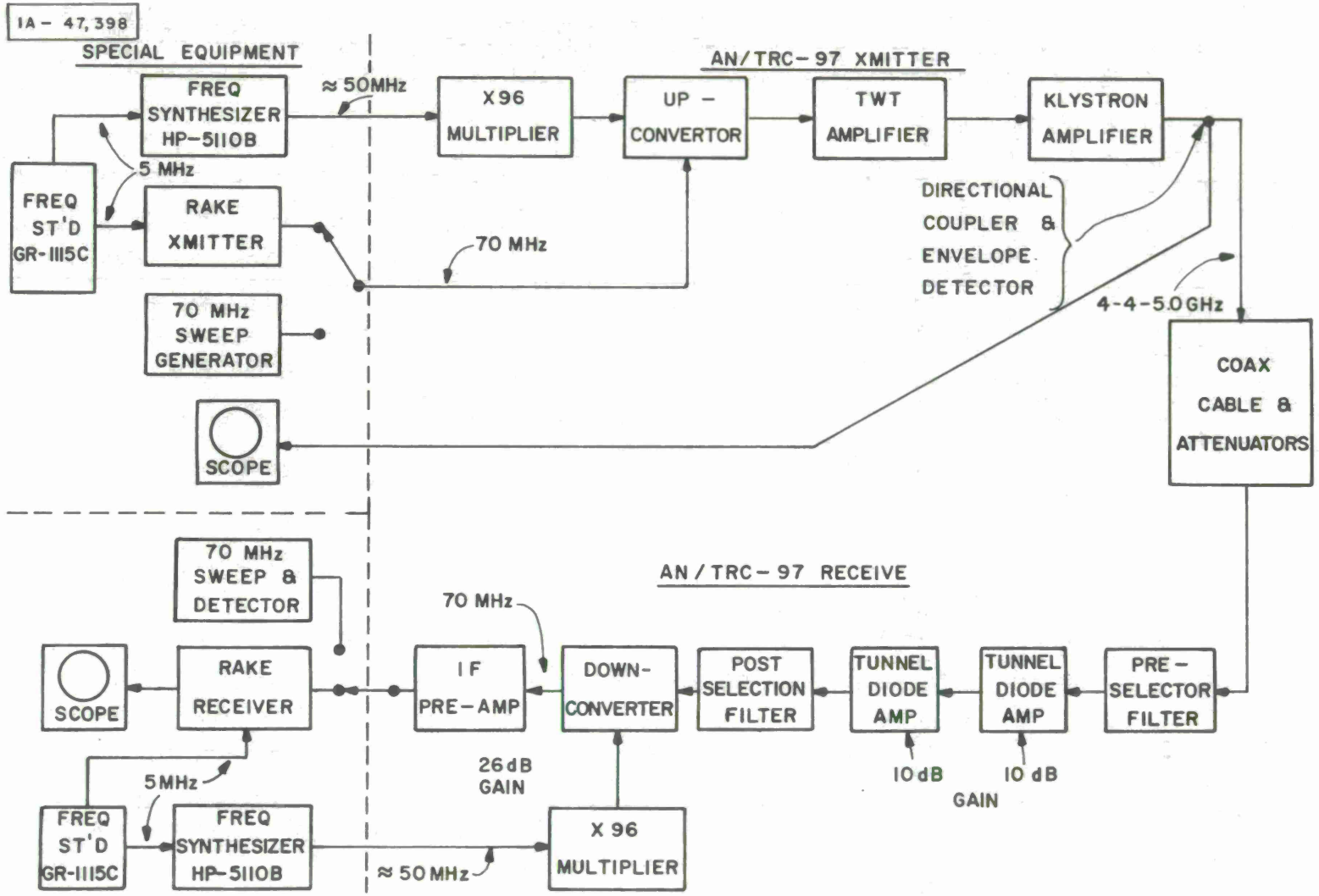

Figure 2-6. RAKE/Radio Integration Tests

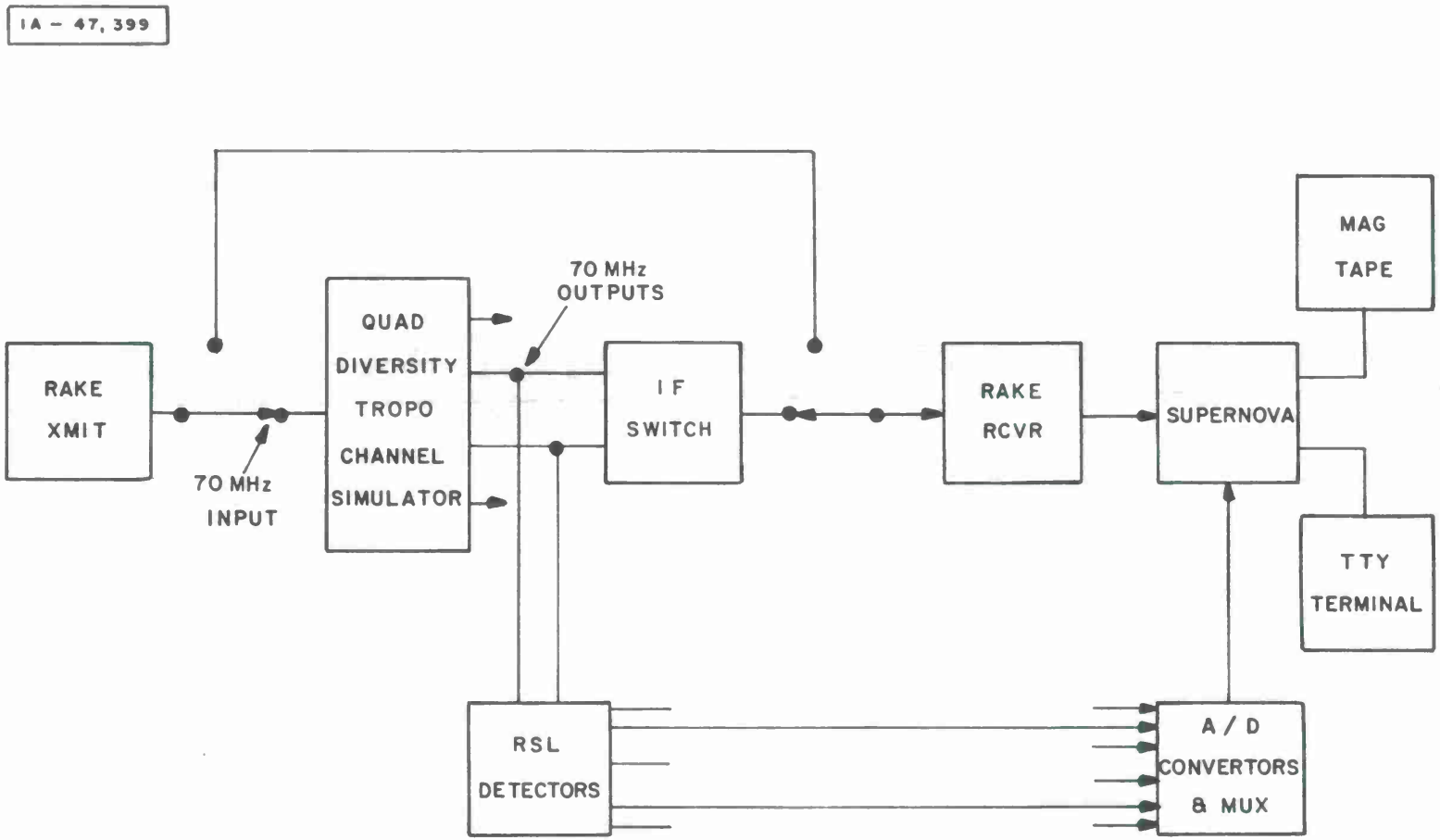

Figure 2-7. RAKE/Channel Simulator Tests

Table 2-3

Results of RAKE/Channel Simulator Tests

Tap No.	-90 dBm, 2 Hz Fade Rate		-95 dBm 2 Hz		-105 dBm 2 Hz		-115 dBm 2 Hz		-125 dBm 2 Hz	
	Simulator (S) - dB	RAKE Estimate (R) - dB	(S)	(R)	(S)	(R)	(S)	(R)	(S)	(R)
1	-∞	-26.8	-∞	-21.6	-∞	-19	-∞	-21	-∞	-23.1
2	0	0	0	0	0	0	0	0	0	0
3	-∞	-22.2	-3	- 2.9	-3	- 2.9	-3	- 2.5	-3	- 3.2
4	-∞	-29.9	-7	- 7.2	-7	- 6.9	-7	- 6.9	-7	- 6.6
5	-∞	-31.0	-12	-11.9	-12	-11.7	-12	-11.4	-12	-11.9
6	-∞	-31.3	-17	-16.7	-17	-16.6	-17	-16.1	-17	-16.1
7	-∞	-31.5	-23	-21.9	-23	-21.3	-23	-21.0	-23	-20
8	-∞	-31.9	-29	-25.3	-29	-24.6	-29	-24.9	-29	-22.4
9	-∞	-31.8	-∞	-28.9	-∞	-28.2	-∞	-29.1	-∞	-24.2
10	-∞	-31.3	-∞	-28.8	-∞	-27.8	-∞	-28.9	-∞	-24.2

Tap No.	-95 dBm 0.2 Hz		-95 dBm 2 Hz		-95 dBm 0.5 Hz		-95 dBm 2 Hz		-115 dBm 2 Hz		-95 dBm 2 Hz	
	(S)	(R)	(S)	(R)	(S)	(R)	(S)	(R)	(S)	(R)	(S)	(R)
1	-∞	-19.8	-∞	-24	-∞	-27.6	-3	- 2.8	-3	- 2.8	-∞	-20.2
2	0	0	0	0	0	0	0	0	0	0	0	0
3	-3	- 2.1	-6	- 6.2	-6	- 5.2	-1	- 1.1	-1	- 1.1	-∞	-21.1
4	-7	- 6.8	-14	-13.8	-14	-13	-3	- 2.8	-3	- 2.7	-∞	-21.1
5	-12	-11.8	-23	-21.8	-23	-21.4	-5	- 4.9	-5	- 4.8	0	0
6	-17	-17.1	-34	-27.8	-34	-26.5	-7	- 7.0	-7	- 6.8	-9	- 8.8
7	-23	-21.1	-∞	-29.4	-∞	-28.8	-10	- 9.7	-10	- 9.2	-16	-15.9
8	-29	-24.7	-∞	-30.1	-∞	-29.4	-12	-12.5	-12	-11.9	-∞	-27.6
9	-∞	-28.2	-∞	-30.1	-∞	-29.2	-15	-14.7	-15	-14.2	-∞	-28.4
10	-∞	-28.4	-∞	-29.7	-∞	-29.8	-18	-19.6	-18	-18.9	-∞	-27.7

SECTION III

TEST AND METEOROLOGICAL DATA, AND DATA REDUCTION SOFTWARE

3.1 TROPO CHANNEL CHARACTERIZATION TEST DATA

All channel characterization test data collected on data tapes at the Verona test site have been placed on a single master tape using a set of computer routines. Data from 942 tests which were recorded on eleven tapes at the test site have been transferred onto a master tape in chronological order, the first test being November 11, 1974 and the last August 7, 1975. The master tape is formatted such that the data set for each test consists of the header data (date, time, test identification number and length of test) and the following specific test data: PDF and CDF of the received signal level, path loss, fade rate, multipath profile, mean path delay, RMS multipath delay spread, and the transmit and receive antenna sizes (usually two receivers).

Figure 3-1 is a sample print-out that shows the data from a test performed on December 20, 1974 in the master tape format. Data for channel 0 on the data tapes correspond to test data from Receiver 1 and data for channel 1 on the data tapes correspond to test data from Receiver 2. This is true except for the first 79 tests on the master tape (and corresponding tests on two of eleven original data tapes) where, for the multipath power profile and values of the mean delay and RMS multipath delay spread, the reverse is true; i.e., data for channel 0 correspond to test data from Receiver 2 and data for channel 1 correspond to test data from Receiver 1.

TAPE REC NO. 93

WB DATA DATE 12 20 74 TEST LEN= 3 ID NO.= 12065 TIME 12 40 REC#1= 15 REC#2= 8 XMIT= 8

CHANNEL NO. 0

MED= -93 P-LOSS= 230 F-RATE= 9

	LEVEL	PDF	CUM
1	-110	10	0
2	-109	3	0
3	-108	0	0
4	-107	8	1
5	-106	2	1
6	-105	5	1
7	-104	16	2
8	-103	41	4
9	-102	39	6
10	-101	59	10
11	-100	80	14
12	-99	201	25
13	-98	211	37
14	-97	178	47
15	-96	193	58
16	-95	213	69
17	-94	195	80
18	-93	145	88
19	-92	111	95
20	-91	63	98
21	-90	17	99
22	-89	10	100
23	-88	0	100
24	-87	0	100
25	-86	0	100
26	-85	0	100
27	-84	0	100
28	-83	0	100
29	-82	0	100
30	-81	0	100
31	-80	0	100
32	-79	0	100
33	-78	0	100
34	-77	0	100
35	-76	0	100
36	-75	0	100
37	-74	0	100
38	-73	0	100
39	-72	0	100
40	-71	0	100
41	-70	0	100

CHANNEL NO. 1

MED= -99 P-LOSS= 232 F-RATE= 16

	LEVEL	PDF	CUM
1	-110	310	17
2	-109	35	19
3	-108	65	22
4	-107	37	24
5	-106	68	28
6	-105	50	31
7	-104	151	39
8	-103	133	47
9	-102	175	56
10	-101	123	63
11	-100	139	71
12	-99	208	83
13	-98	154	91
14	-97	93	96
15	-96	44	99
16	-95	15	100
17	-94	0	100
18	-93	0	100
19	-92	0	100
20	-91	0	100
21	-90	0	100
22	-89	0	100
23	-88	0	100
24	-87	0	100
25	-86	0	100
26	-85	0	100
27	-84	0	100
28	-83	0	100
29	-82	0	100
30	-81	0	100
31	-80	0	100
32	-79	0	100
33	-78	0	100
34	-77	0	100
35	-76	0	100
36	-75	0	100
37	-74	0	100
38	-73	0	100
39	-72	0	100
40	-71	0	100
41	-70	0	100

LEGEND

TEST LEN(gth): Minutes

ID NO. = xxyyy: xx = Month, yyy = Test Number

TIME: Hr., Min, Local

REC # = x : x = Antenna Size Ft.

MED: Median RSL, dBm

P-LOSS: Path Loss, dB

F-Rate: Fade Rate - Med. Crossings per min.

LEVEL: dBm

PDF: No. of Samples at Level

CUM: Cumulative Distribution in percent.

Figure 3-1. Sample of Test Data

```
PROB.ERR. GAIN INT BW NO.SAMPLES       0   6   1    0   5632   5632

        TO                PO              RDBO
0.9999997E-07     0.1166773E 04     -.2500374E 02
0.1999999E-06     0.1374227E 04     -.2429301E 02
0.2999999E-06     0.2548109E 06     -.1611673E 01
0.3999999E-06     0.3693066E 06     0.0
0.4999998E-06     0.8022331E 05     -.6630795E 01
0.5999998E-06     0.5550383E 04     -.1823044E 02
0.6999998E-06     0.1154068E 04     -.2505128E 02
0.7999997E-06     0.1021341E 04     -.2558189E 02
0.8999997E-06     0.1130977E 04     -.2513905E 02
0.9999994E-06     0.1035841E 04     -.2552066E 02

MEAN PATH DELAY=0.3790282E-06     RMS MULTIPATH SPREAD=0.1493819E-06

        T1                P1              RDB1
0.9999997E-07     0.1120886E 04     -.2215457E 02
0.1999999E-06     0.5396930E 04     -.1532879E 02
0.2999999E-06     0.1676324E 06     -.4068395E 00
0.3999999E-06     0.1840952E 06     0.0
0.4999998E-06     0.1304398E 05     -.1149620E 02
0.5999998E-06     0.1611909E 04     -.2057680E 02
0.6999998E-06     0.1112295E 04     -.2218799E 02
0.7999997E-06     0.1058000E 04     -.2240532E 02
0.8999997E-06     0.1081068E 04     -.2231165E 02
0.9999994E-06     0.1054114E 04     -.2242131E 02

MEAN PATH DELAY=0.3612351E-06     RMS MULTIPATH SPREAD=0.1582226E-06

CORRECTED RMS MULTIPATH SPREAD,CH.0= 0.1349999E-06     CORRECTED RMS MULTIPATH SPREAD,CH. 1= 0.1217999E-06
```

Legend

TO: Relative Path Delay, Channel 0.

PO: Relative Power, Channel 0.

RDBO: Relative Power in dB, Channel 0.

Figure 3-1. (Concluded)

At Verona, data from each test were recorded on a tape as a file. To ease and facilitate the reading and processing of test data on MITRE's IBM 370/155 computer facility, an intermediate tape was generated which converted the data files from the original tapes to a series of records. This intermediate tape is generated by a computer program which takes a number, say N, of files (tests) from an original test data tape and creates a tape with a single file having N records. The data in a record correspond to data in a file on the test data tape. In addition, the program outputs a message whenever a "bad" (unreadable) file has been encounted, skips the "bad" file and then continues processing the next file. These "bad" files are usually the result of tape drive or computer system malfunction at the test site.

The header data plus median RSL and path loss values are read from the intermediate data tape and printed by a "Read Tape" routine. The output from this "Read Tape" routine is then manually checked against a test log kept by the operators at the test site. Corresponding header data for each test are checked and errors are noted, e.g., date, time, length of test, etc. Besides the median RSL and path loss values, the site test log also contains corrected RMS multipath spread values and the sizes of the transmit and receive antennas for each test. The corrected RMS multipath spread values and the antenna sizes are not part of the data on the intermediate data tape since they are not part of the data on the original test data tapes from Verona. The operator corrected the RMS multipath delay spread values at the test site by viewing the output of the multipath delay profile at the completion of a particular test, determining the power value at a particular tap to be the noise floor, and recalculating the RMS multipath delay spread on a Hewlitt-Packard programmable desk calculator. The uncorrected RMS multipath delay, i.e., RMS delay calculated by the test

program software, includes power values from all taps even if many of these tap values are only noise. Because of the maintenance of the test log during the test program, all data on a "bad" file are not lost; the information on the test log for those files which could not be read are placed on the master tape.

The corrections to the header data and the additional data (corrected RMS multipath delay spread values and antenna sizes) are added to the corresponding set of data for each test on the intermediate tape and a computer routine transfers this new set of data to the master tape. The entire procedure was performed on each of the eleven test data tapes to generate a master tape.

From this master tape, a second "normalized" master tape was created. Since transmit powers ranged from 300 W to 1 KW during the testing period, median RSL values and path loss values were "normalized" (for the TRC-97 paths) to reflect transmit power as being 1 KW. This "normalized" master tape is the tape used to obtain results presented in the next section. Thus, the test data gathered at Verona over the duration of the test program, November 1974 through August 1975, are available on three different sets of magnetic tapes:

- Eleven original data tapes (uncorrected),
- A master tape, and
- A "normalized" master data tape.

3.2 DATA REDUCTION SOFTWARE

The basic software to process the data on the master tape consists of six different routines integrated into a single computer program package.

Various data reduction and output options are selected by user inputs to the program. (In addition to the basic software, a number of shorter programs were written for processing test data with meteorological data as described in the next section).

The six basic routines are:

a) A routine that reads the master tape and collates data according to user designation of type of data, antenna sizes and time. The time designation can be with respect to months (1 - 12), hours of the day (interval of the day prescribed by minimum and maximum values, 0 - 23), or by tape record numbers (since data from each test were written on the master tape as a record in chronological order). The tape read routine compensates for the transition from EST to EDT made on February 24, 1975; all times used were EST.

b) A routine which correlates two sets of data.

c) A graph routine that calls appropriate CALCOMP plotter routines to generate a tape for the plotter; scatter or probability plots.

d) A routine that generates data arrays of RMS multipath delay and path loss data for input to the correlation routine or the graph routine (scatter plot).

e) A routine to generate a data array of RMS multipath delay spread values for input to the graph routine (probability plot).

f) A routine to generate a data array of median RSL values for input to the graph routine (probability plot).

Basically, Routines (d), (e), and (f) accomplish similar functions. The data collated by the tape read routine are checked to determine whether they fall within an interval determined by prescribed minimum and maximum values of RMS multipath delay spread, path loss or median RSL. That data falling within the prescribed interval are stored in data arrays compatible with the CALCOMP plotter routines. The axis lengths of the plots can be from 10 to 20 inches. For the probability plots, the probability and cumulative distributions of the data are computed. The probability axis scale on the plot is determined from a table of cumulative normal distribution values for increments of 1/10 sigma (over a range of ± 3 sigma).

3.3 METEOROLOGICAL DATA

The USAF Environmental Technical Applications Center (USAFETAC) supplied three different types of meteorological data to the program: surface data from Rochester, Buffalo, Utica and Syracuse; wind shear data from Albany and Buffalo; and upper air data (rawinsonde data) from Albany and Buffalo. A tape containing data for each type and for each of the following time intervals was received: October - December 1974, January - February 1975, March, April, May, June, July, August and September 1975, for a total of 27 tapes.

The surface data (hourly) from Buffalo, Utica, Syracuse and Rochester consist of the station number, date, hour (Zulu time), sea level pressure, temperature, dewpoint and surface refractive modulus. An example of surface data from Syracuse for June 1, 2 and part of June 3, 1975 is shown in Figure 3-2.

The wind shear data (twice daily, 0 and 12 Z) from Buffalo and Albany consist of time, date, number of levels, station number, pressure level,

1 LISTING OF SELECTED SURFACE OBSERVATION ELEMENTS
FOR INDICATED STATIONS AND TIMES

BLKSTN NUM	YR	MO	DAY	HR	SEA LVL PRESS MB	TEMP DEG C	DEWPT DEG C	REMCD N UNITS
72519C	1975	6	1	07	1007.5	20	17	250.8
72519C	1975	6	1	12	1006.8	20	16	256.1
72519C	1975	6	1	27	1007.1	19	18	257.7
72519C	1975	6	1	32	1006.9	19	18	257.6
72519C	1975	6	1	47	1006.6	19	18	257.5
72519C	1975	6	1	52	1005.8	19	17	251.8
72519C	1975	6	1	67	1005.2	19	17	251.7
72519C	1975	6	1	72	1004.5	18	17	252.0
72519C	1975	6	1	87	1003.5	19	17	251.2
72519C	1975	6	1	92	1003.0	19	17	251.1
72519C	1975	6	1	102	1003.6	19	18	256.8
72519C	1975	6	1	112	1004.9	18	17	253.1
72519C	1975	6	1	127	1006.2	17	16	246.6
72519C	1975	6	1	132	1007.0	17	16	246.9
72519C	1975	6	1	147	1007.9	17	15	245.1
72519C	1975	6	1	167	1009.1	17	14	240.7
72519C	1975	6	1	177	1009.1	19	14	237.9
72519C	1975	6	1	182	1009.7	19	14	238.0
72519C	1975	6	1	197	1010.0	19	14	238.1
72519C	1975	6	1	202	1010.4	19	14	238.2
72519C	1975	6	1	217	1010.4	21	14	235.4
72519C	1975	6	1	227	1010.7	21	13	231.2
72519C	1975	6	1	237	1010.9	20	11	224.6
72519C	1975	6	2	07	1011.2	18	11	227.3
72519C	1975	6	2	17	1011.9	17	11	228.8
72519C	1975	6	2	22	1012.5	17	12	232.9
72519C	1975	6	2	37	1013.0	17	12	237.3
72519C	1975	6	2	42	1013.3	16	12	238.7
72519C	1975	6	2	57	1013.8	14	12	237.4
72519C	1975	6	2	62	1014.0	15	13	240.3
72519C	1975	6	2	77	1014.7	15	13	240.5
72519C	1975	6	2	87	1015.9	13	9	227.8
72519C	1975	6	2	92	1015.9	11	9	230.5
72519C	1975	6	2	107	1016.5	11	8	227.1
72519C	1975	6	2	112	1017.4	12	9	228.2
72519C	1975	6	2	127	1018.1	15	9	225.7
72519C	1975	6	2	132	1018.4	16	9	224.5
72519C	1975	6	2	147	1018.3	17	11	230.5
72519C	1975	6	2	157	1018.6	18	11	229.2
72519C	1975	6	2	167	1018.8	19	11	228.0
72519C	1975	6	2	177	1018.5	21	11	225.3
72519C	1975	6	2	182	1018.3	21	8	214.9
72519C	1975	6	2	197	1018.0	22	6	207.7
72519C	1975	6	2	202	1017.3	22	6	207.5
72519C	1975	6	2	212	1017.0	22	6	207.4
72519C	1975	6	2	227	1017.0	21	6	208.6
72519C	1975	6	2	237	1017.0	21	6	208.6
72519C	1975	6	3	07	1016.5	18	6	212.1
72519C	1975	6	3	17	1016.4	16	7	217.4

Figure 3-2. Meteorological Data: Surface

height, wind direction, wind speed, wind direction change and speed shear. An example of wind shear data from Buffalo for July 1, 1975 is shown in Figure 3-3. Values of meteorological data that are shown as all 9's, e.g., 999.9, denote missing data.

The upper air (rawinsonde) data (twice daily, 0 and 12Z) from Buffalo and Albany consist of the station number, date, time, number of levels, atmospheric pressure, height, wind direction, density, temperature, dewpoint, relative humidity, refractive modulus in "N" units, refractive index gradient, modified refractive modulus in "M" units, equivalent potential temperature, and stability (gradient of equivalent potential temperature). An example of rawinsonde data from Buffalo for January 1, 1975 is shown in Figure 3-4.

Computer routines to read each of the three types of meteorological data tapes have been written so that the data tapes could be used with MITRE's IBM 370/155 computer. A computer program has been written integrating the three different tape read routines and having routines to collate various meteorological data, compute statistical parameters, and compute the effective earth radius from radiosonde data.

WINDS FOR 07 DAY 1 MONTH 7 YEAR 1975 19 LEVELS FOR STATION 725280

PRESSURE LEVEL (MB)	HEIGHT (METERS)	WIND DIR	WIND SPEED KNOTS	WIND DIR CHANGE	SPEED SHEAR KTS/100M
999999.	218.	41.	9.	**	99.99
999999.	610.	45.	13.	+	1.04
999999.	914.	50.	11.	+	0.79
999999.	1219.	29.	7.	-	1.27
850.	1605.	325.	7.	-	0.00
999999.	2134.	5.	6.	+	0.22
999999.	2438.	25.	6.	+	0.00
999999.	2743.	30.	8.	+	0.70
700.	3223.	55.	11.	+	0.61
999999.	3962.	30.	16.	-	0.68
999999.	4267.	35.	17.	NC	0.32
999999.	4877.	45.	13.	+	0.64
500.	5900.	35.	16.	-	1.28
999999.	7010.	360.	24.	-	0.72
400.	7600.	360.	23.	NC	0.15
999999.	9144.	5.	23.	+	0.00
300.	9670.	360.	27.	-	0.78
250.	10910.	345.	32.	-	0.39
200.	12360.	345.	34.	NC	0.15

Figure 3-3. Meteorological Data: Wind Shear

STATION 725280 BUFFALO, NEW YORK YEAR 1975 MONTH 1 DAY 1 TIME 02 NO. OF LEVELS IN REPORT 18

PRES LVL (MB)	HEIGHT (METERS)	WIND (DEG	KTS)	DENSITY (GM/M3)	TEMP (C)	DEWPT (C)	REL HUM (PERCENT)	REF MOD (N UNITS)	REF GRAD (DN/100M)	M UNITS	THETAE (K)	STABILITY (DEG/100M)
992.0	224	90	6	1265.658	-0.7	-1.4	94	310.2	999.9	345.3	281.8	99.9
916.0	859	999	999	1179.191	-3.1	-3.1	99	288.0	-3.5	422.7	285.4	0.6
875.0	1222	999	999	1121.102	-1.9	-1.9	99	277.2	-3.0	468.9	291.7	1.7
850.0	1443	230	16	1093.211	-2.9	-2.9	99	269.2	-3.6	495.5	292.4	0.4
780.0	2125	999	999	1001.429	-2.5	-2.5	99	249.5	-2.9	582.7	301.5	1.3
700.0	2981	255	27	909.040	-5.5	-5.5	99	224.0	-3.0	691.4	309.4	0.6
627.0	3842	999	999	823.029	-8.3	-8.3	99	201.1	-2.7	803.4	311.9	0.6
500.0	5570	260	80	679.395	-17.1	-17.1	99	160.6	-2.3	1033.9	318.1	0.4
424.0	6785	999	999	597.961	-26.3	-26.9	94	137.4	-1.9	1201.2	316.5	0.0
400.0	7210	260	105	572.606	-29.9	-33.2	72	129.9	-1.8	1260.3	317.8	-0.2
368.0	7798	999	999	537.946	-34.9	-40.9	53	120.9	-1.5	1343.5	317.9	0.0
349.0	8166	999	999	516.287	-37.7	-48.7	30	115.5	-1.5	1395.7	318.4	0.1
300.0	9190	270	130	454.251	-43.1	999.9	999	101.7	-1.3	1542.5	324.9	0.6
250.0	10400	270	140	389.547	-49.6	999.9	999	87.3	-1.2	1717.8	332.8	0.6
200.0	11850	999	999	312.617	-50.3	999.9	999	70.1	-1.2	1928.0	353.7	1.4
150.0	13730	999	999	238.529	-54.1	999.9	999	53.6	-0.9	2206.2	377.8	1.3
100.0	16260	999	999	165.517	-62.7	999.9	999	37.4	-0.6	2586.6	408.3	1.2
70.0	18470	999	999	115.205	-61.5	999.9	999	26.2	-0.5	2921.9	455.7	2.1

Figure 3-4. Meteorological Data: Upper Air

SECTION IV

TEST RESULTS

Literature is available on the results of both theoretical and empirical analyses of troposcatter radio link tests. These results are usually presented as comparisons of collected radio data, probability graphs of radio or meteorological data, comparisons of meteorological data with radio data, or meteorological data or radio data grouped with respect to time. Results of the reduction of test radio data from Verona and the available meteorological data from locations around the test site are presented here in a similar manner; results are in most cases shown as graphs or tables, and the number of data samples used to generate them is stated. Also, because grouping or omission of data can lead to biased results, a description is included of how data is grouped or averaged to obtain hourly, daily or monthly statistical parameters.

As stated in Section 2.2, radio data were obtained over two different path distances, a short path of 86 statute miles and a long path of 168 statute miles. Notations and symbols used in the various tables and graphs denoting different test configurations are given in Table 4-1. The blanks in the table denote that the particular combination of transmit and receive antenna sizes were not used or the number of data samples gathered for that particular combination were not sufficient enough to be reported.

Table 4-1

Test Configurations

Test Configuration Number	Transmit Antenna Size (ft)	Receiver 1 Antenna Size (ft)	Receiver 2 Antenna Size (ft)	Path Length (St. mi)
I	8	8	8	Short (86)
II	8	-	15	Short
III	15	8	-	Short
IV	15	-	15	Short
V	28	28	28	Long (168)

Time block designations used are those given in the National Bureau of Standards Technical Note 101 (See Reference 14, p. III -45) in which eight time blocks are denoted as TB1, TB2...., TB8. These and additional notations TXX, TB0, and TB9, which define "all data", all "winter" data, and all "summer" data for the period of the RADC tests, are designated in Table 4-2. The test radio data were gathered at Verona from November 1974 to August 1975; TXX denotes the set of all test data for a particular test configuration in Table 4.1 during this testing interval. Similarly, TB0 denotes the set of all test data for the "winter" months, which are November 1974 through April 1975, while TB9 denotes the set of all test data for the "summer" months, May 1975 to August 1975. Of primary interest for these tests are "time of day" designations TB1, TB2, TB4, and TB5, which represent the intervals for which sufficient data were collected.

Table 4-2

Time Block Notations

Notation	Time Interval	Time of Day Interval (EST)
TXX	Nov. 1974-Aug. 1975 (Winter & Summer - all data)	0000 - 2400
TB0	Nov. 1974-Apr. 1975 (Winter - all data)	0000 - 2400
TB1	Nov. - Apr. (Winter morning)	0600 - 1300
TB2	Nov. - Apr. (Winter afternoon)	1300 - 1800
TB3	Nov. - Apr. (Winter evening)	1800 - 2400
TB4	May - Oct. (Summer morning)	0600 - 1300
TB5	May - Oct. (Summer afternoon)	1300 - 1800
TB6	May - Oct. (Summer evening)	1800 - 2400
TB7	May - Oct. (Summer night)	0000 - 0600
TB8	Nov. - Apr. (Winter night)	0000 - 0600
TB9	May 1975 - Aug. 1975 (Summer - all data)	0000 - 2400

4.1 SCATTER PLOTS: PATH LOSS VERSUS RMS MULTIPATH DELAY SPREAD

In this subsection, scatter plots of path loss versus root-mean-square (RMS) multipath delay spread (two sigma) for the various test configurations and time blocks in Tables 4-1 and Table 4-2, respectively, are shown. Nineteen scatter plots are presented in Figures 4-1 through 4-11 at the end of this section. For easier access to a particular plot, the figure numbers that correspond to the various test configurations and time blocks are given in Table 4-3.

Correlation values of the path loss and RMS multipath delay spread test data used to generate the scatter plots are given in Table 4-4. It should be noted that all test data available for test Configuration I (TXX, TB9, TB4, and TB5) were not used to generate the corresponding scatter plots or to compute the correlation values. From May 1975 until the end of testing in August 1975, when modem tests were being conducted, up to four or five test results within an hour were being obtained for test Configuration I, whereas in the early months of testing the time intervals between tests during the day were generally about an hour. Thus, for test Configuration I, test results from May - August 1975 were arbitrarily selected about an hour apart where necessary.

Table 4-3

Scatter Plots

Figure Number	Test Configuration	Time Block Notation	Receiver Number
4-1a	I	TXX	1
4-1b	I	TXX	2
4-2a	I	TB0	1
4-2b	I	TB0	2
4-3a	I	TB9	1
4-3b	I	TB9	2
4-4a	I	TB1	1
4-4b	I	TB1	2
4-5a	I	TB2	1
4-5b	I	TB2	2
4-6a	I	TB4	1
4-6b	I	TB4	2
4-7a	I	TB5	1
4-7b	I	TB5	2
4-8a	V	TXX	1
4-8b	V	TXX	2
4-9	II	TXX	2
4-10	III	TXX	1
4-11	IV	TXX	2

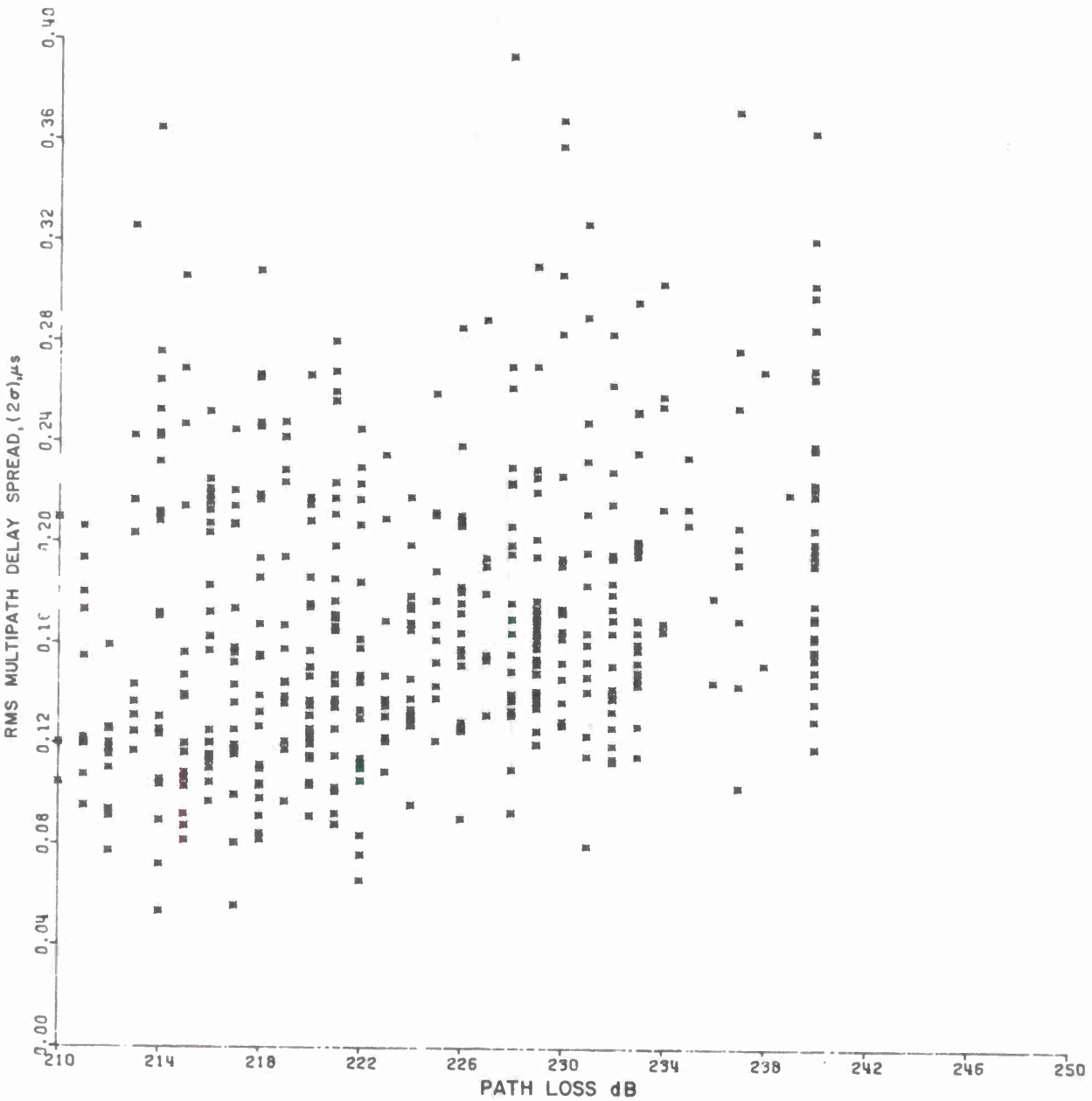

Figure 4-1(a). RMS Delay Spread VS Path Loss — XMIT 8 Ft., RCVR 8 Ft., All Data (RCVR 1)

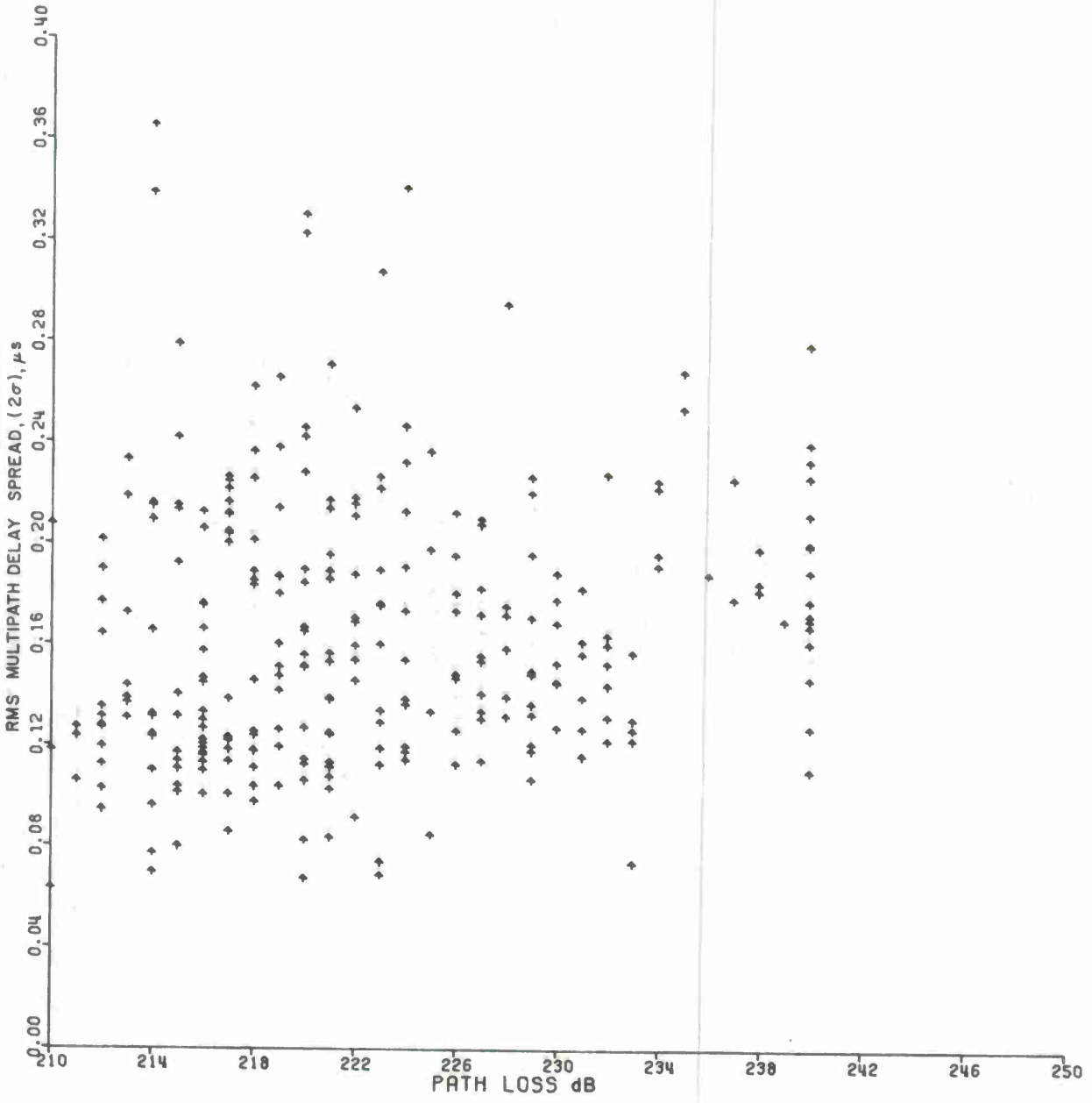

Figure 4-1(b). RMS Delay Spread VS Path Loss – XMIT 8 Ft., RCVR 8 Ft., All Data (RCVR 2)

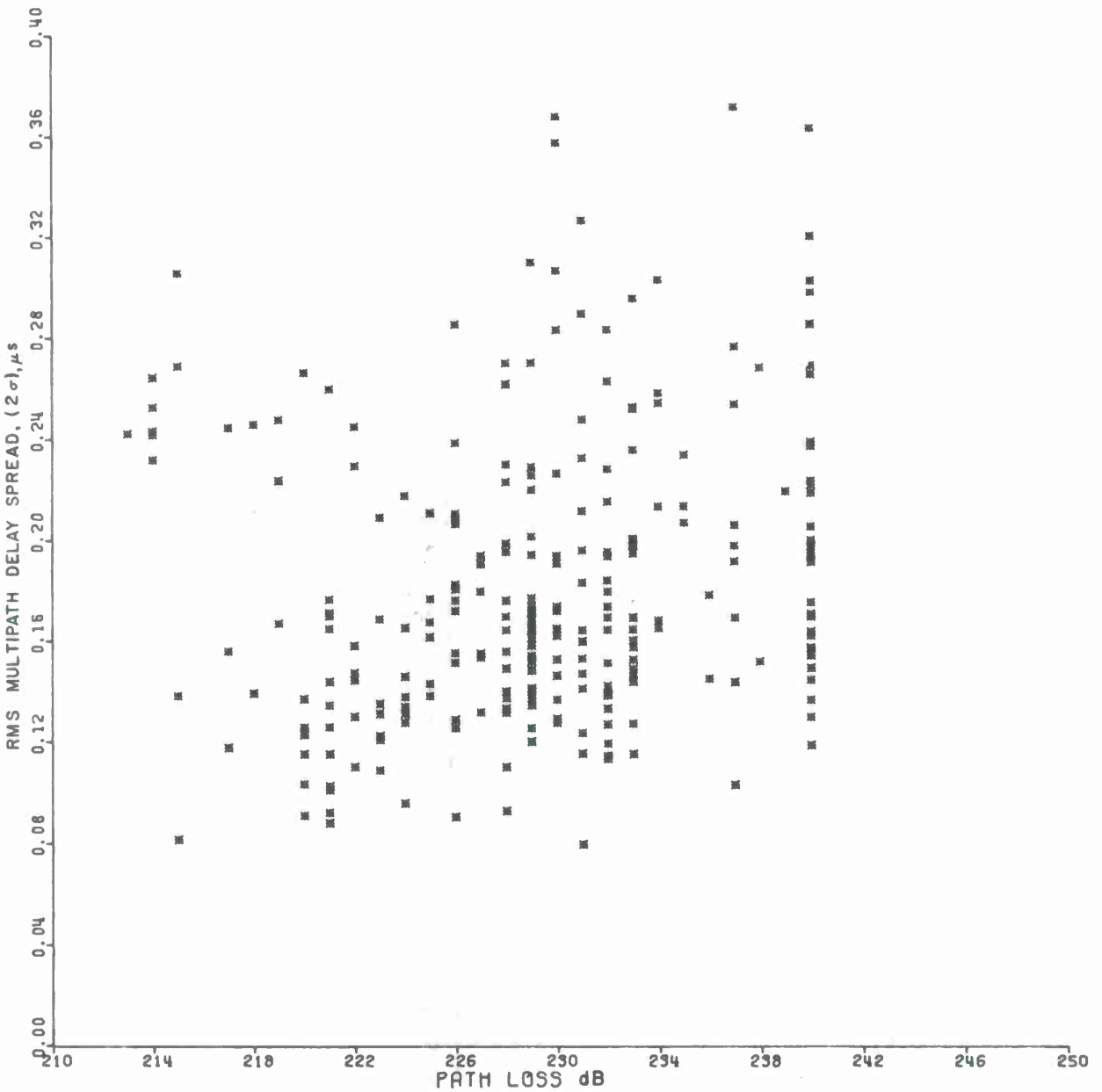

Figure 4-2(a). RMS Delay Spread VS Path Loss — XMIT 8 Ft., RCVR 8 Ft., Winter Data (RCVR 1)

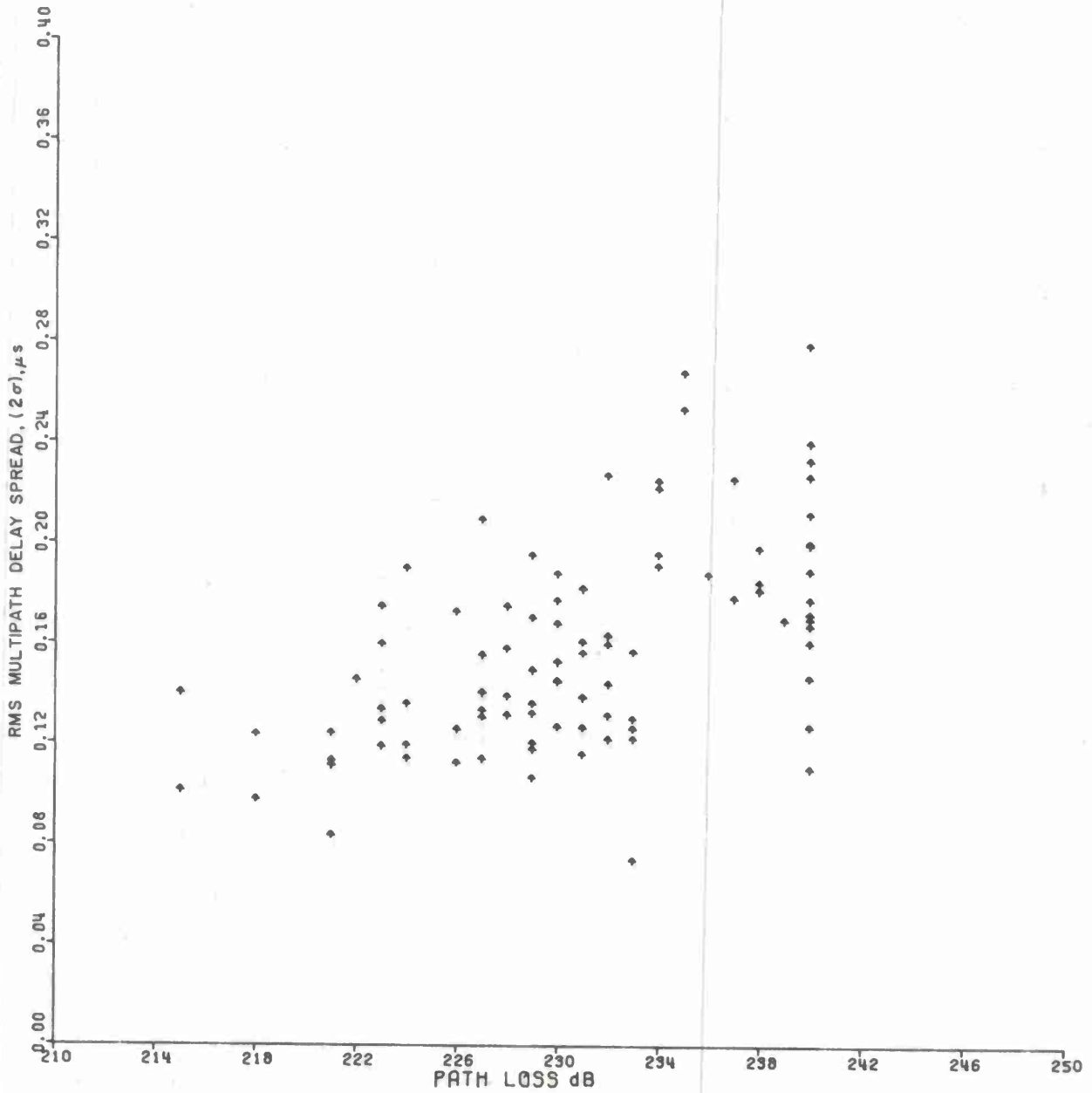

Figure 4-2(b). RMS Delay Spread VS Path Loss — XMIT 8 Ft., RCVR 8 Ft., Winter Data (RCVR 2)

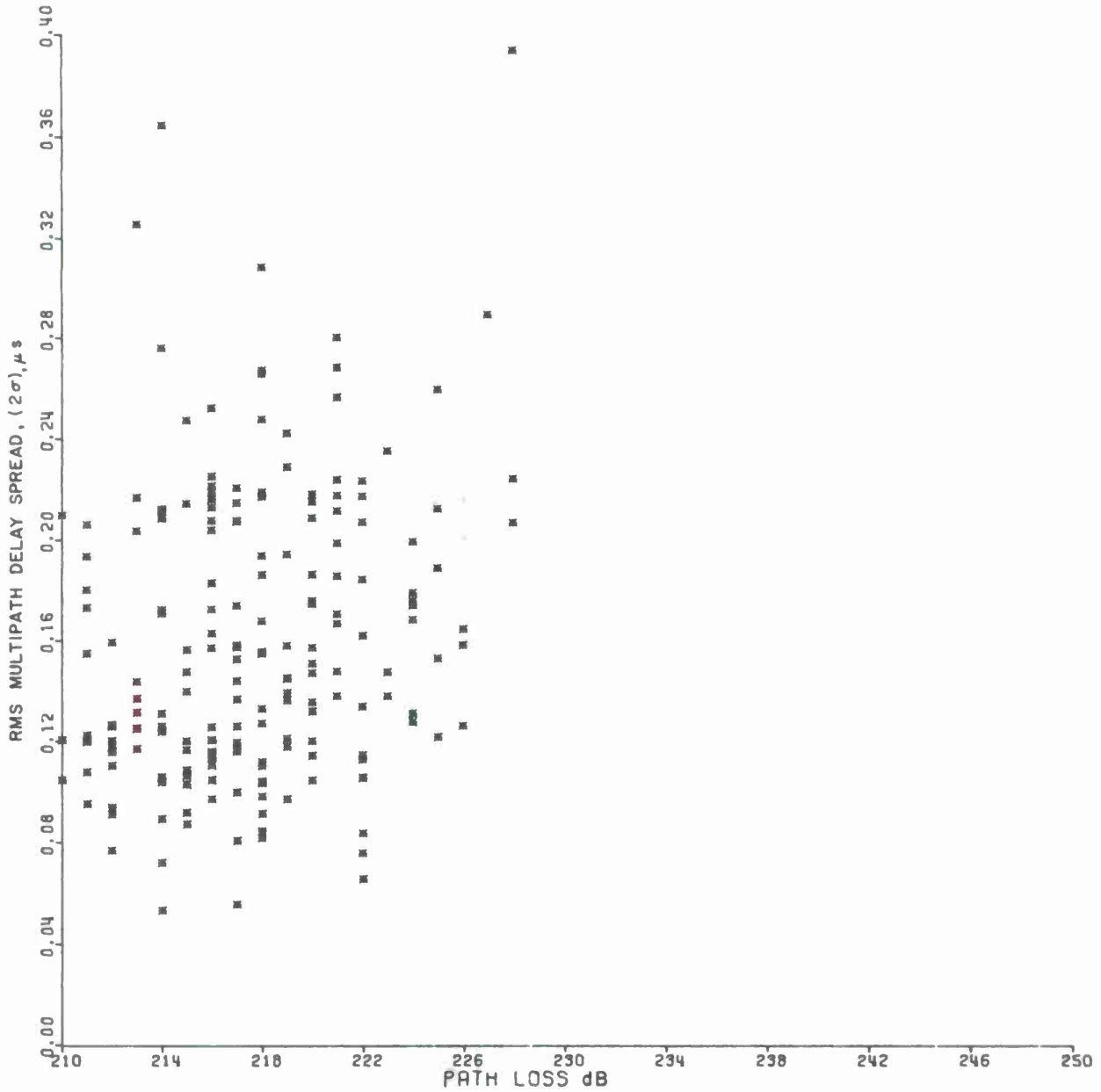

Figure 4-3(a). RMS Delay Spread VS Path Loss — XMIT 8 Ft., RCVR 8 Ft., Summer Data (RCVR 1)

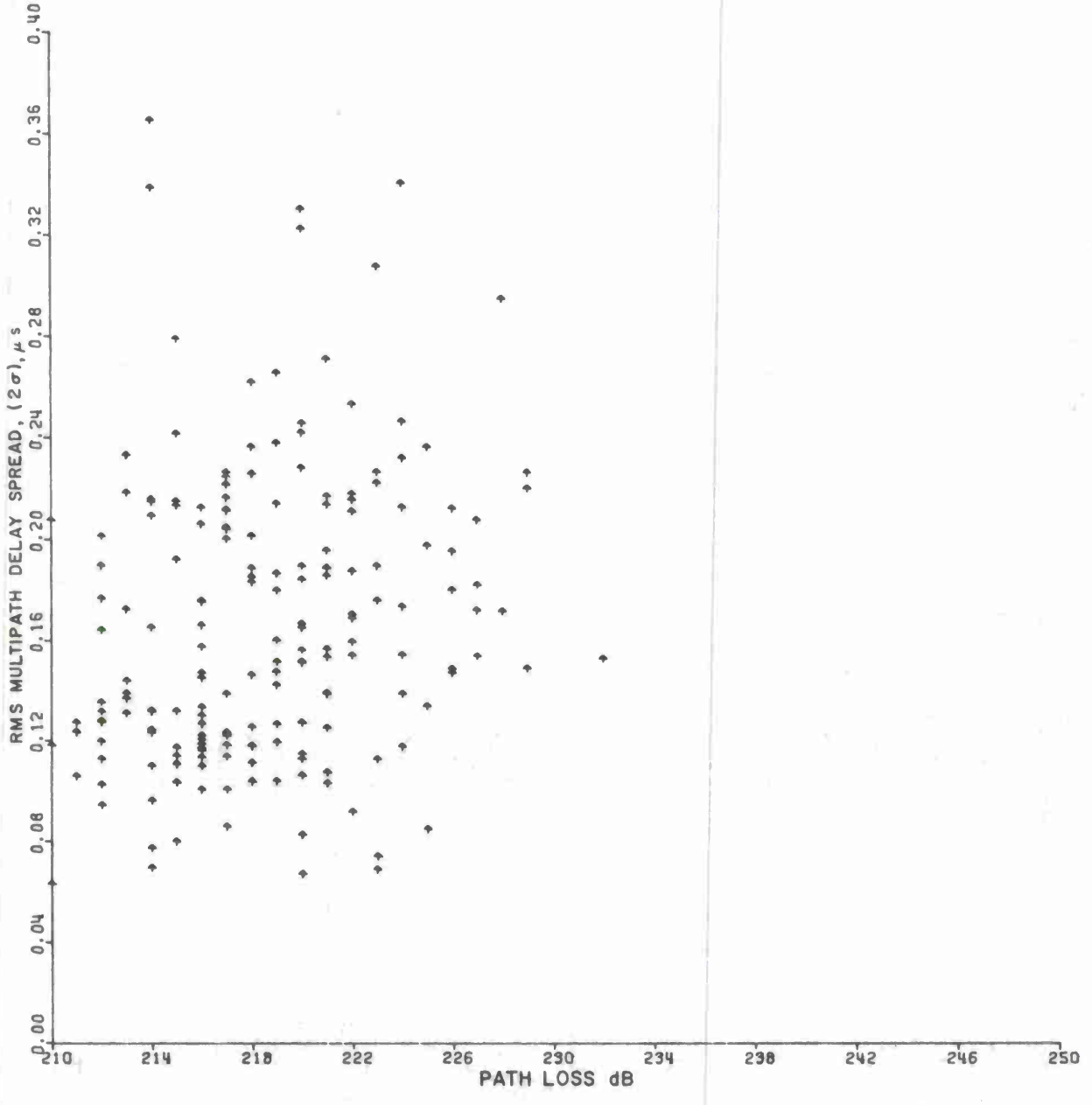

Figure 4-3(b). RMS Delay Spread VS Path Loss — XMIT 8 Ft., RCVR 8 Ft., Summer Data (RCVR 2)

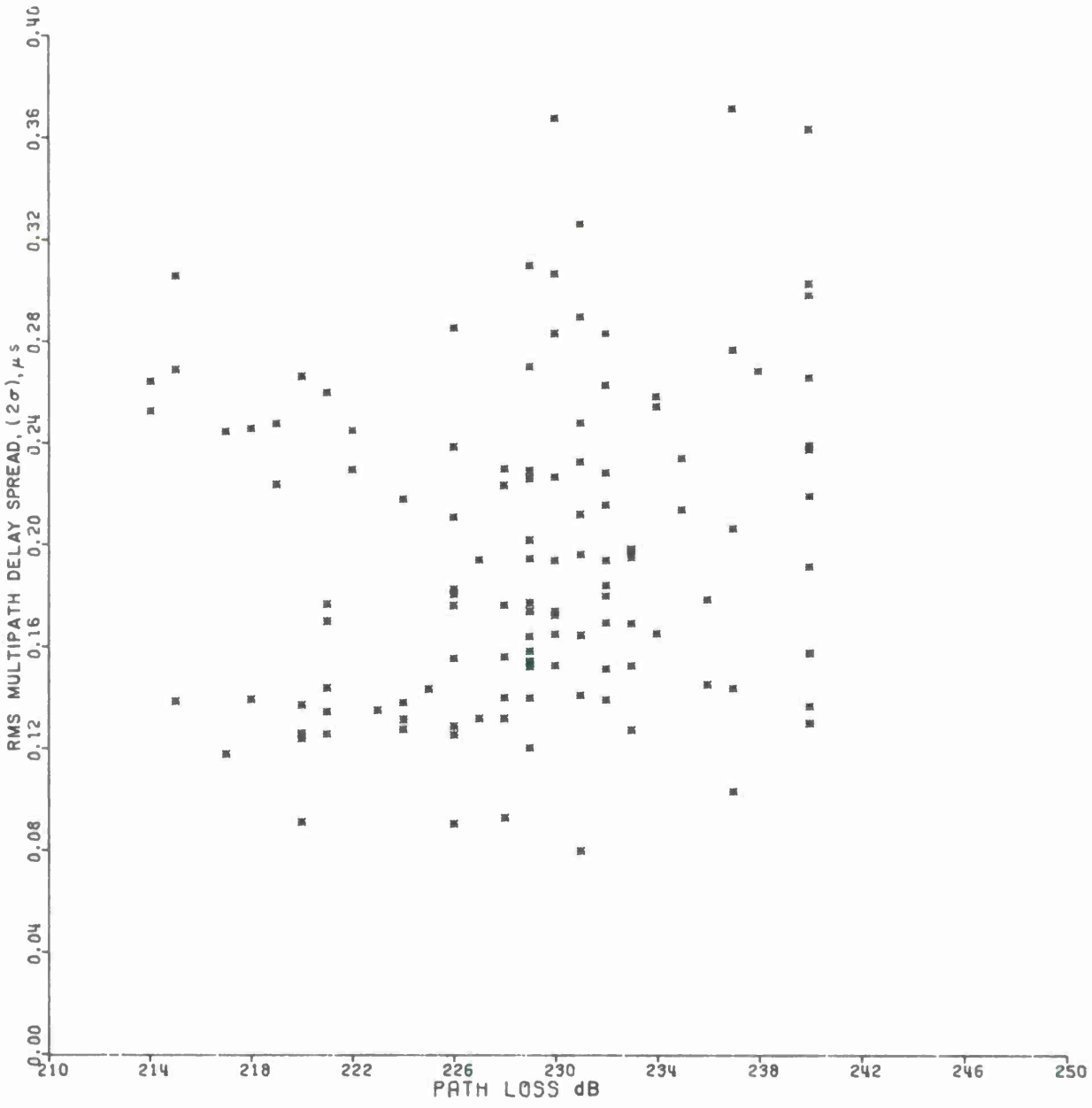

Figure 4-4(a). RMS Delay Spread VS Path Loss — XMIT 8 Ft., RCVR 8 Ft., Winter Morning Data (RCVR 1)

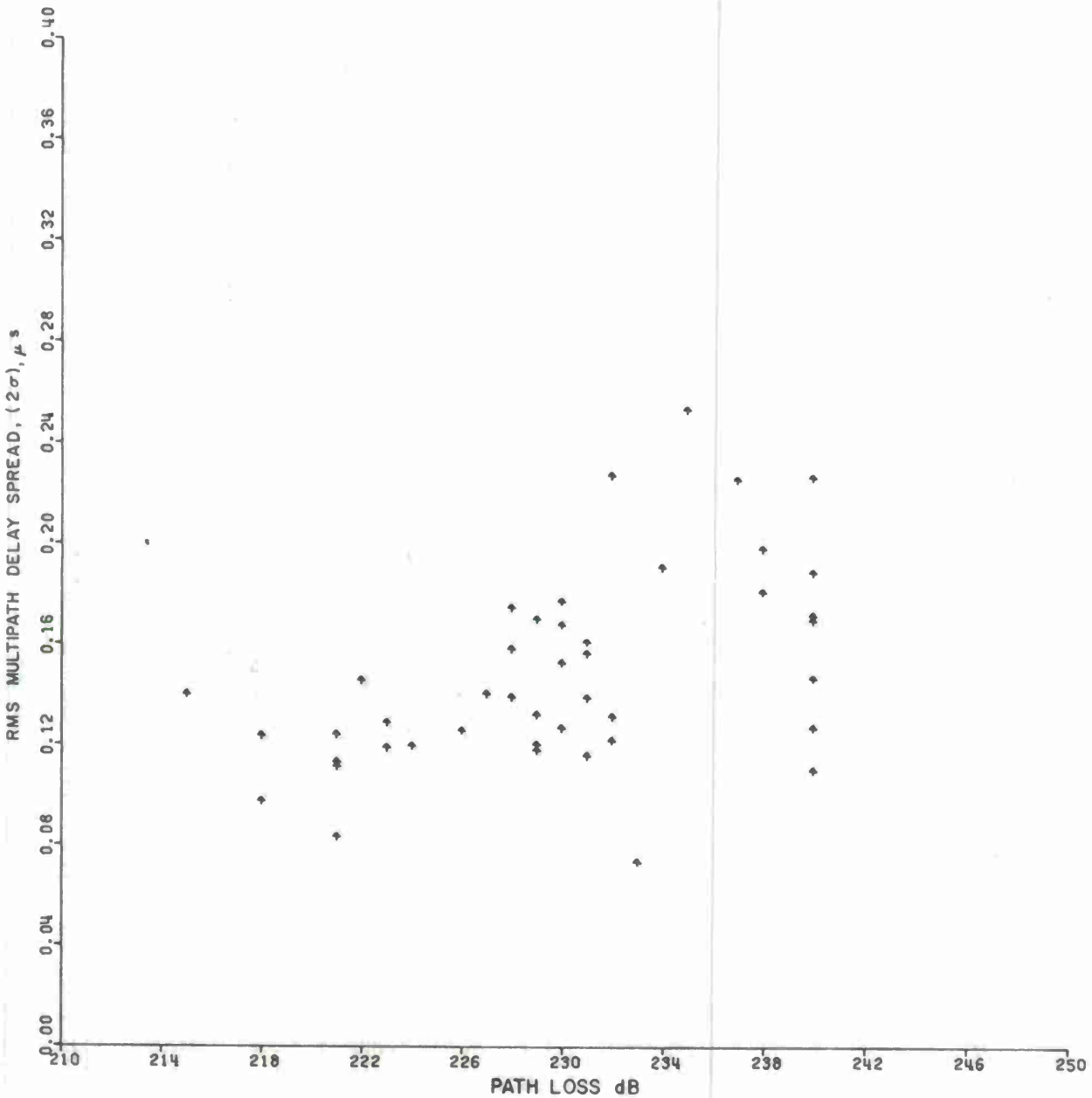

Figure 4-4(b). RMS Delay Spread VS Path Loss — XMIT 8 Ft., RCVR 8 Ft., Winter Morning Data (RCVR 2)

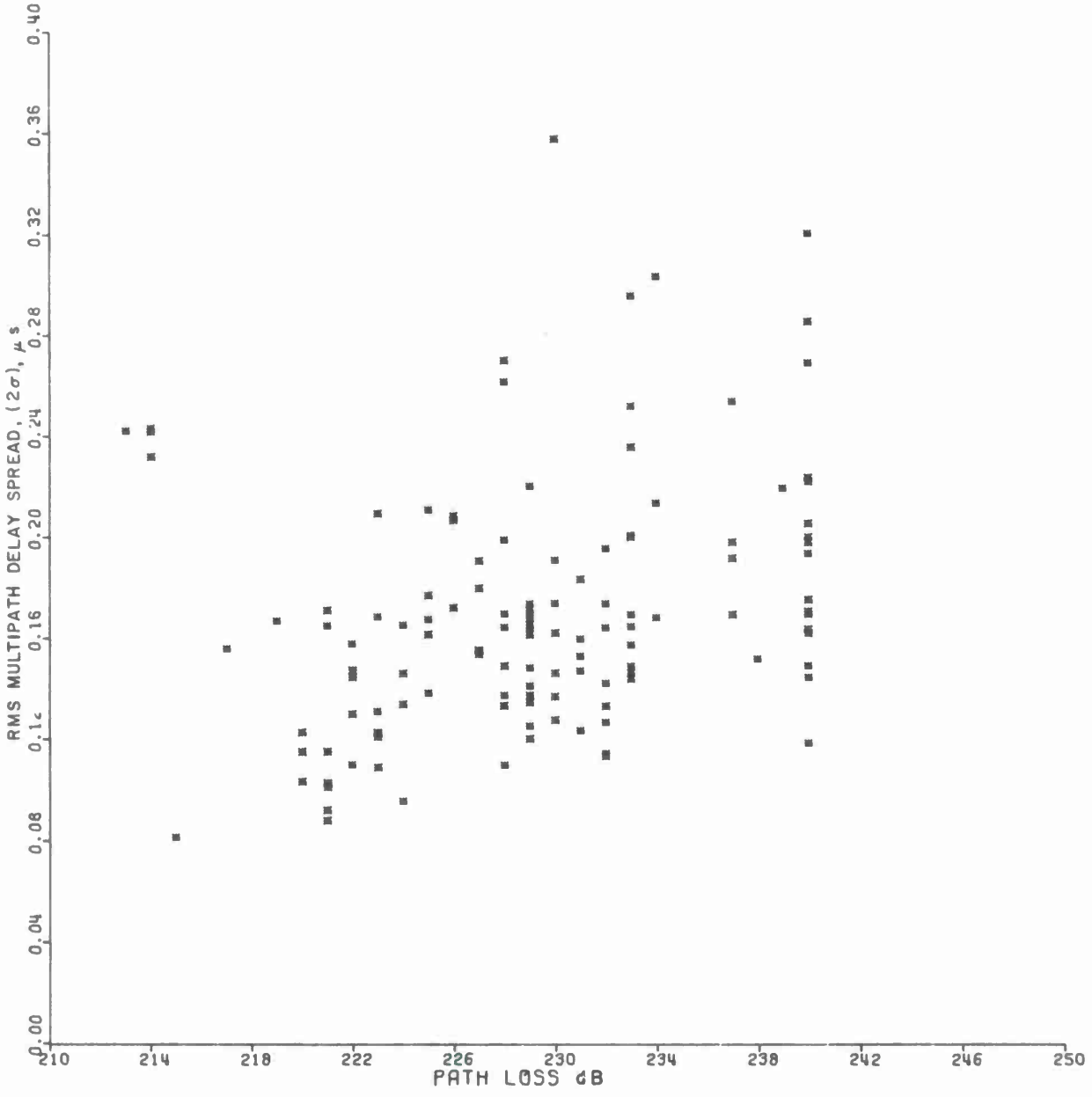

Figure 4-5(a). RMS Delay Spread VS Path Loss — XMIT 8 Ft., RCVR 8 Ft., Winter Afternoon Data (RCVR 1)

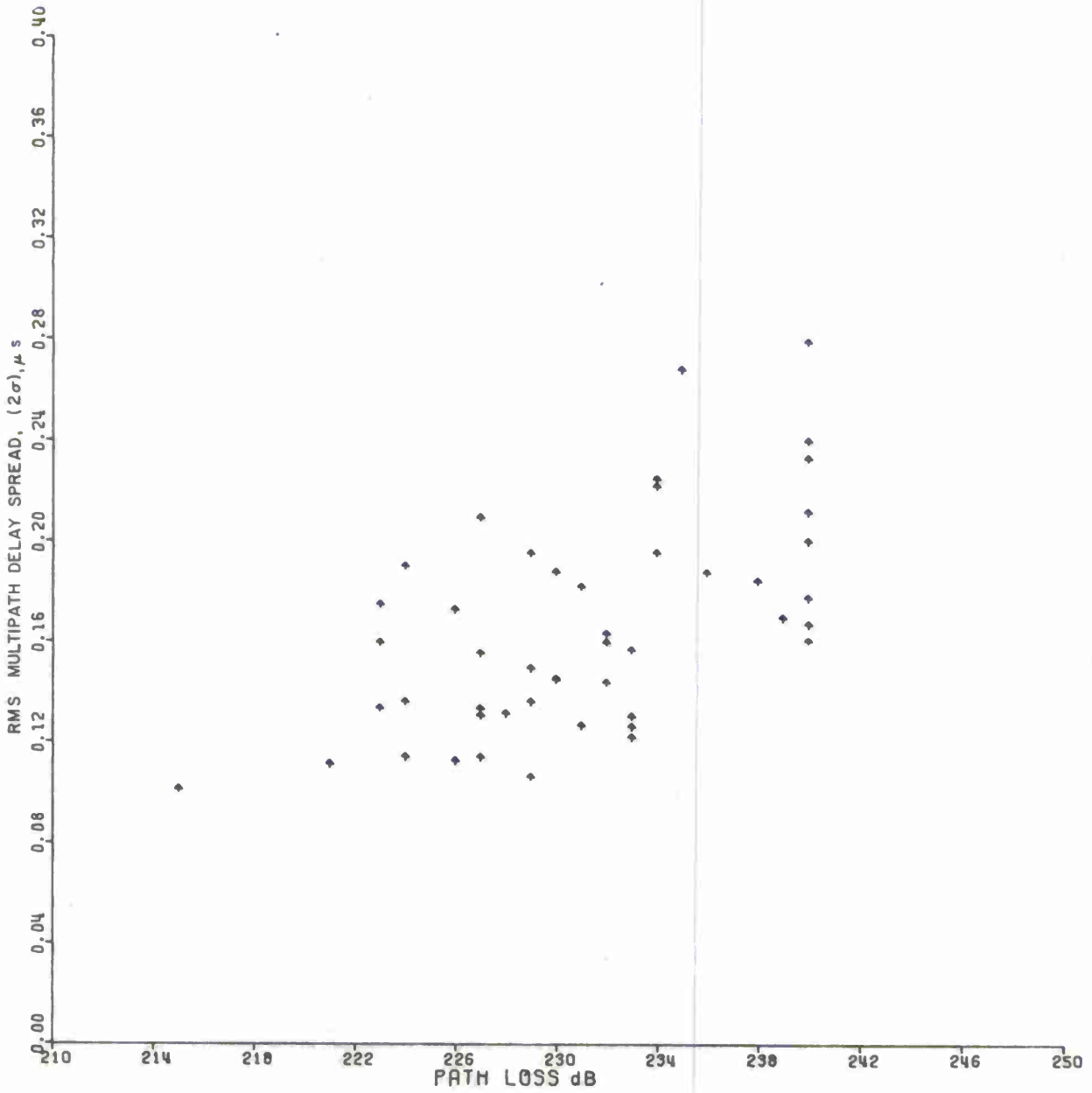

Figure 4-5(b). RMS Delay Spread VS Path Loss — XMIT 8 Ft., RCVR 8 Ft., Winter Afternoon Data (RCVR 2)

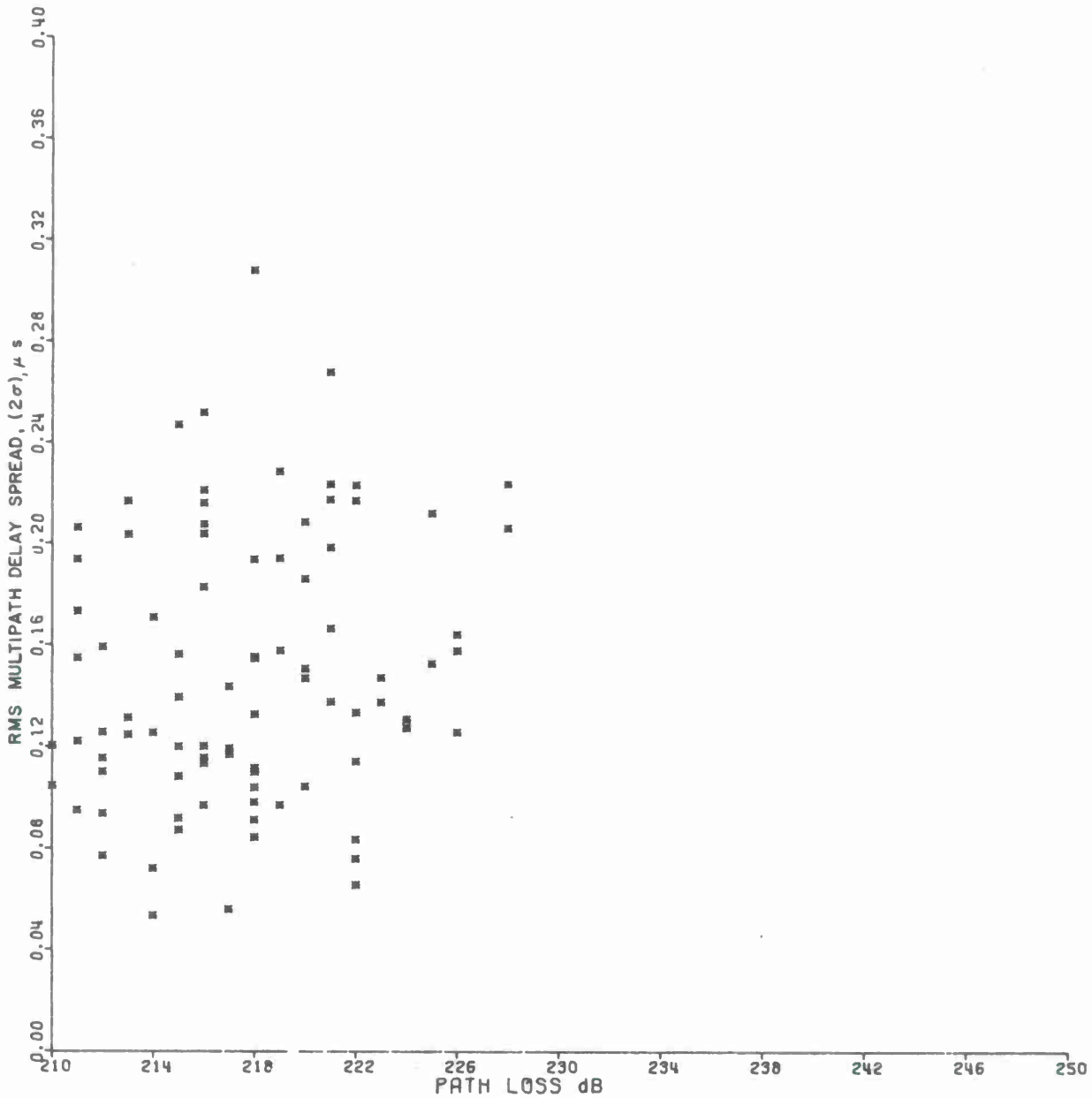

Figure 4-6(a). RMS Delay Spread VS Path Loss — XMIT 8 Ft., RCVR 8 Ft., Summer Morning Data (RCVR 1)

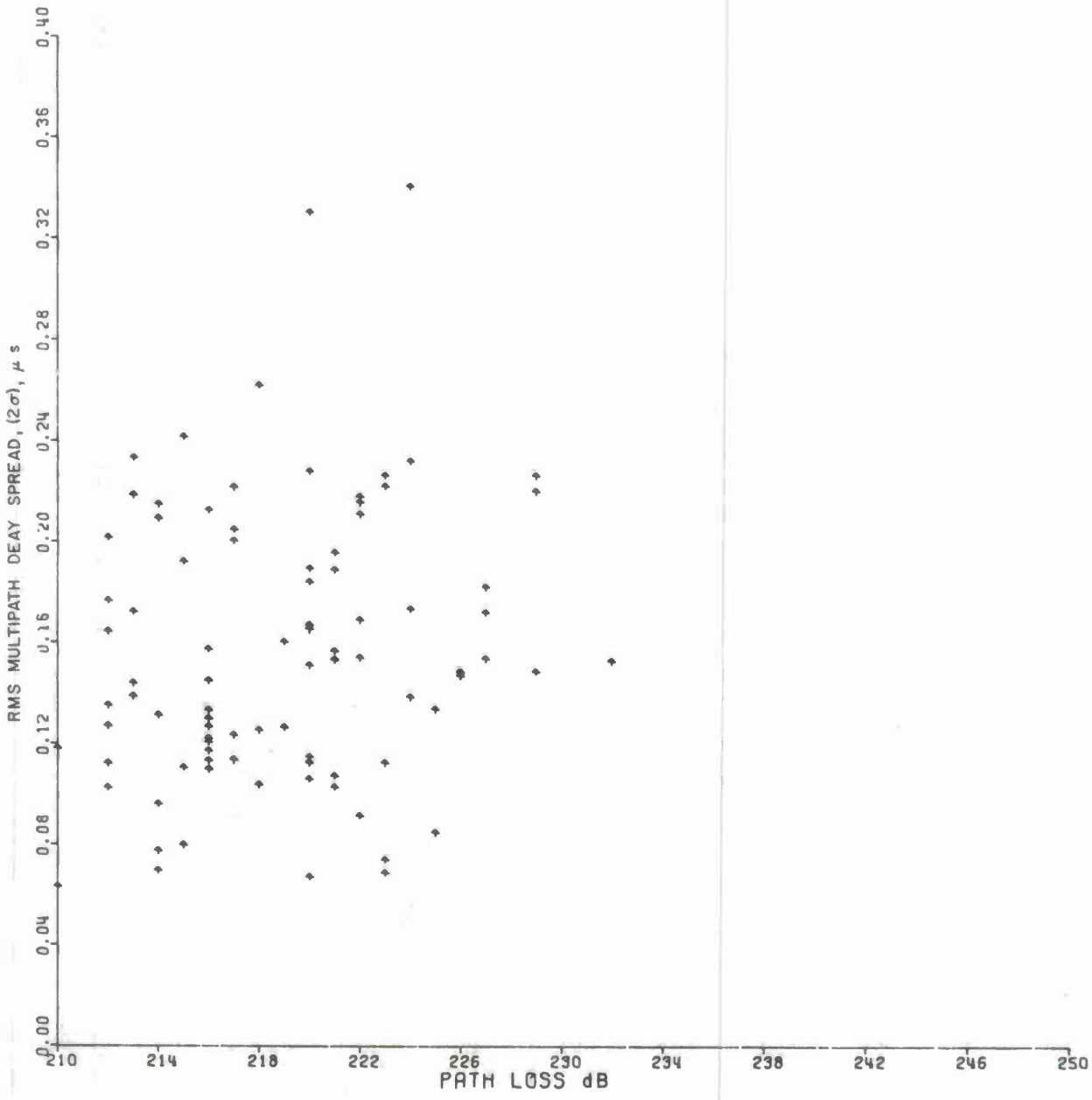

Figure 4-6(b). RMS Delay Spread VS Path Loss — XMIT 8 Ft., RCVR 8 Ft., Summer Morning Data (RCVR 2)

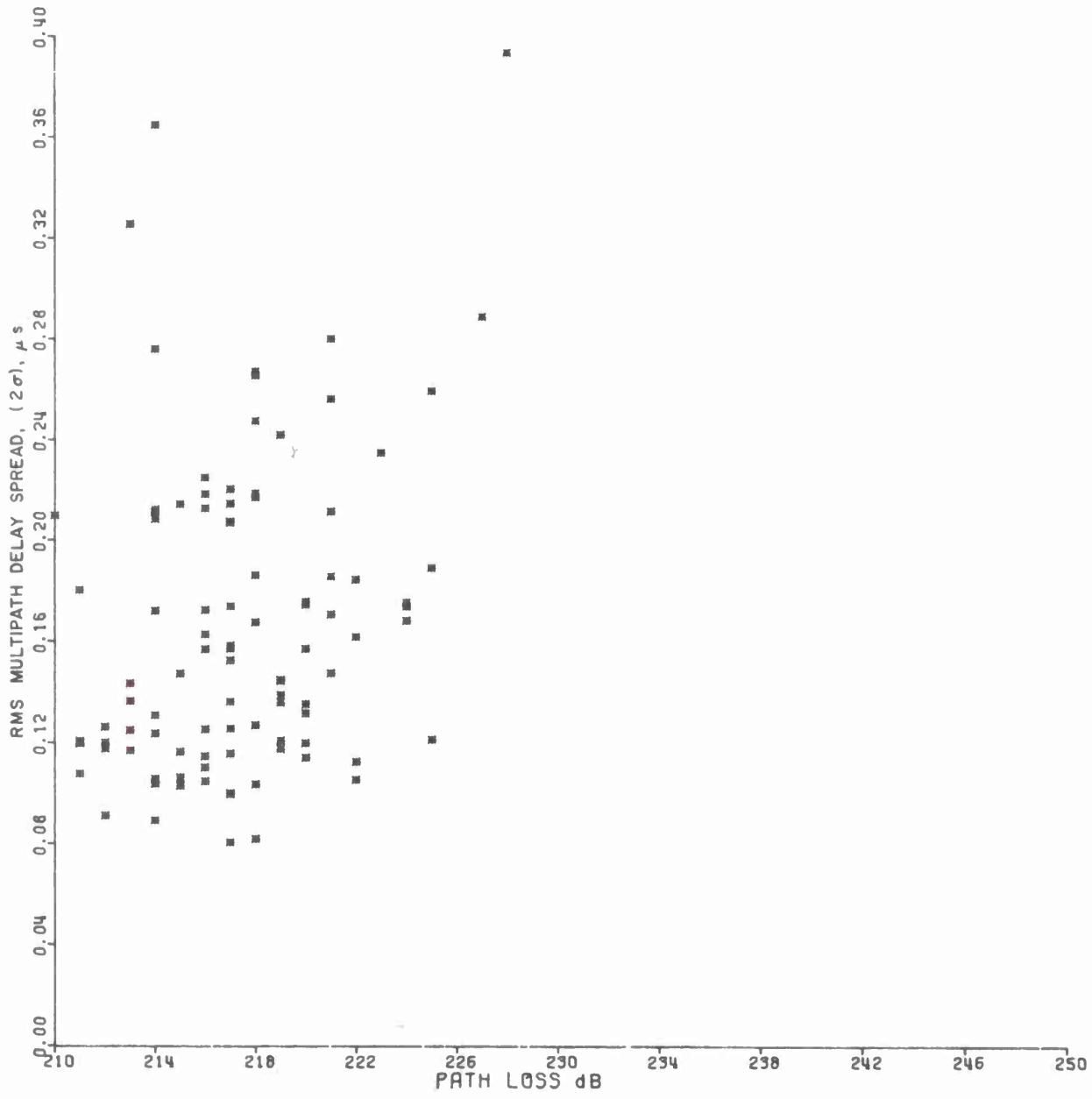

Figure 4-7(a). RMS Delay Spread VS Path Loss — XMIT 8 Ft., RCVR 8 Ft., Summer Afternoon (RCVR 1)

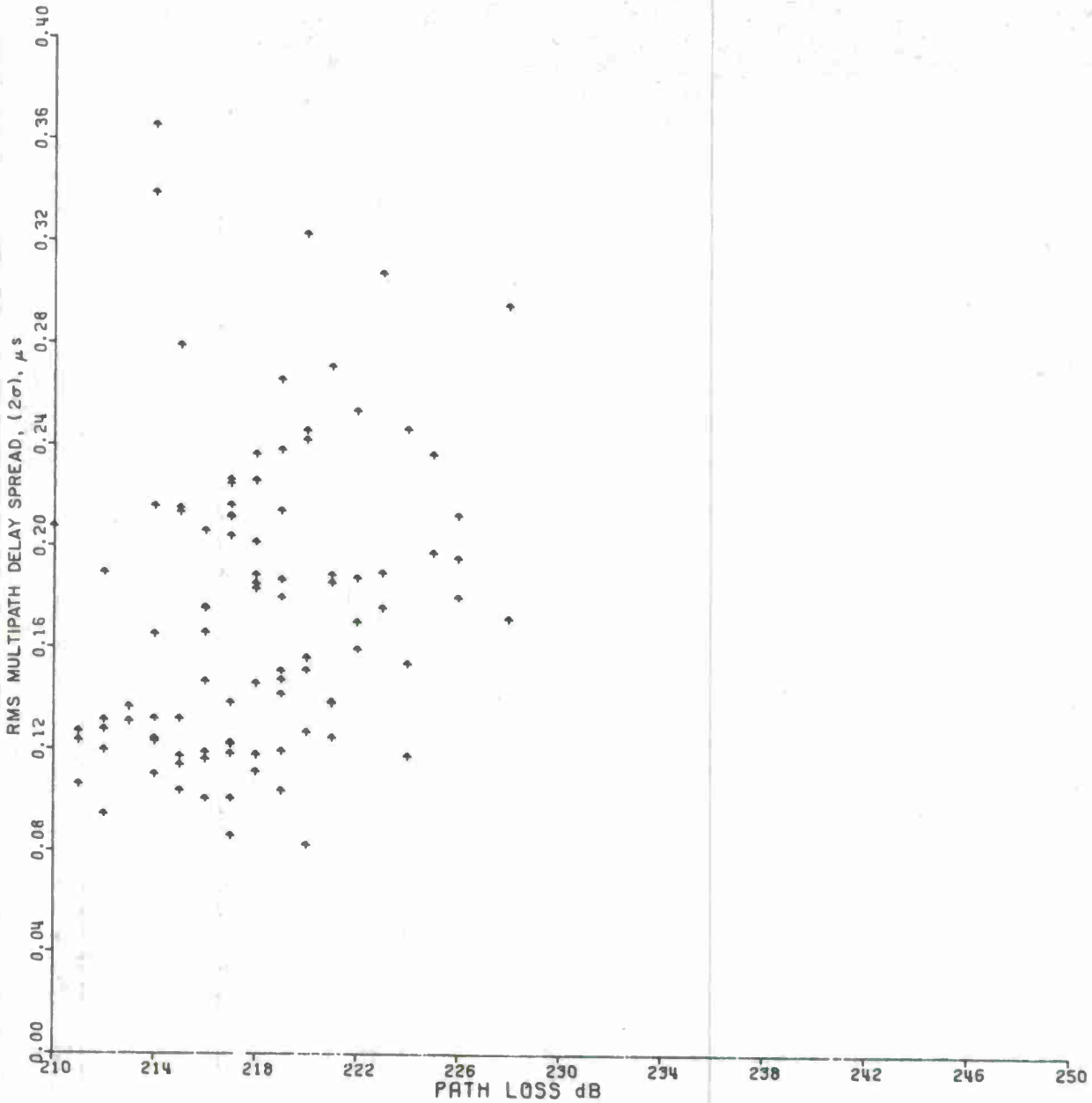

Figure 4-7(b). RMS Delay Spread VS Path Loss — XMIT 8 Ft., RCVR 8 Ft., Summer Afternoon (RCVR 2)

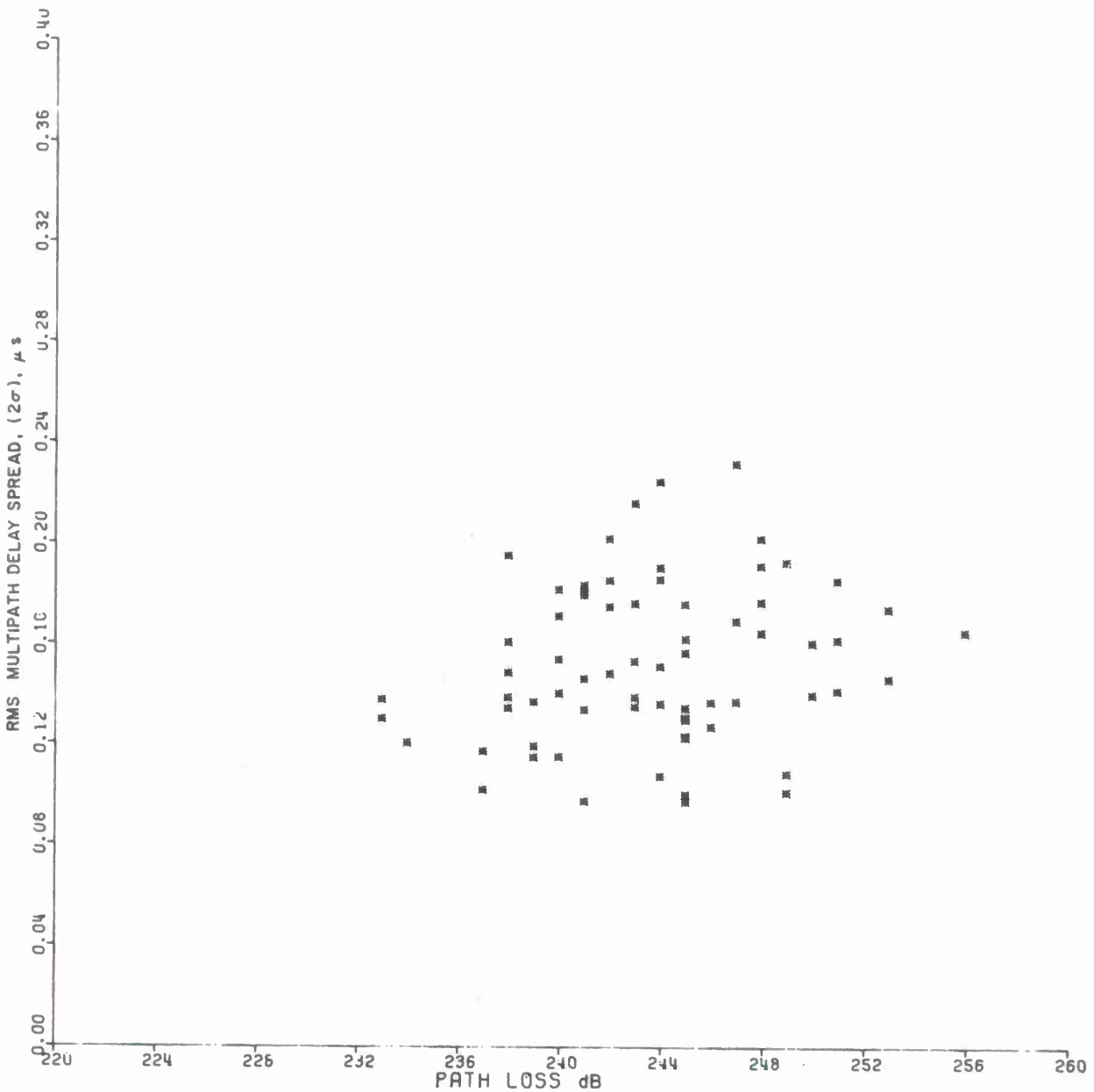

Figure 4-8(a). RMS Delay Spread VS Path Loss — XMIT 28 Ft., RCVR 28 Ft., All Data (RCVR 1)

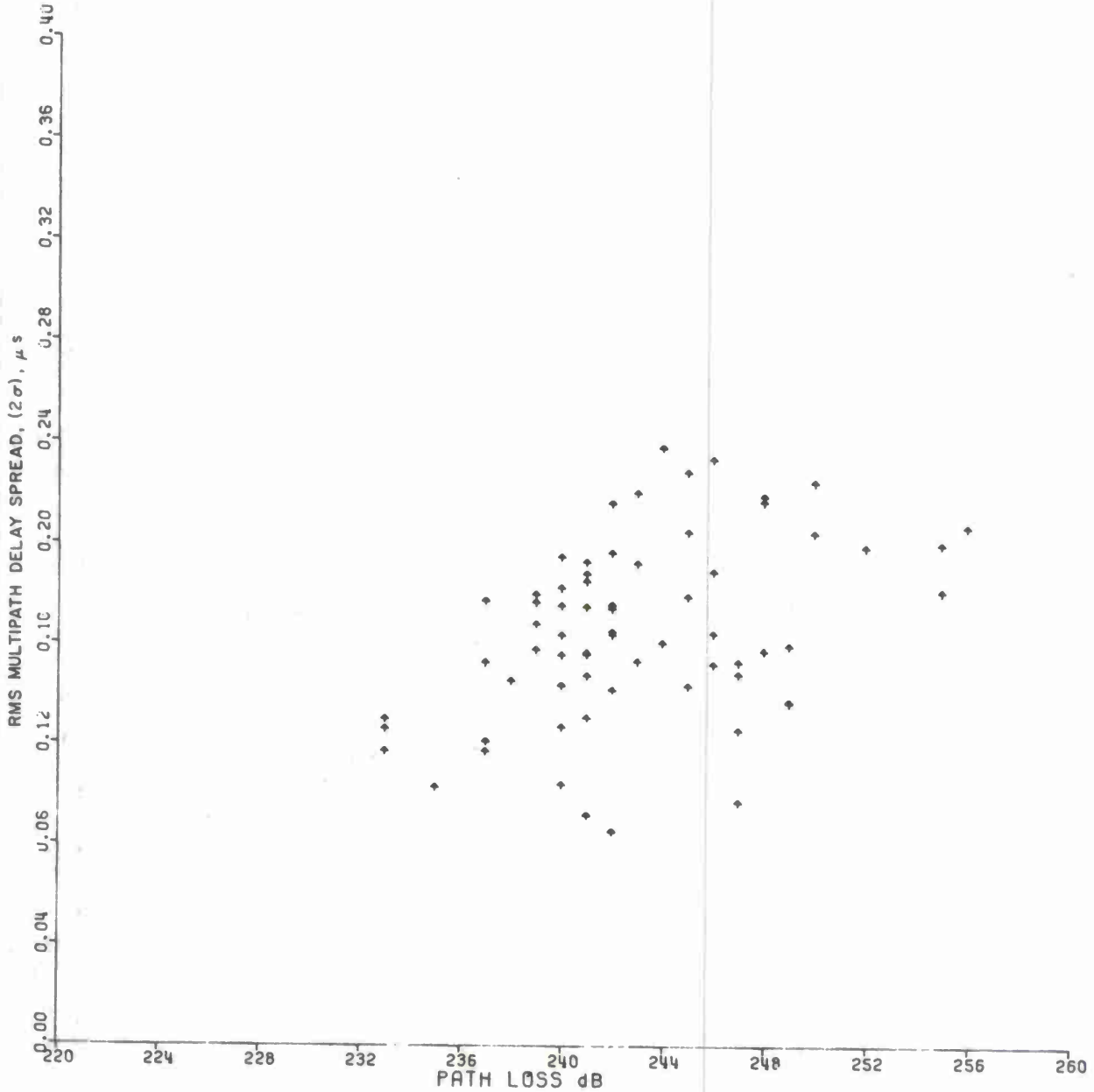

Figure 4-8(b). RMS Delay Spread VS Path Loss — XMIT 28 Ft., RCVR 28 Ft., All Data (RCVR 2)

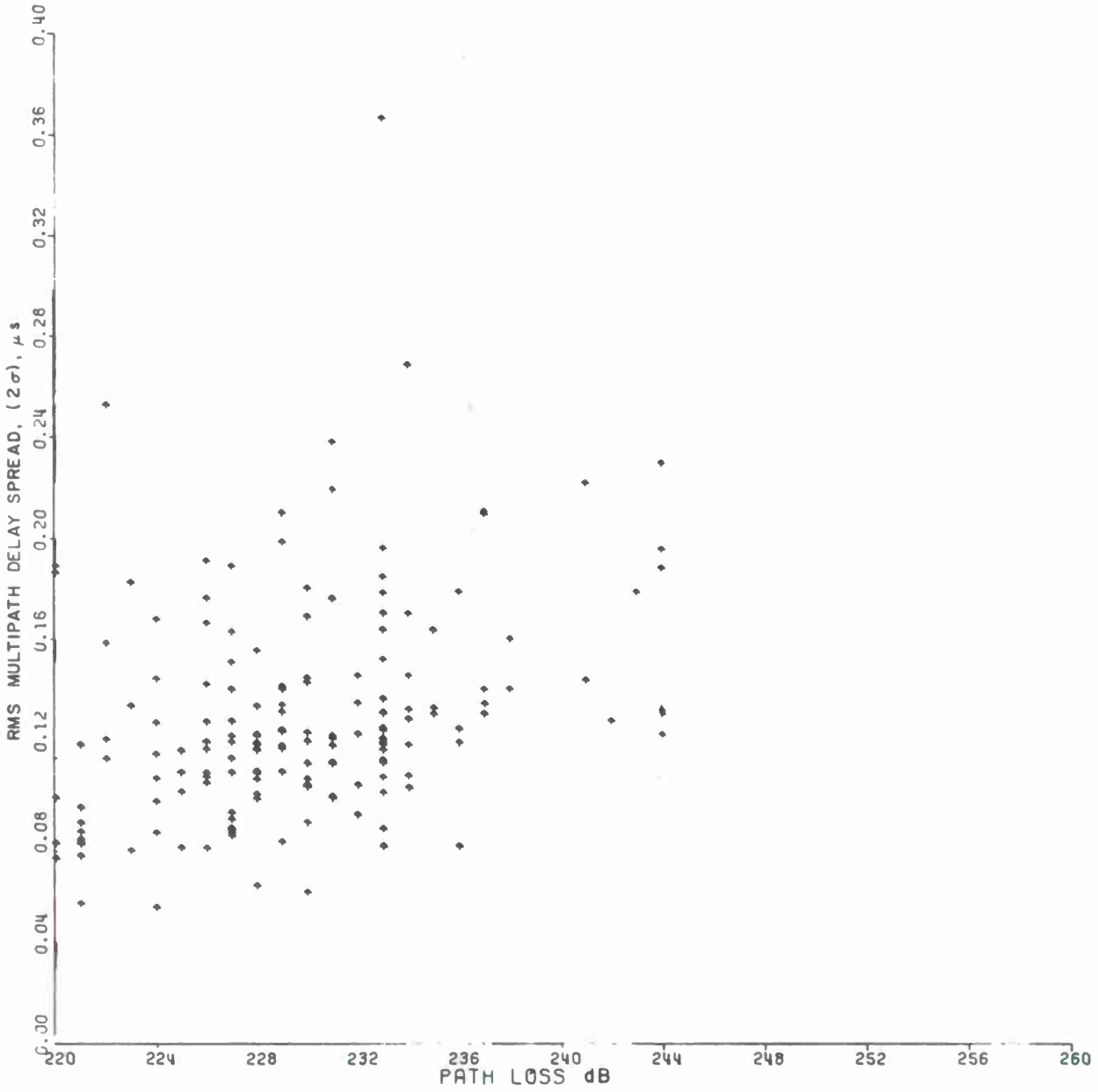

Figure 4-9. RMS Delay Spread VS Path Loss — XMIT 8 Ft., RCVR 15 Ft., All Data (RCVR 2)

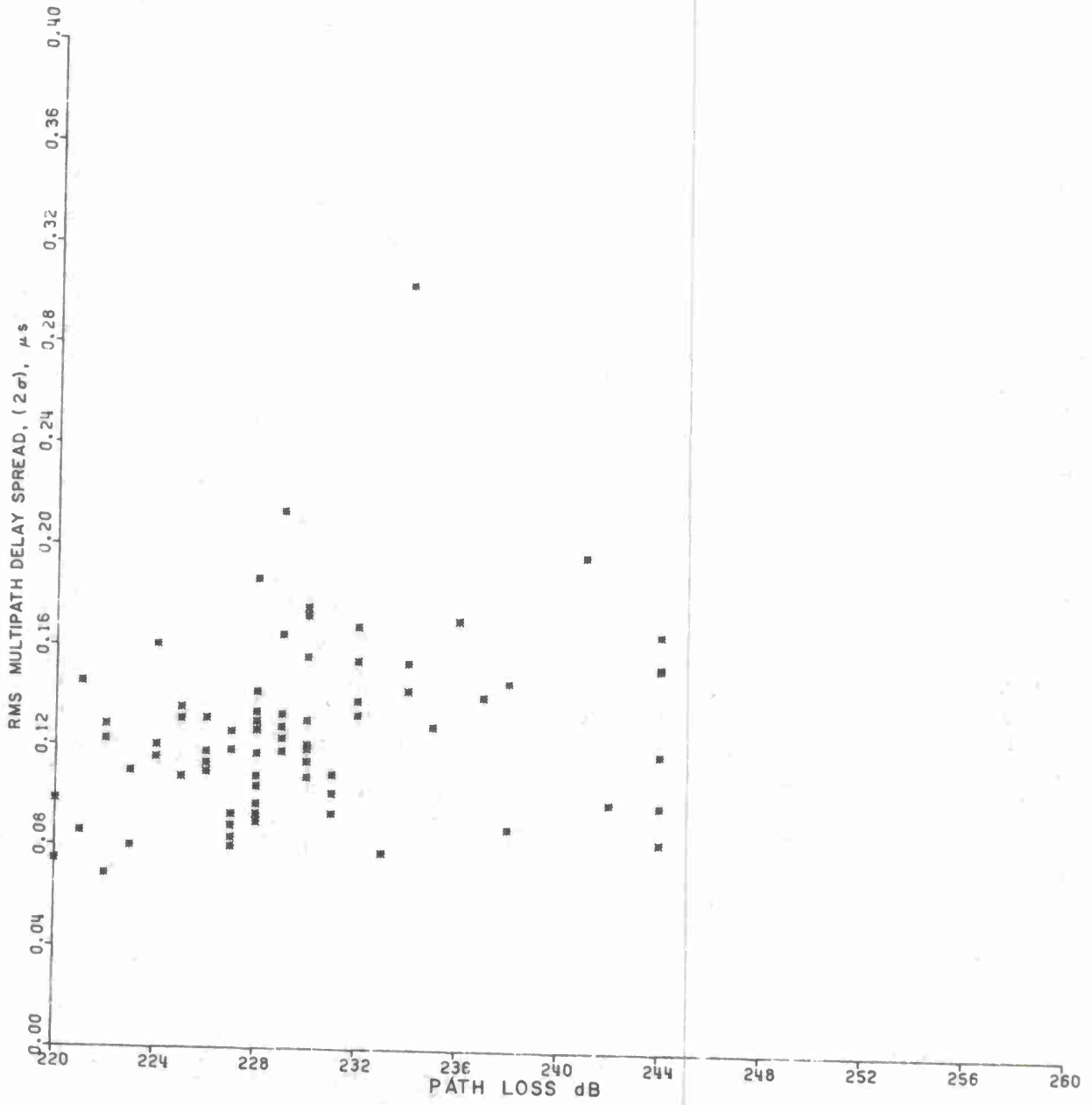

Figure 4-10. RMS Delay Spread VS Path Loss — XMIT 15 Ft., RCVR 8 Ft., All Data (RCVR 1)

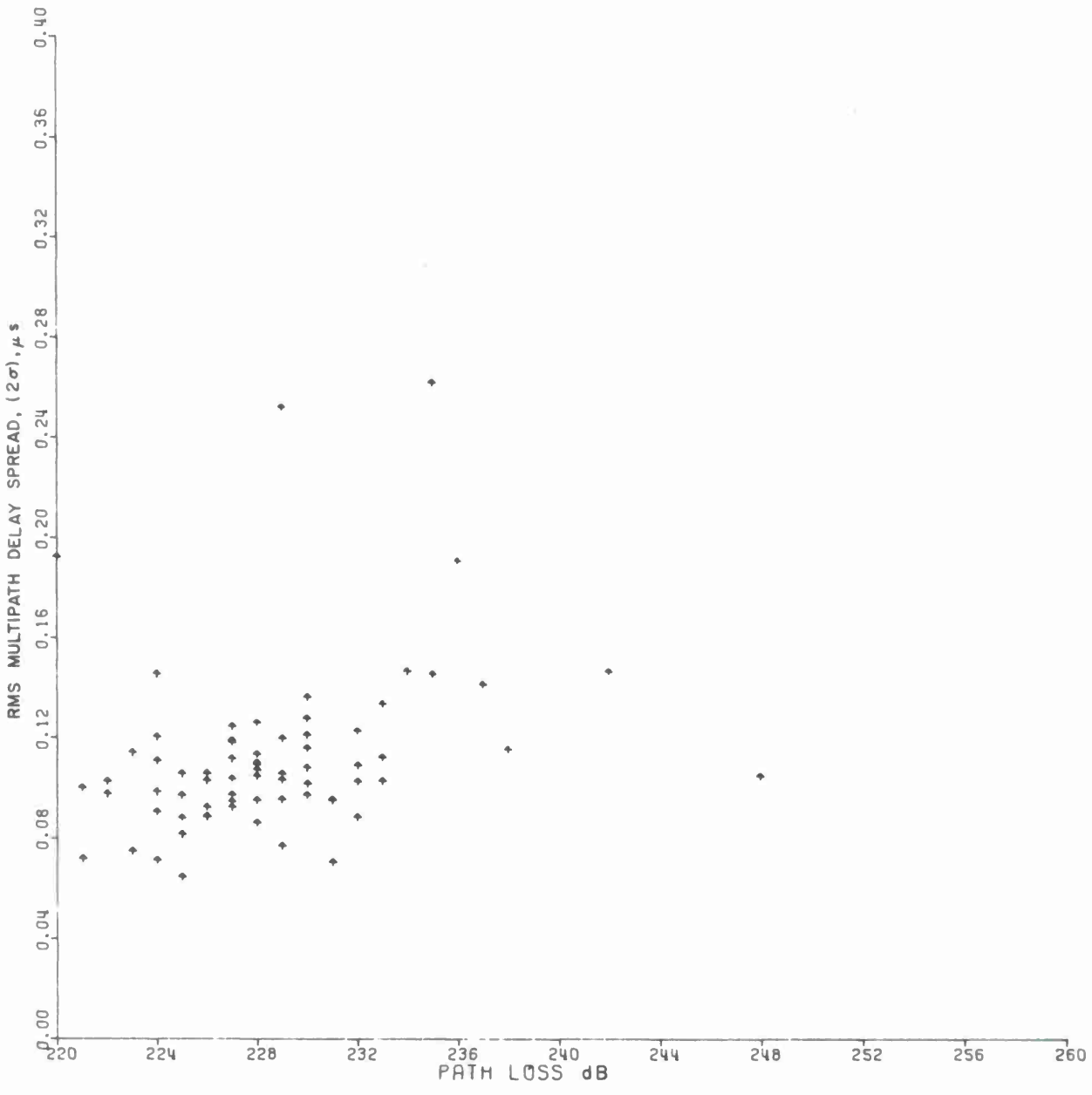

Figure 4-11. RMS Delay Spread VS Path Loss —XMIT 15 Ft., RCVR 15 Ft., All Data (RCVR 2)

Table 4-4

Correlation Values: RMS Delay Spread vs Path Loss

Configuration	Time Block or Interval	Receiver 1		Receiver 2	
		No. of Samples	Correlation Values	No. of Samples	Correlation Values
I	TXX	454	.271	284	.149
	TB0	261	.194	94	.559
	TB9	193	.236	190	.214
	TB1	122	.139	44	.508
	TB2	126	.310	47	.586
	TB4	89	.174	88	.182
	TB5	99	.283	98	.264
V	TXX (April - May 1975)	69	.198	68	.405
II	TXX (Dec. 1974 - April 1975)	-	-	174	.328
III	TXX (Dec. 1974 - May 1975)	74	.248	-	-
IV	TXX (Feb. - Apr. 1975)	-	-	71	.292

It can be readily seen from Table 4-4 that the correlation values of the RMS multipath delay spread and path loss data for the various combinations of test configurations and time blocks are generally between .17 and .41. The exception to this is the correlation value for test Configuration I, Receiver 2, TB0 (TB1, TB2). A possible explanation for these higher correlation values is that the data samples for time block TB0 for Receiver 2, test Configuration I, were all obtained (except for one sample in January) during the two-month period of November-December 1974. On the other hand, the data samples for Receiver 1 were obtained over the entire period denoted by TB0, and the number of data samples for Receiver 2 is much less than that for Receiver 1. A second possible explanation is that test instrumentation or test procedures associated with Receiver 2 were causative factors; however, this is not indicated by looking at the other correlation values obtained for data from Receiver 2.

It should be noted that care needs to be exercised in interpreting experimental results obtained from a limited number of tests for a relatively short period of time. For example, if the experimental program ran only for the time period November - December 1974, and the test data obtained were only for Receiver 2 over this period, then one might conclude that a relatively strong correlation exists. However, from one such test result, no conclusion can be drawn as to how frequent such a relatively high correlation value can be expected.

4.2 PROBABILITY PLOTS: RMS MULTIPATH DELAY SPREAD

Various combinations of test configurations and time blocks of RMS multipath delay spread data plotted against a probability scale are shown in Figures 4-12(a,b), 4-13(a-d), 4-14(a-d), and 4-15(a,b). The number of data samples used to generate these 12 graphs was given in Table 4-4.

Figures 4-12(a) and 4-12(b) are comparison plots of all RMS delay spread data (TXX), all "winter" data (TB0) and all "summer" data (TB9), respectively, for Receivers 1 and 2. There exists a distinguishable, almost uniform, difference between the winter and summer plots for Receiver 1, whereas for Receiver 2 a distinguishable difference cannot be said to exist. This lack of separation of the winter and summer plots in Figure 4-12 (b) may have occurred because the winter test data for Configuration I, Receiver 2, are available from two months only, November - December 1974 (see Section 4.1).

Figures 4-13(a-d) are comparison probability plots of winter and summer morning (0600-1300) and afternoon (1300-1800) RMS delay spread data for test Configuration I, Receivers 1 and 2. From Figures 4-13(a), and 4-13(b), distinguishable separation of the plots can be seen for the morning and afternoon data. The RMS delay spread is greater in the winter morning than winter afternoon (Figure 4-13a) while in the summer the opposite occurs (Figure 4-13 b). This phenomenon occurs for summer morning and afternoon hours for Receiver 2 (Figure 4-13d) but does not occur for winter data (Figure 4-13c). However, for reasons stated previously about winter test data available for test Configuration I, Receiver 2, the winter plot may be different if sufficient data from months other than just November and December were available. A conjecture, which appears reasonable, is that the RMS multipath spread is greater in winter morning

hours than winter afternoon hours, while in the summer the converse is true. This conjecture is reinforced somewhat by Figure 4-29 in Section 4.7 where hourly averages of RMS delay spreads for two summer and two winter months are plotted. Any statements on the statistical validity of such a conjecture require further testing.

Figures 4-14(a-d) are comparison probability plots of winter and summer morning and winter and summer afternoon RMS delay spread data for test Configuration I, Receiver 1 and Receiver 2. A separation between the winter morning and summer morning plots can be readily seen in Figure 4-14(a), whereas no separation of the plots basically exist for other combinations in Figures 4-14(b), (c), and (d).

Figures 4-15(a) and 4-15(b) are comparison probability plots of the different test Configurations I-V (Table 4-1) of the RMS delay spread data for the winter months (TB0). Except for test Configuration I, the test samples available are basically within the time period of November 1974 - April 1975 (with additional test data for test configurations other than Configuration I from the first 12 days in May).

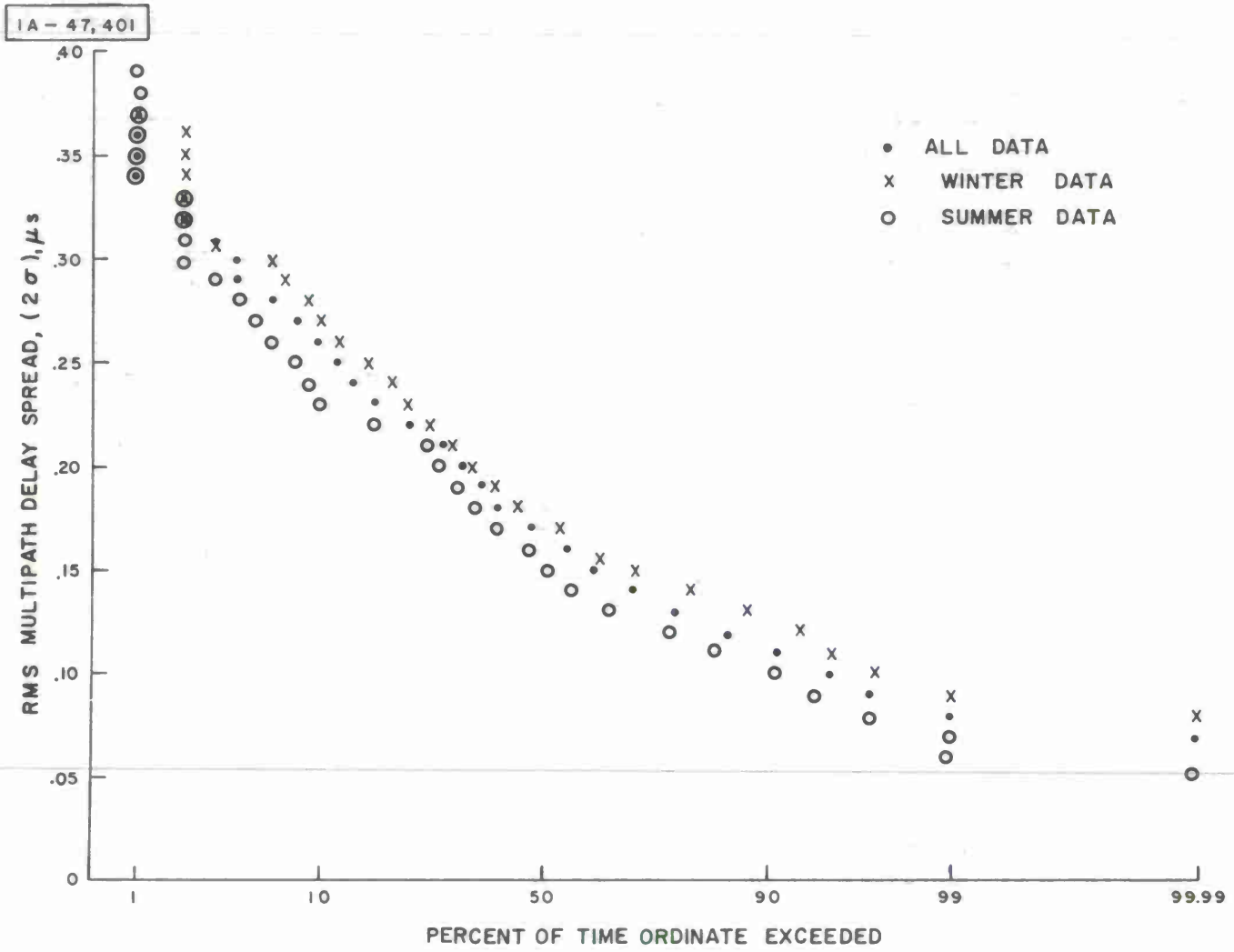

Figure 4-12(a). RMS Delay Spread Distributions — XMIT 8 Ft., RCVR 8 Ft., All Data, Winter and Summer Data (RCVR 1)

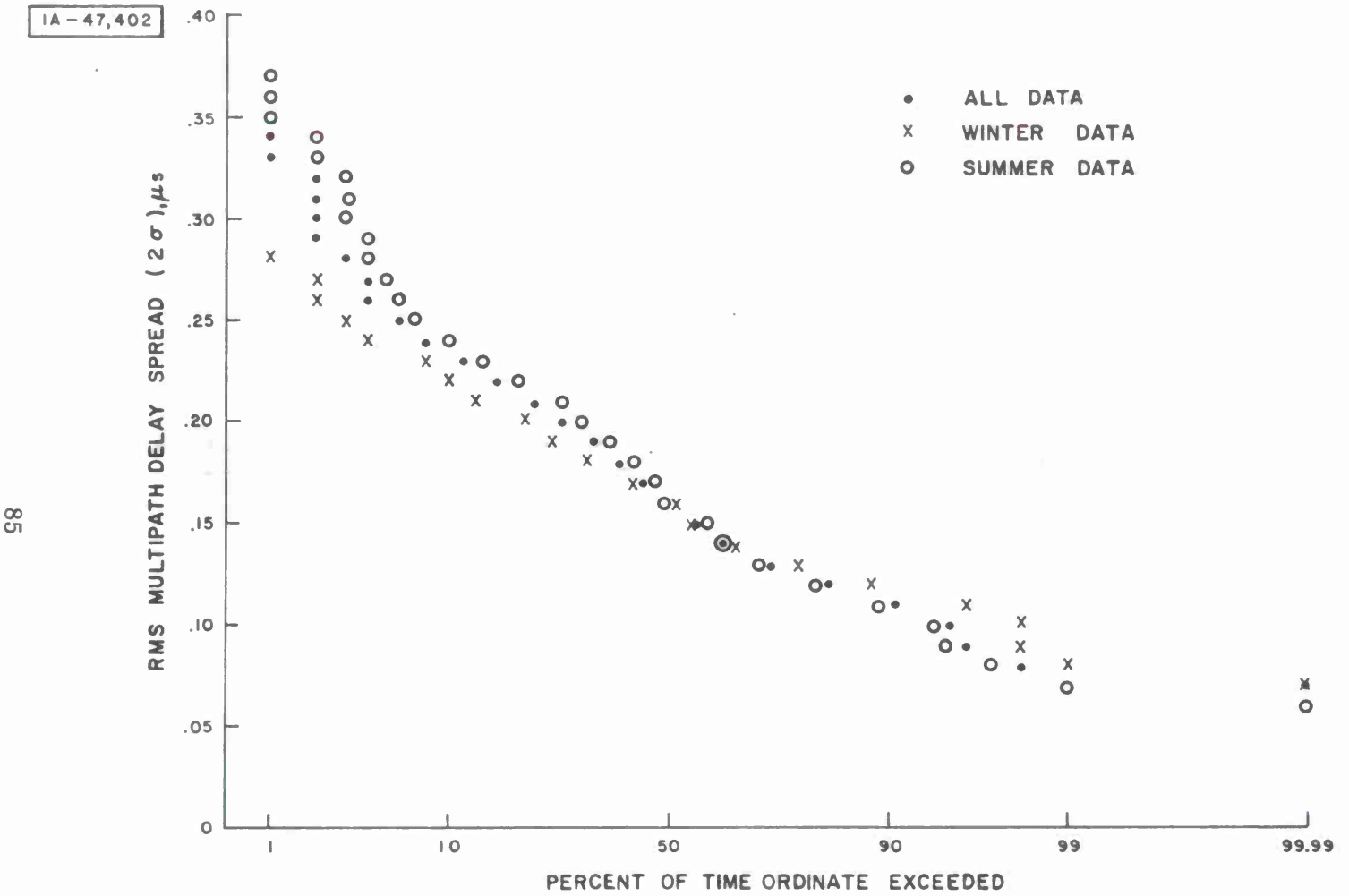

Figure 4-12(b). RMS Delay Spread Distributions — XMIT 8 Ft., RCVR 8 Ft., All Data, Winter and Summer Data (RCVR 2)

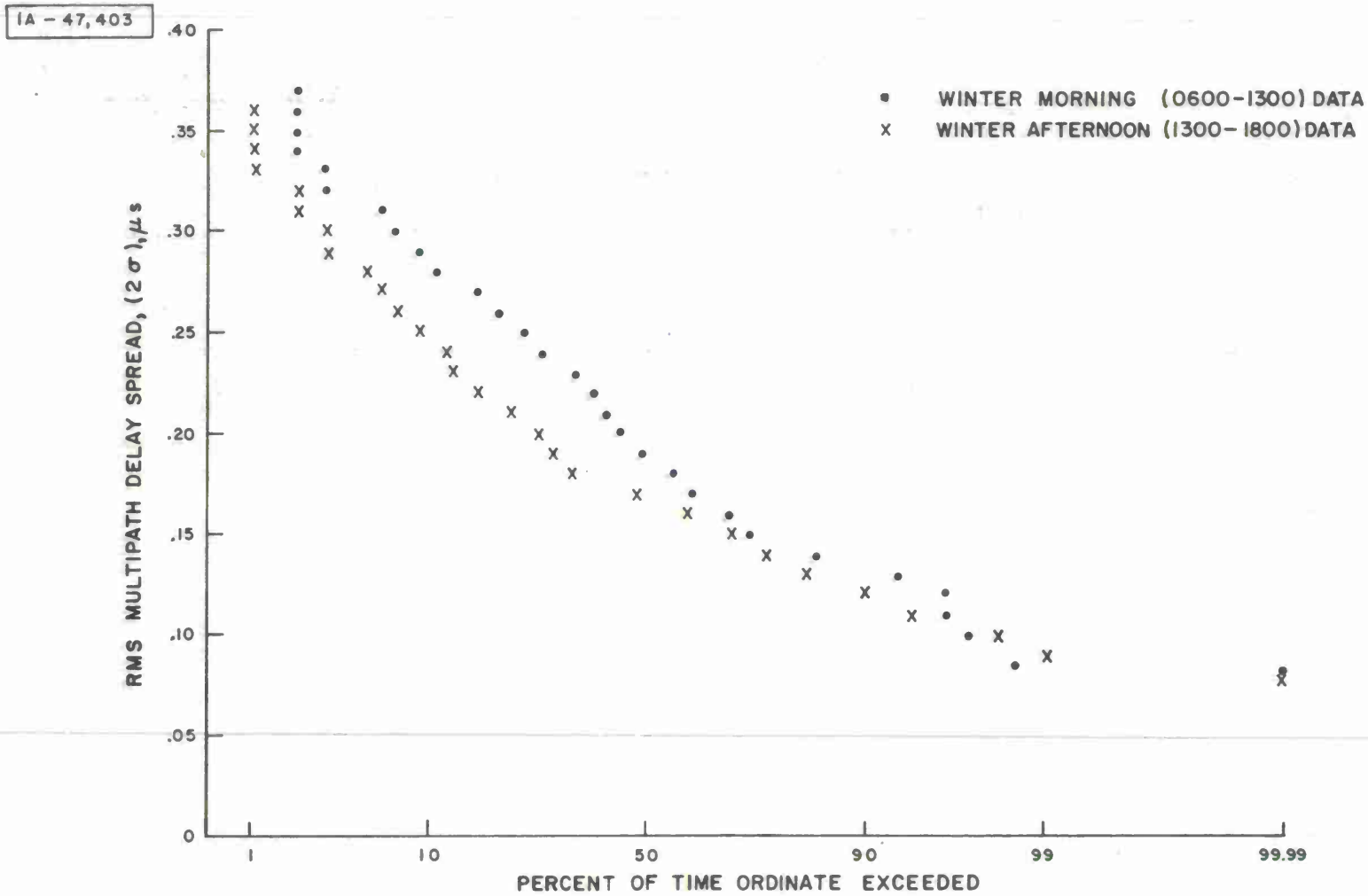

Figure 4-13(a). RMS Delay Spread Distributions — XMIT 8 Ft., RCVR 8 Ft., Winter Morning and Winter Afternoon Data (RCVR 1)

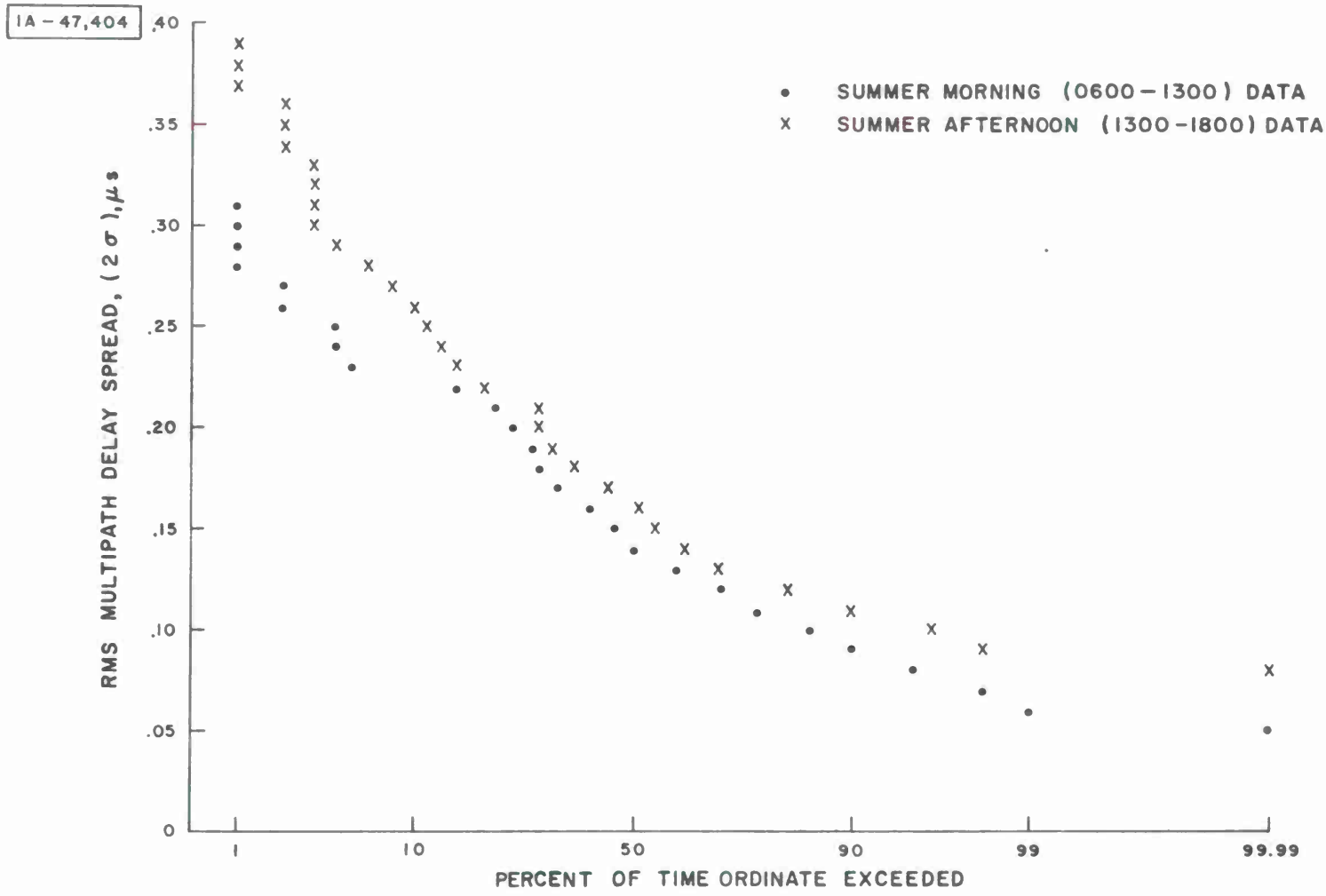

Figure 4-13(b). RMS Delay Spread Distributions — XMIT 8 Ft., RCVR 8 Ft., Summer Morning and Summer Afternoon Data (RCVR 1)

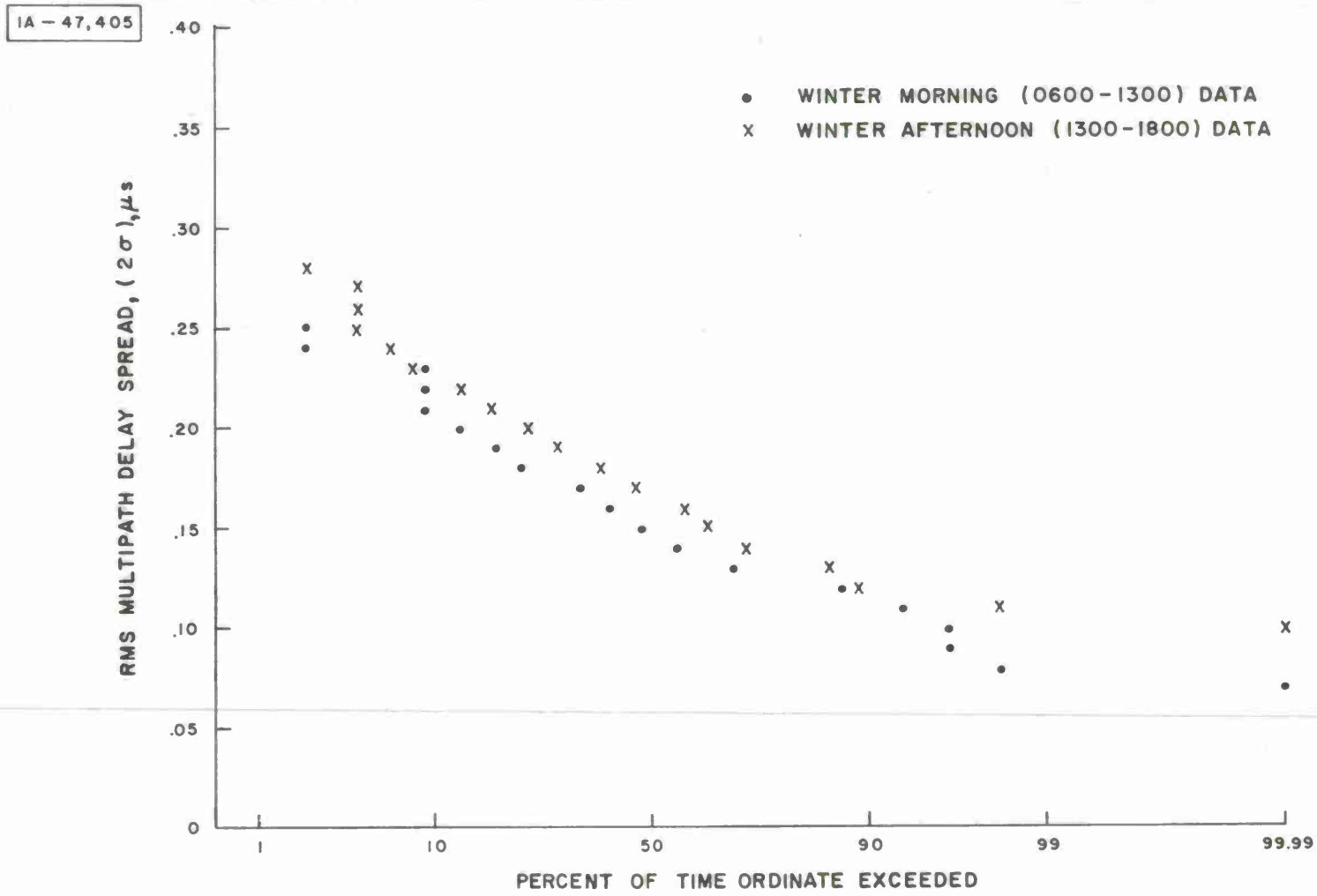

Figure 4-13(c). RMS Delay Spread Distributions — XMIT 8 Ft., RCVR 8 Ft., Winter Morning and Winter Afternoon Data (RCVR 2)

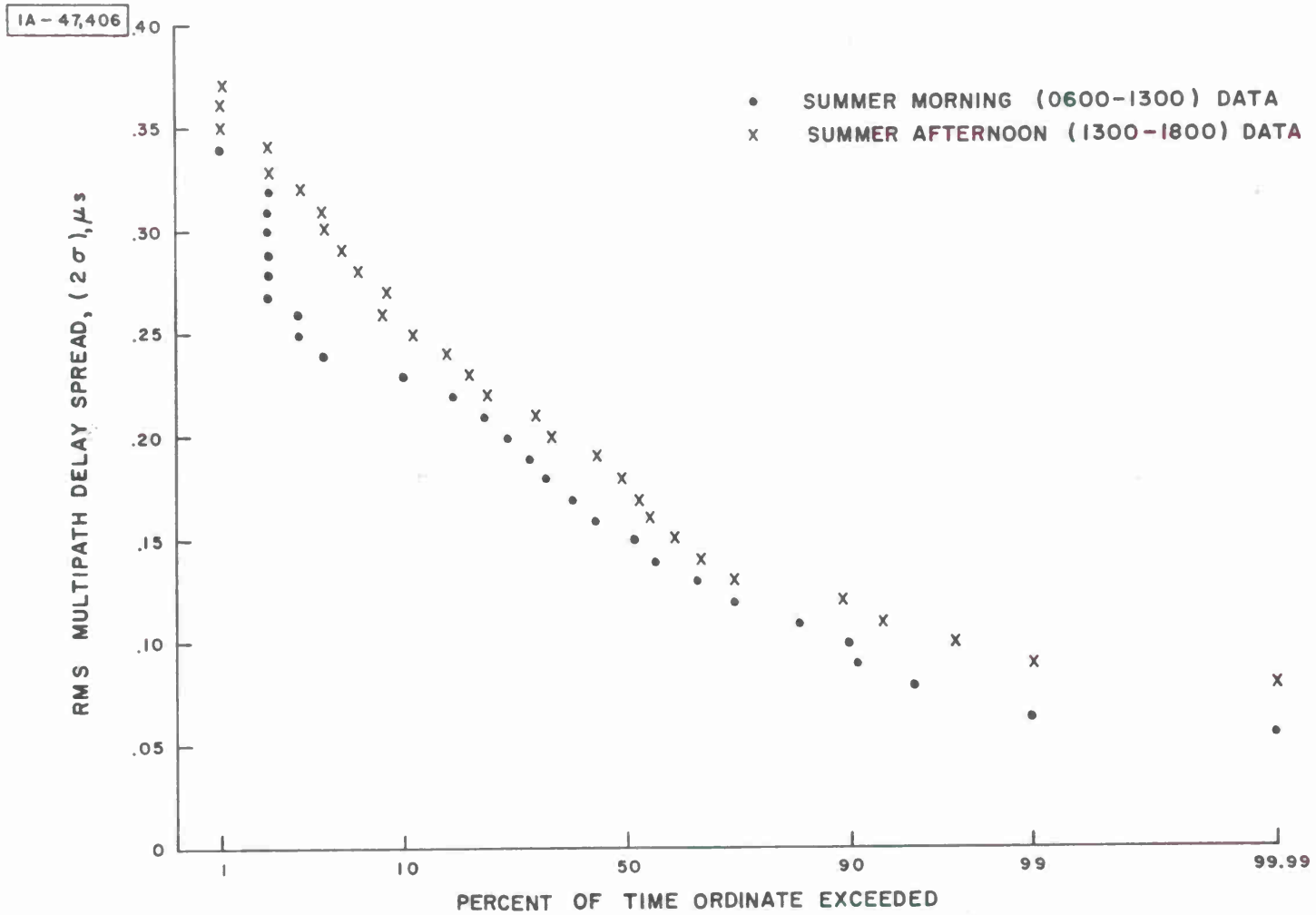

Figure 4-13(d). RMS Delay Spread Distributions — XMIT 8 Ft., RCVR 8 Ft., Summer Morning and Summer Afternoon Data (RCVR 2)

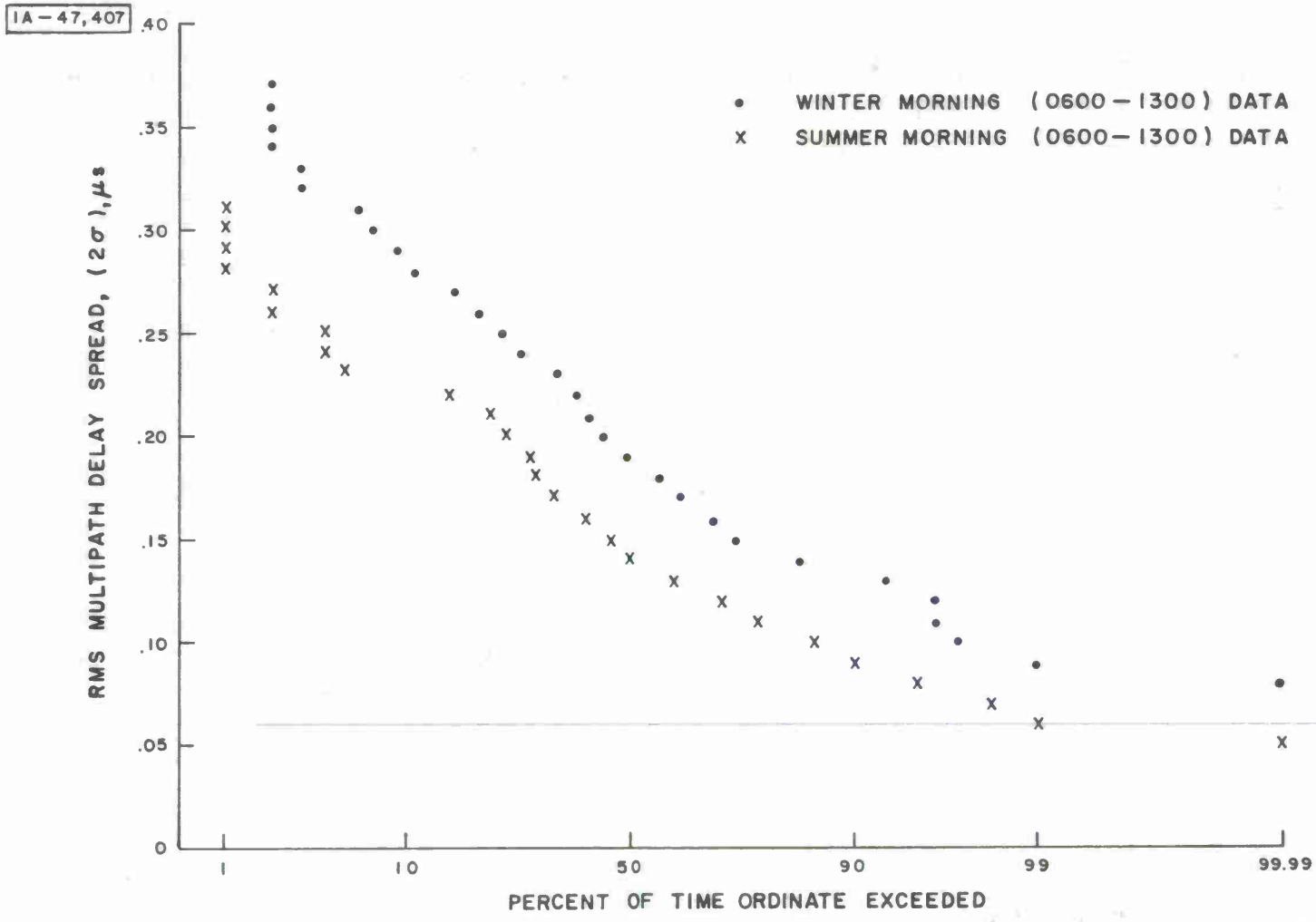

Figure 4-14(a). RMS Delay Spread Distributions — XMIT 8 Ft., RCVR 8 Ft., Winter Morning and Summer Morning Data (RCVR 1)

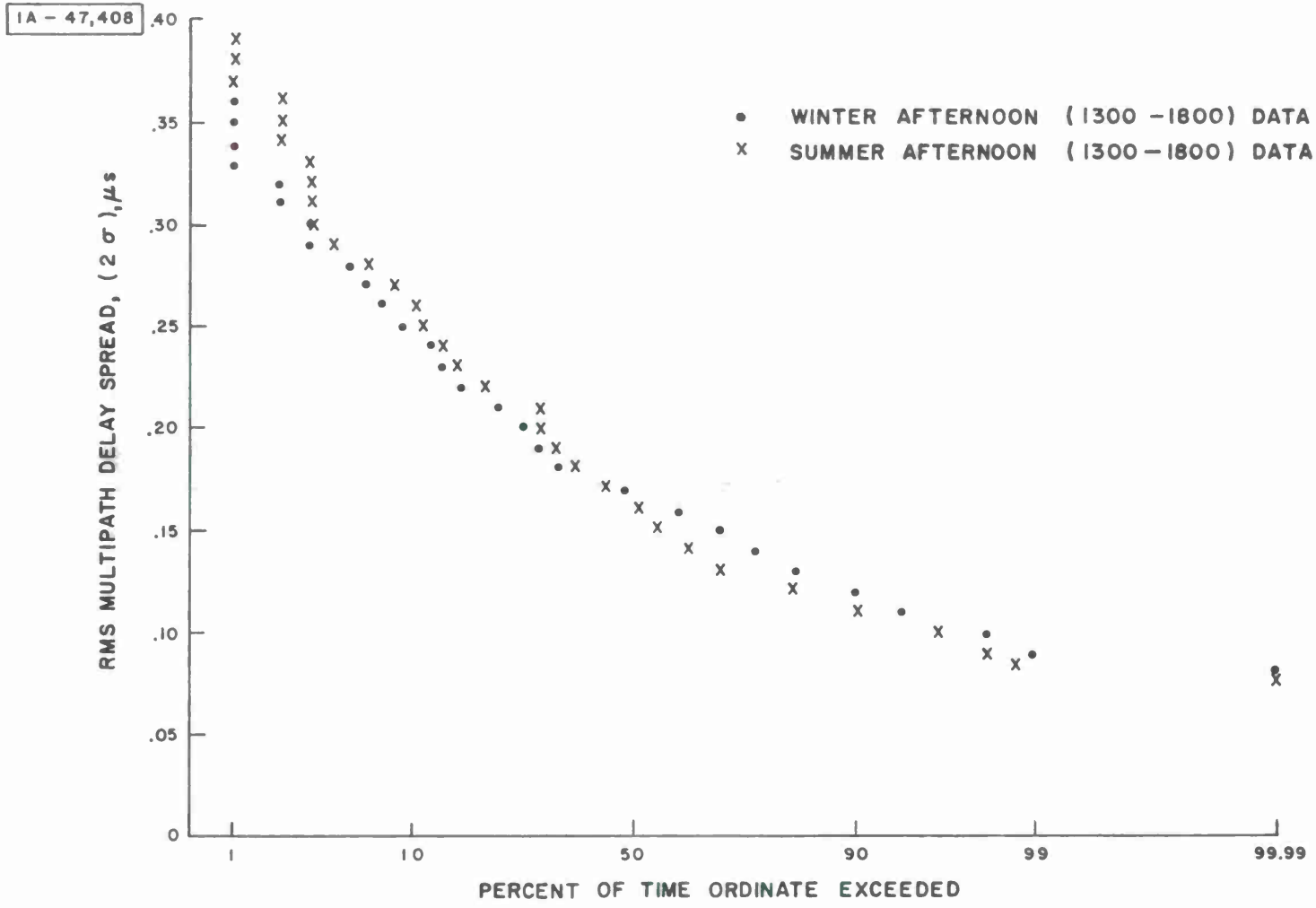

Figure 4-14(b). RMS Delay Spread Distributions — XMIT 8 Ft., RCVR 8 Ft., Winter Afternoon and Summer Afternoon Data (RCVR 1)

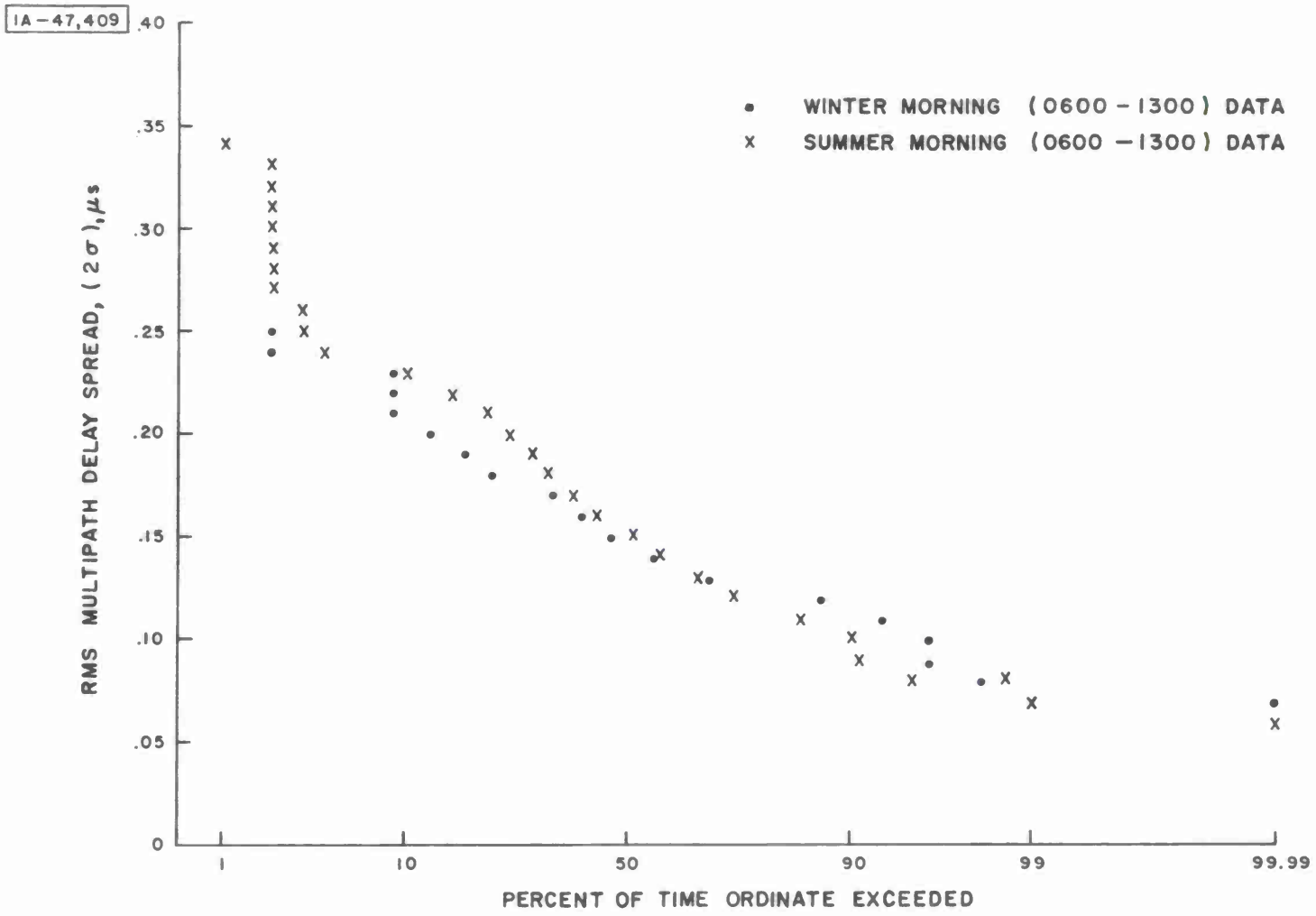

Figure 4-14(c). RMS Delay Spread Distributions — XMIT 8 Ft., RCVR 8 Ft., Winter Morning and Summer Morning Data (RCVR 2)

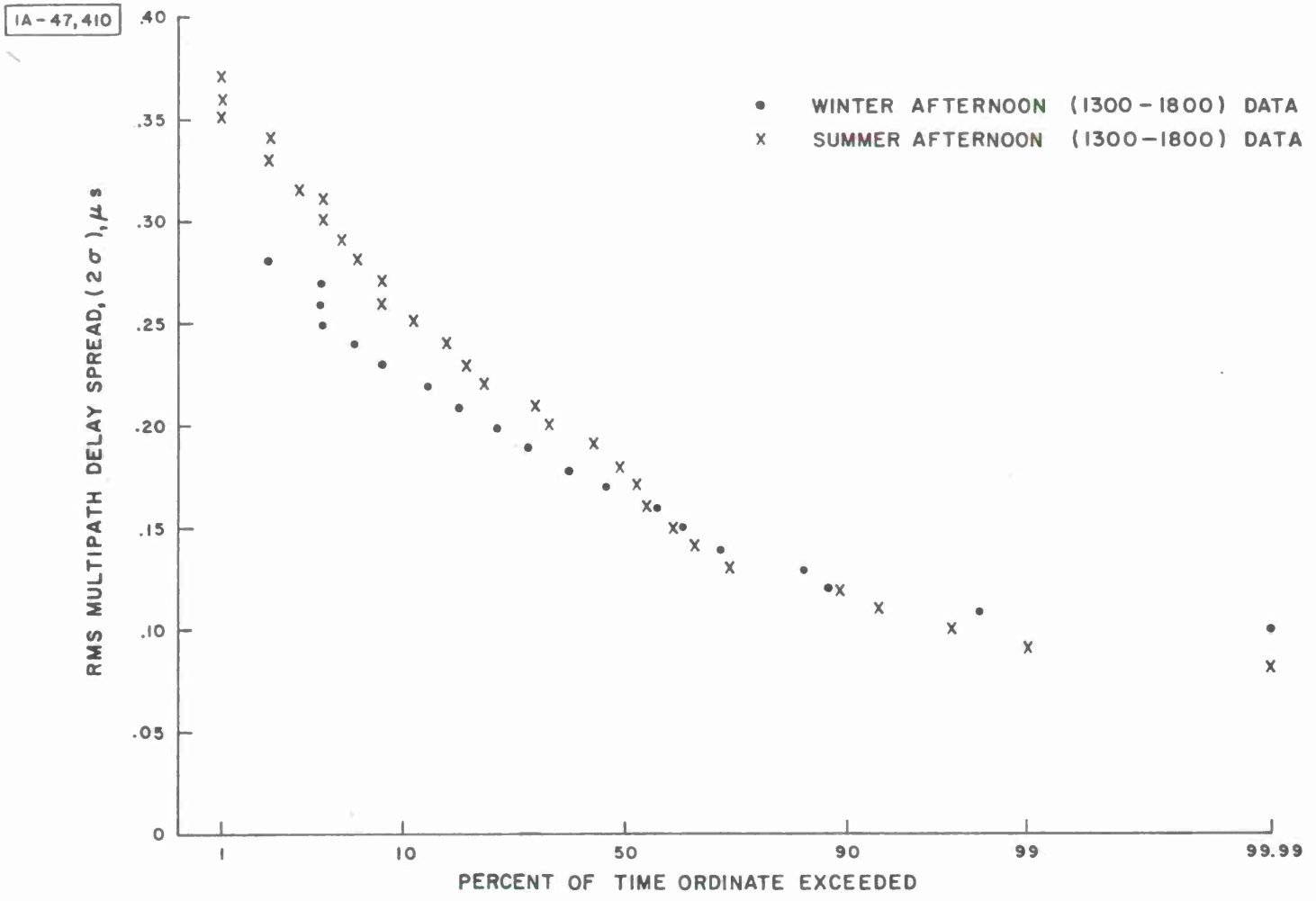

Figure 4-14(d). RMS Delay Spread Distributions — XMIT 8 Ft., RCVR 8 Ft., Winter Afternoon and Summer Afternoon Data (RCVR 2)

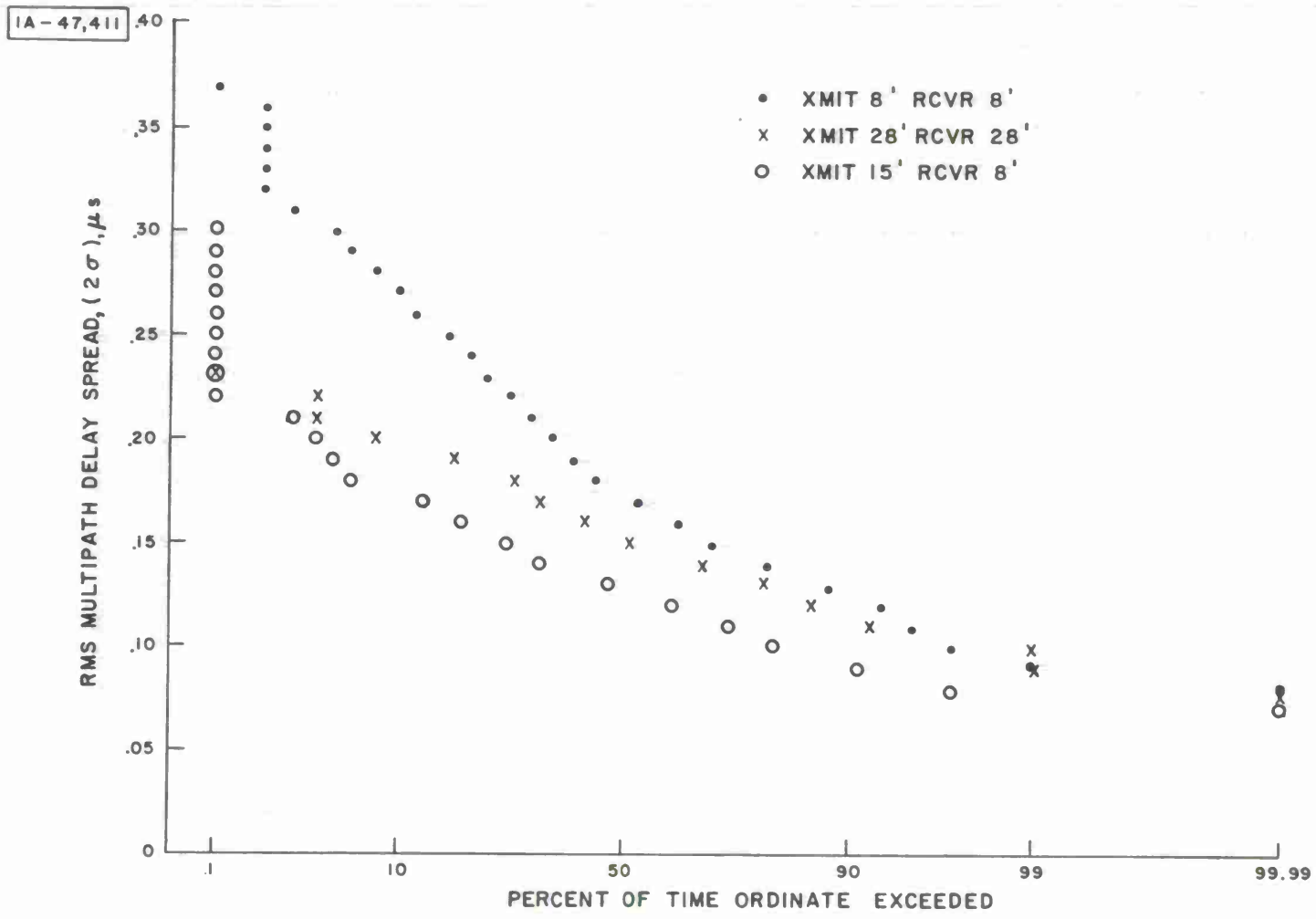

Figure 4-15(a). RMS Delay Spread Distributions — Configurations I, III, and V, Winter Data (RCVR 1)

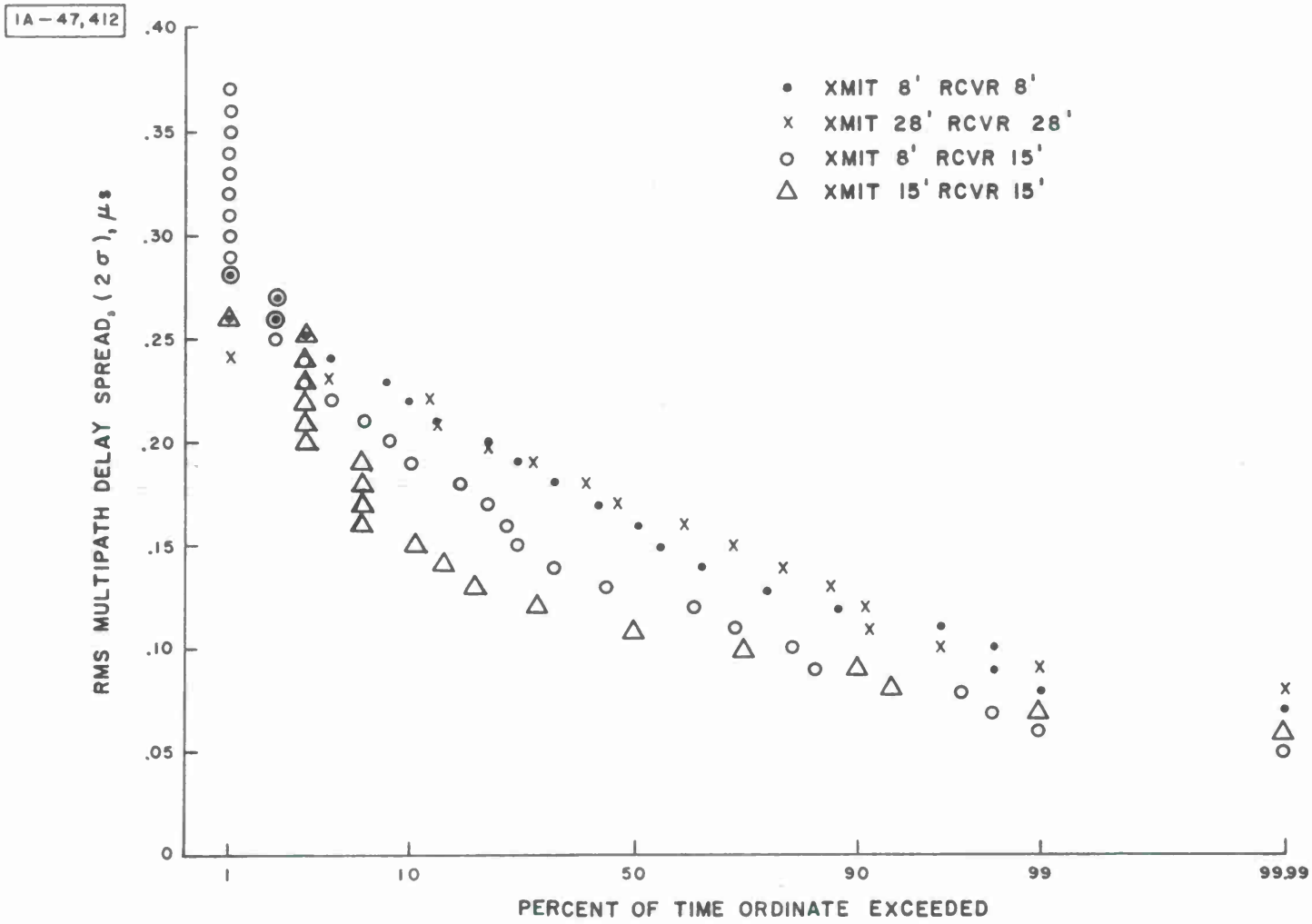

Figure 4-15(b). RMS Delay Spread Distributions — Configurations I, II, IV, and V, Winter Data (RCVR 2)

4.3 PROBABILITY PLOTS: MEDIAN RSL

The median received signal level (RSL) data plotted against a probability scale are shown in Figures 4-16(a) and 4-16(b), 4-17(a) and 4-17(b), and 4-18(a) and 4-18(b) for different combinations of the test configurations and time blocks. The number of data samples used to generate these graphs is given in Table 4-4.

Figures 4-16(a) and 4-16(b) are comparison plots of all RSL data for the testing period (TXX), all winter data (TB0) and all summer data (TB9) for test Configuration I, Receiver 1 and Receiver 2. These two graphs show that the seasonal variation of received signal levels in a temperate climate is what was expected; the signal levels are higher in the summer than in the winter for both receivers, [15, 16].

Figures 4-17(a) and 4-17(b) are comparison plots of median RSL data for test Configuration I, Receivers 1 and 2, for winter and summer, mornings and afternoons. As one can readily see, there is basically no separation between the summer morning and afternoon or winter morning and afternoon plots for either receiver. Since there are insufficient median RSL test data for the nighttime period, comparison of nighttime and daytime signal levels could not be made.

Figures 4-18(a) and 4-18(b) are comparison plots for median RSL data for the different test configurations (Table 4-2) for the winter months. Other than for test Configuration I, the test data are generally within the time period of November 1974 - April 1975 (with additional test data for test configurations other than I from the first 12 days in May).

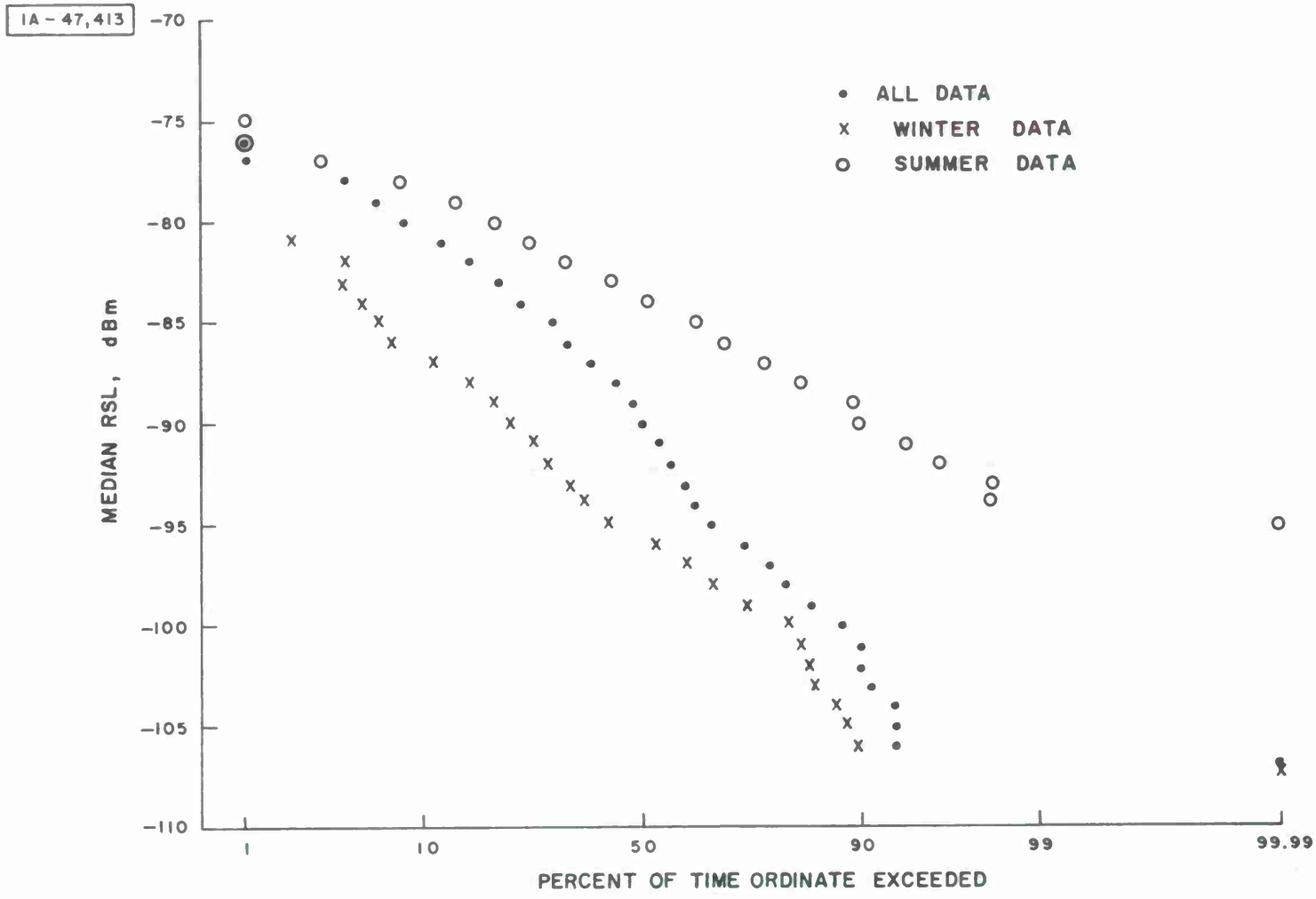

Figure 4-16(a). Median RSL Distributions — XMIT 8 Ft., RCVR 8 Ft., All Data, Winter and Summer Data (RCVR 1)

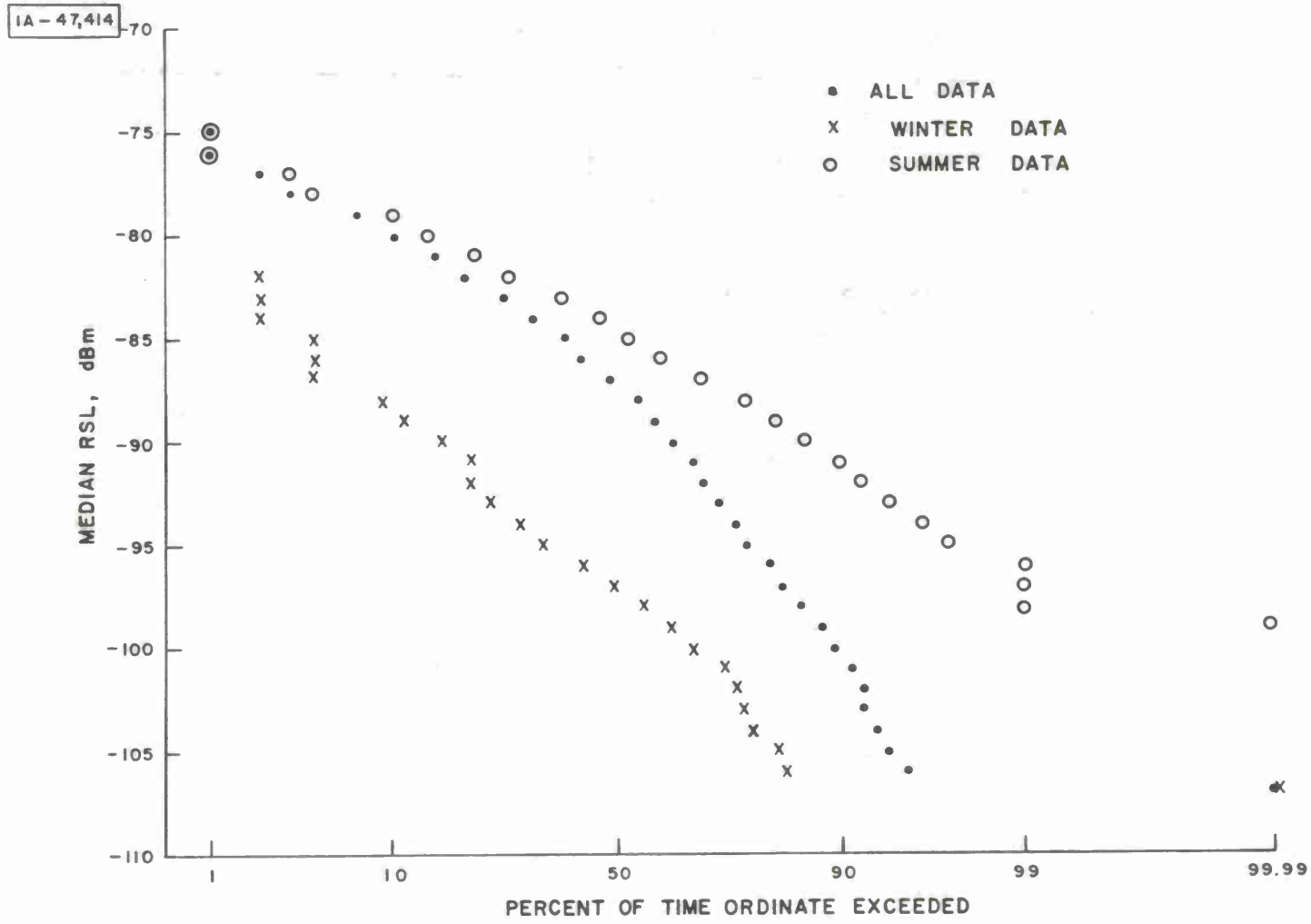

Figure 4-16(b). Median RSL Distributions — XMIT 8 Ft., RCVR 8 Ft., All Data, Winter and Summer Data (RCVR 2)

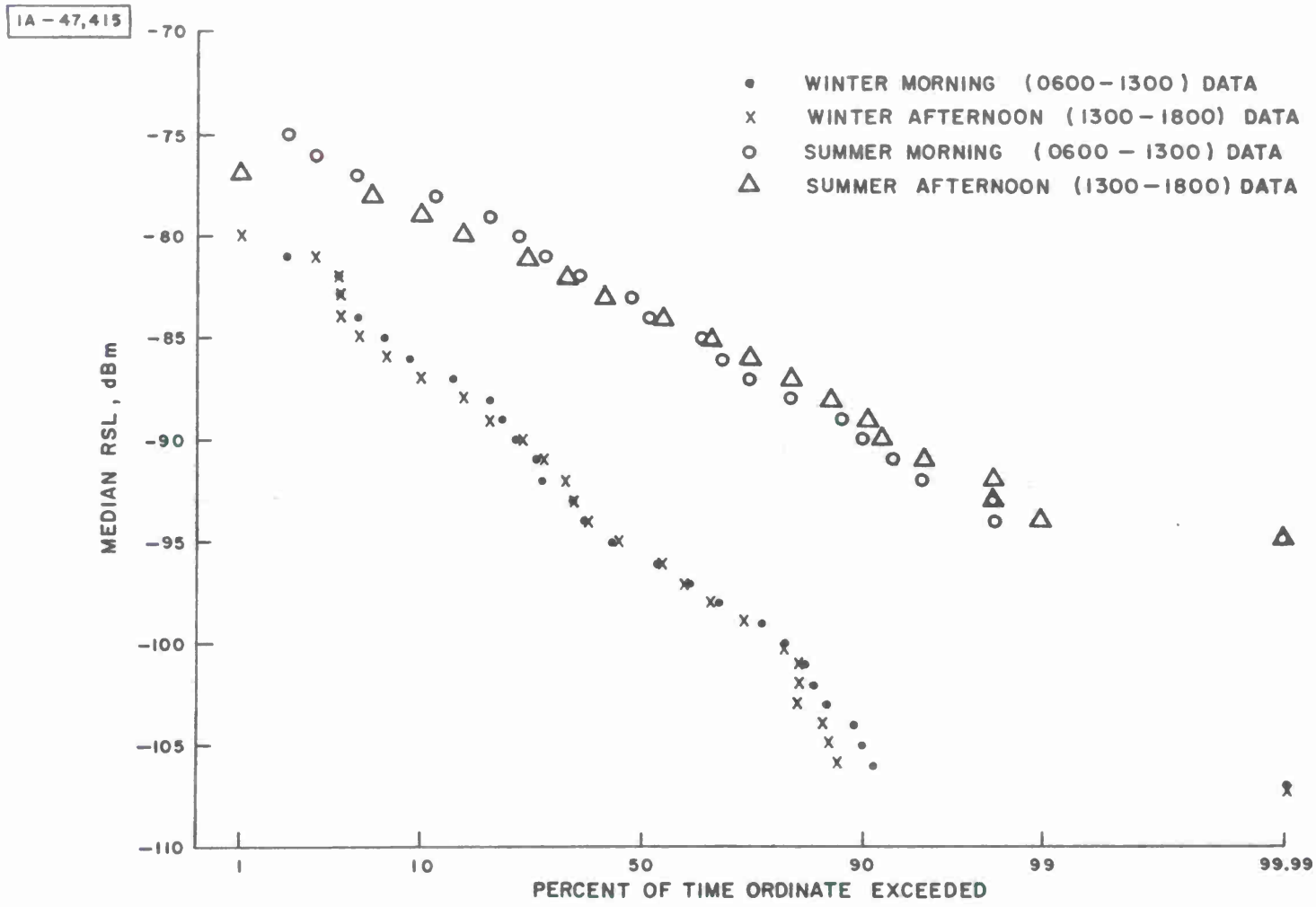

Figure 4-17(a). Median RSL Distributions — XMIT 8 Ft., RCVR 8 Ft., Winter Morning and Afternoon Data, Summer Morning and Afternoon Data (RCVR 1)

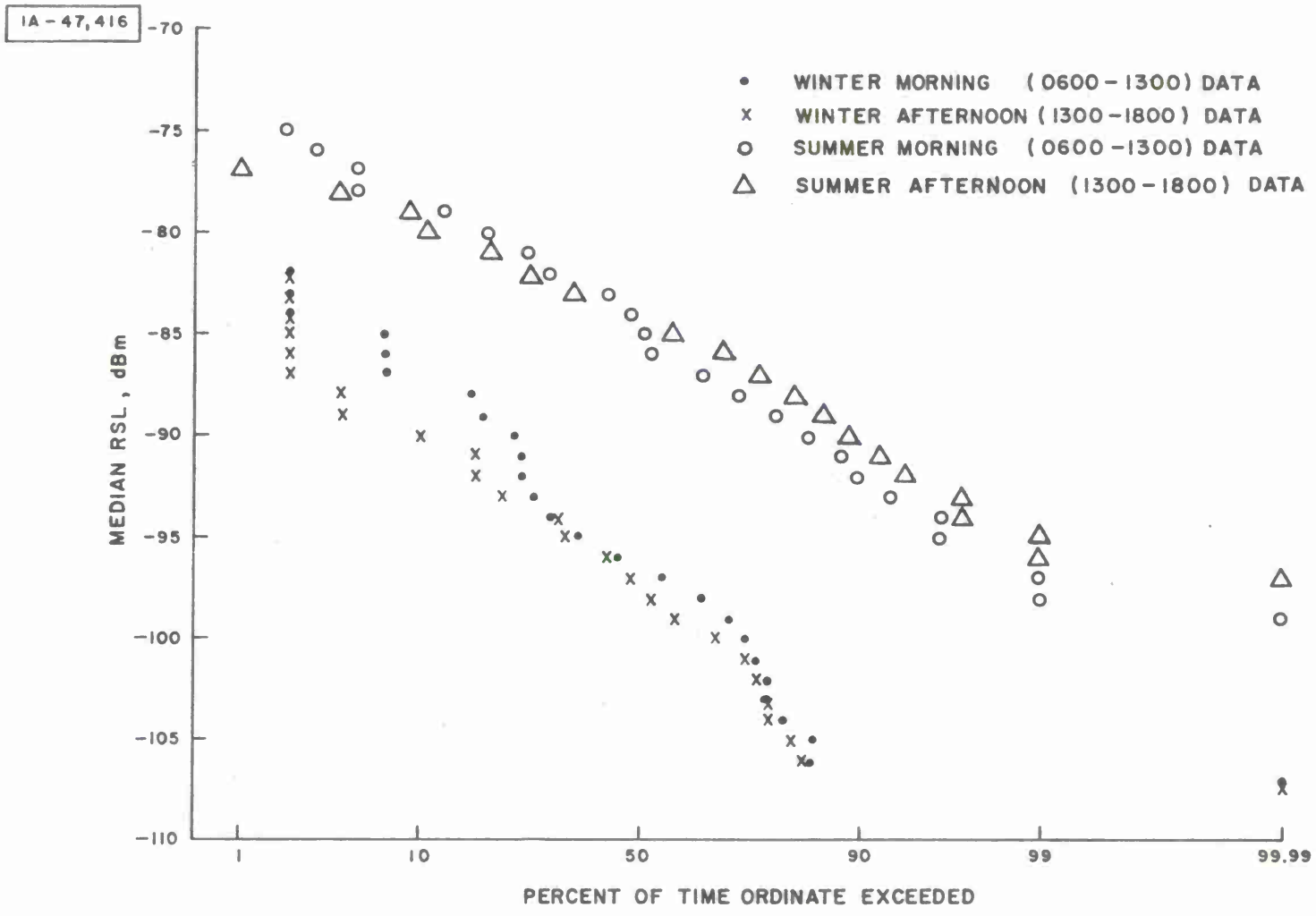

Figure 4-17(b). Median RSL Distributions — XMIT 8 Ft., RCVR 8 Ft., Winter Morning and Afternoon Data, Summer Morning and Afternoon Data (RCVR 2)

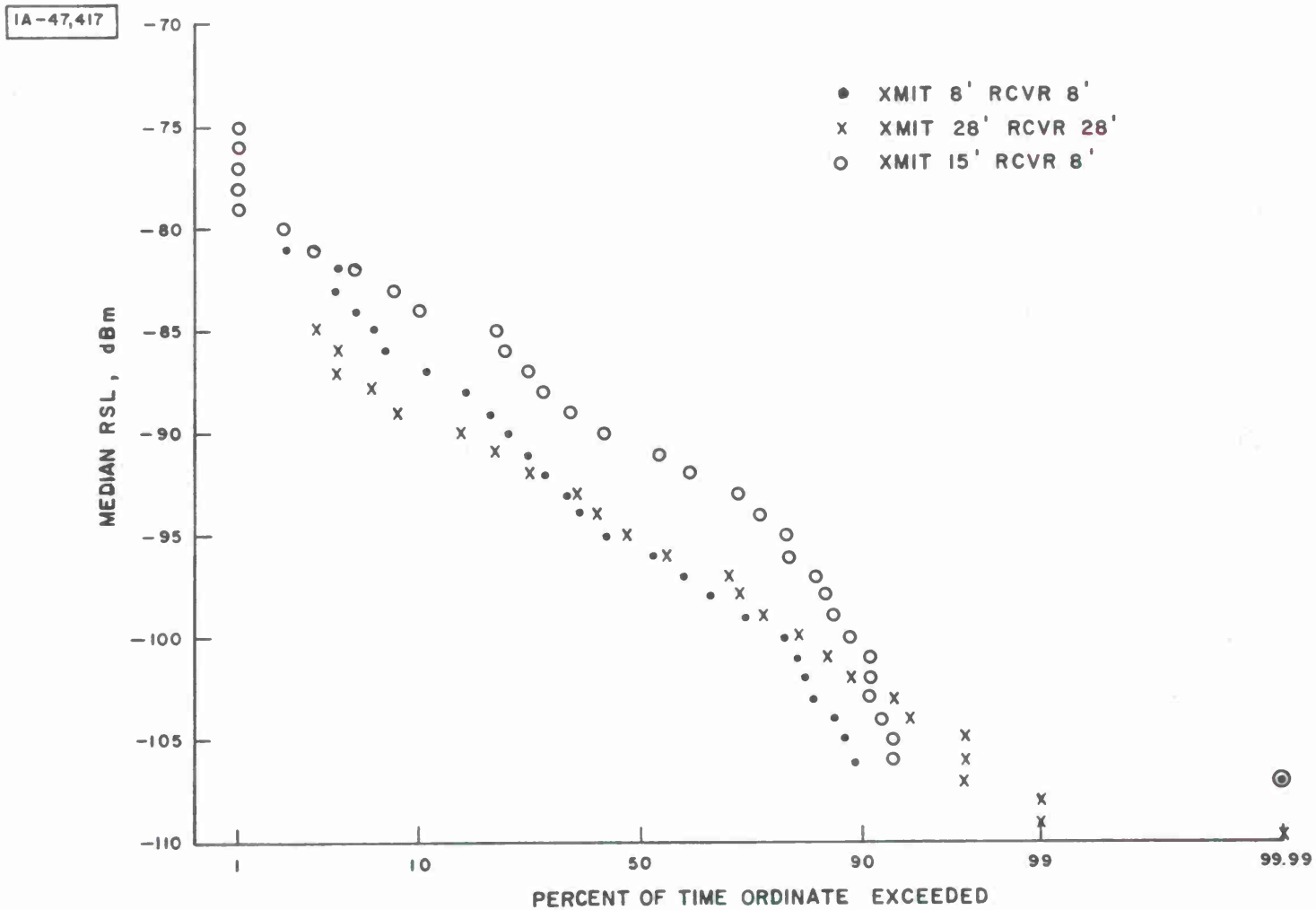

Figure 4-18(a). Median RSL Distributions — Configurations I, III, and V, Winter Data (RCVR 1)

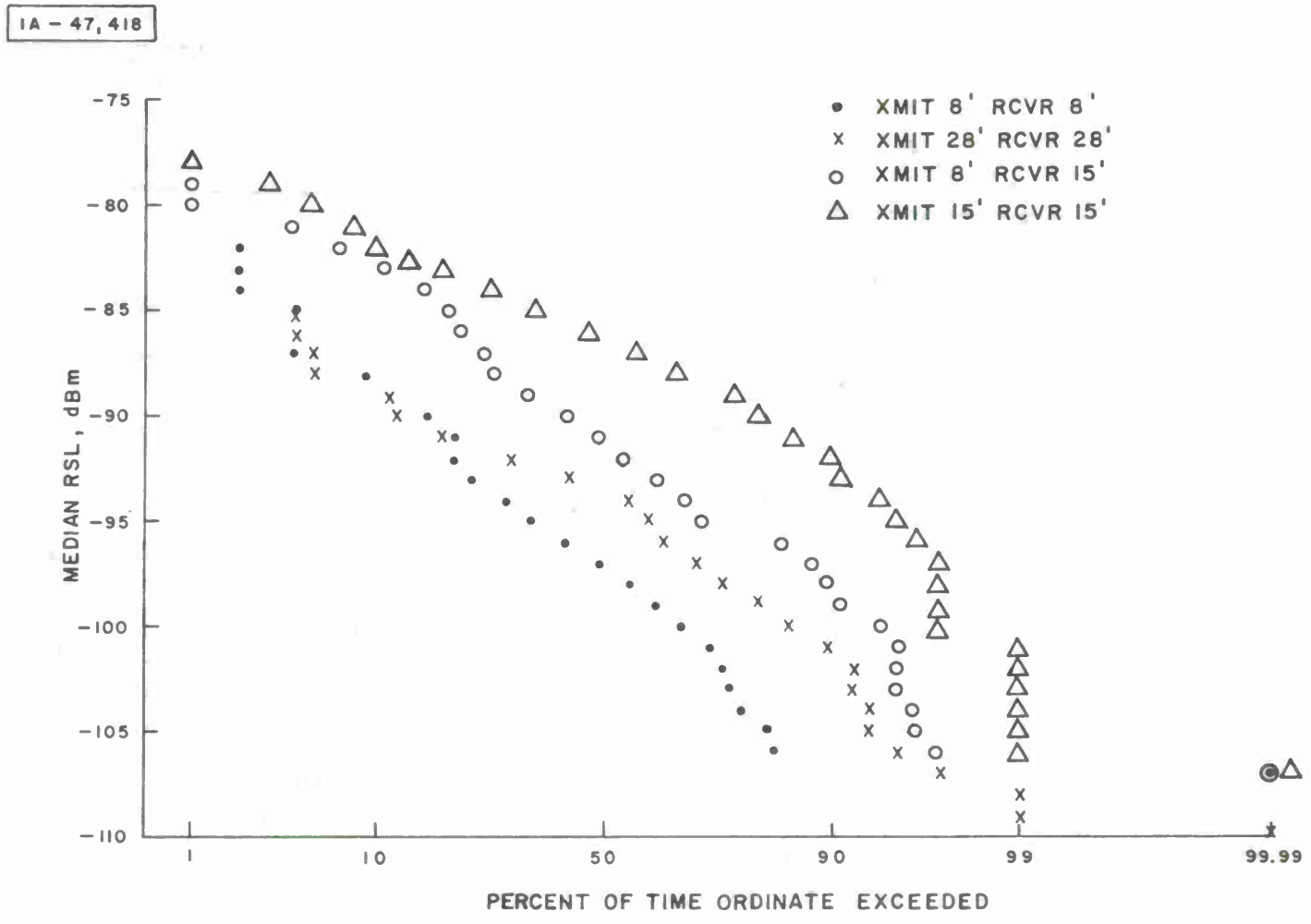

Figure 4-18(b). Median RSL Distributions — Configurations I, II, IV, and V, Winter Data (RCVR 2)

4.4 SCATTER PLOT: MEDIAN RSL VERSUS FADE RATE

Reference 15 (p. 488) presents scatter plots of experimental RSL data versus fade rate for January, April and July. Fade rate is defined as the number of times the signal level exceeds a prescribed level during a unit time interval. For the experimental data shown in the plots, it can be seen that on a monthly basis, high fade rate corresponds to low signal level. Although this is stated as not true for the year, it is true on a monthly basis for data shown for the three months.

To determine whether such a phenomenon exists for the test data from Verona, two scatter plots are shown in Figures 4-19(a) and 4-19(b), which are scatter plots of the median RSL data versus fade rate from test data obtained for January and June 1975, test Configuration I, Receiver 1. Fade rate test data obtained at Verona are numbers of signal level crossing per minute over "running" median levels computed after each minute of the test interval. For a particular test run, say for the nominal 3-minute test interval, fade rate value is not determined for the first minute of testing. Using the median level obtained from signal level samples during the first minute, the number of signal samples crossing this median value is counted for the second minute of testing. After the second minute of testing, the median signal level is determined for the first two minutes of test data, and the number of signal levels crossing this new median level is counted for the third minute of testing. *

The data points in the two scatter plots are hourly median RSL and fade rate test data where, if data are available, all median RSL and fade rate test data between the time interval x minus 29 minutes and x plus 30 minutes (x being the hour) are averaged. The fade rate data are plotted on a logarithmic scale. Figures 4-19(a), and 4-19(b) do not indicate that high fade rates correspond to low signal levels on a monthly basis for the Verona test data.

*Details of this procedure are given in the Suyemoto report, MTR-3016.

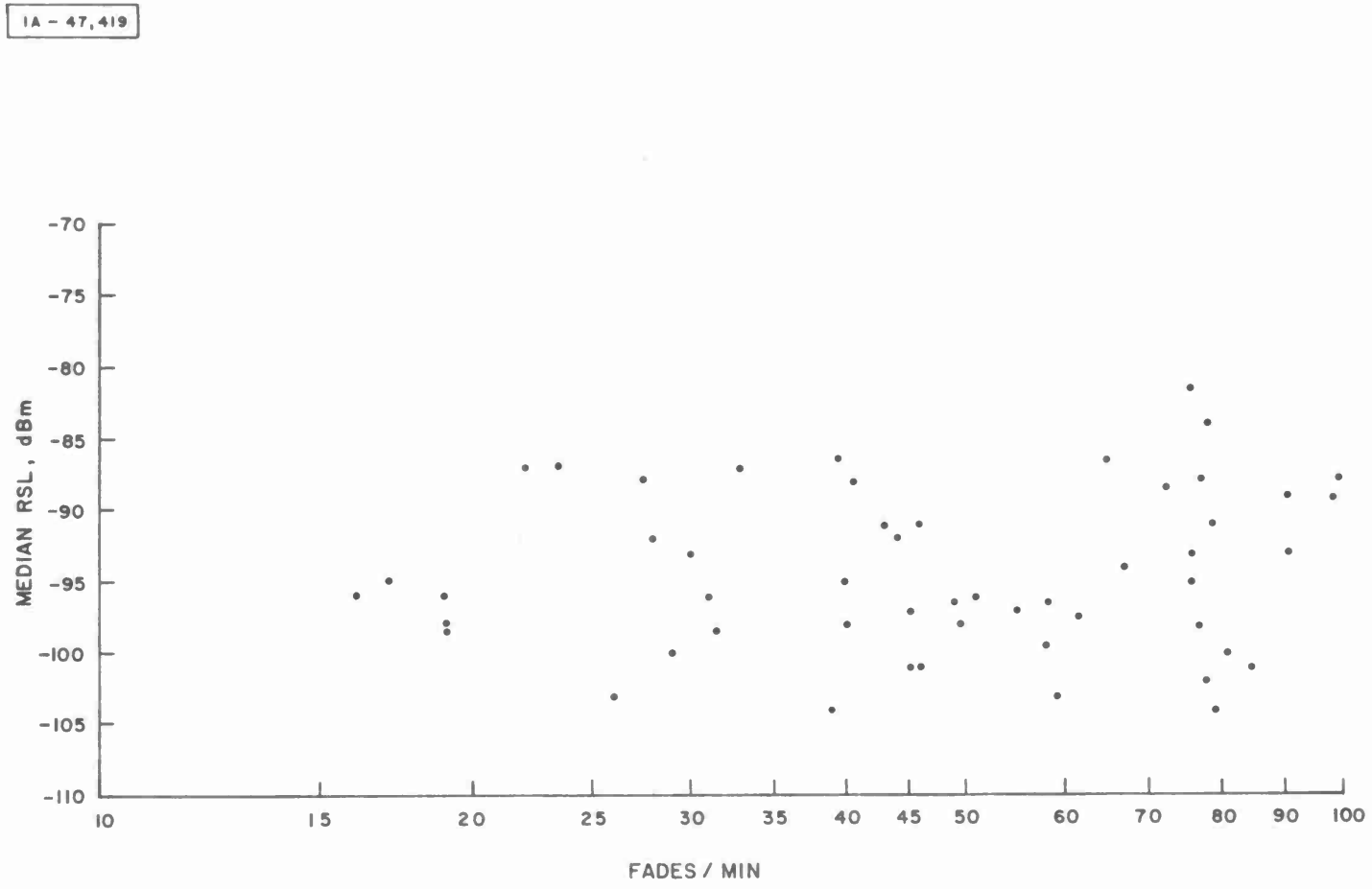

Figure 4-19(a). Median RSL VS Fade Rate — XMIT 8 Ft., RCVR 8 Ft., January 1975 Data (RCVR 1)

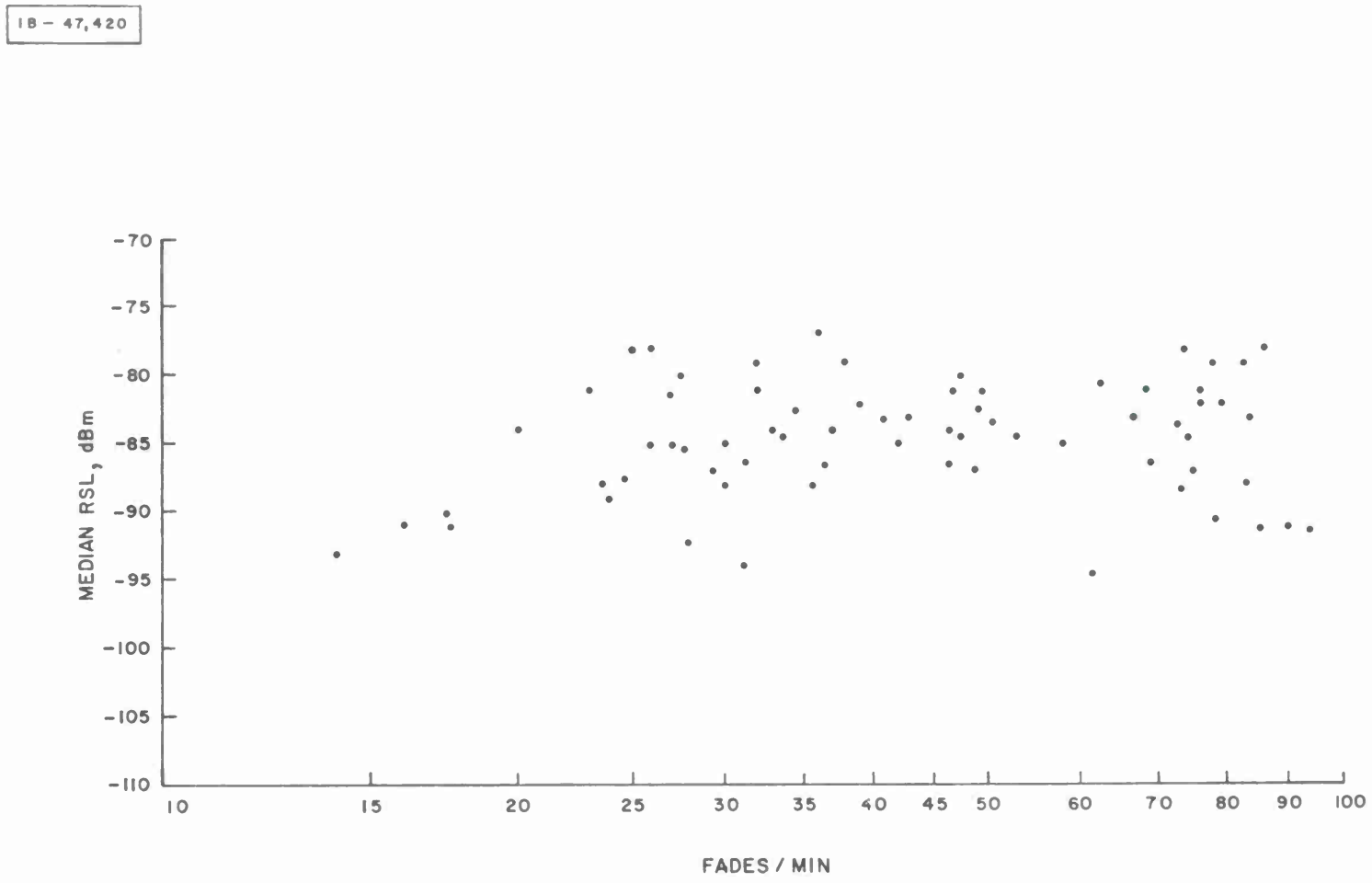

Figure 4-19(b). Median RSL VS Fade Rate — XMIT 8 Ft., RCVR 8 Ft., June 1975 Data (RCVR 1)

4.5 EFFECTIVE EARTH RADIUS COMPUTATIONS

Using radiosonde data obtained at Buffalo for the months November 1974 to August 1975, effective earth radius values are computed as prescribed in Reference 17. The radiosonde data from Buffalo were collected twice daily 0Z (1900 EST) and 12Z (0700 EST). The types of data on the meteorological data tapes provided by USAFETAC have been described in Section 3.

Correlation of the computed effective earth radius values or the refractive index gradients from the Buffalo radiosonde data with the test radio data was not expected. This lack of correlation is seen in results presented in a subsequent subsection. However, the computed effective earth radii are applicable on a long-term and regional basis, i.e., as representative of long-term effective earth radius in the upper New York region. These values are used in Section 4.6 as inputs to a program to compute delay power spectra and these computed values are compared with results in Reference 17, where effective earth radii were computed with radiosonde data from Sola, Norway.

The effective earth radius a is computed from the relation

$$\frac{1}{a} = \frac{1}{R} + \frac{dN}{dZ} \times 10^{-6} \qquad (4\text{-}1)$$

where R is the radius of the earth (R is taken as the mean radius, 6371 Km) and dN/dZ is the average refractivity gradient from the ground to the common volume, N units per Km. The data values of dN/dZ on the

meteorological data tapes are obtained by differencing successive computed values of N at the different levels reported.

The refractivity N (where $N = (n-1)\,10^6$, n being the refractive index), is obtained from the relationship

$$N = 77.6\ \frac{P}{T} + 3.73 \times 10^5\ \frac{e}{T^2} \qquad (4\text{-}2)$$

where P is the total pressure in millibars, T the absolute temperature and e the water vapor pressure in millibars. The value of N is available as part of the data on the meteorological data tape for each of the levels reported.

It is assumed in computing a that the refractivity gradient dN/dZ is constant from the ground to the common volume and that the radio beam is in a near-horizontal direction. The minimum pressure level used is 600 millibars (about 4.2 Km in height), and thus the value of dN/dZ used in (4-1) is the average of dN/dZ values on the data tapes up to the 600-millibar level. This level was chosen since it covers most height intervals used for a troposcatter radio link.

The phenomenon of ducting, superrefraction or subrefraction occurs at the levels in the atmosphere where the refractive index gradient has the following values [18]:

Ducting: $\frac{dN}{dZ} < -159.6$ N units/Km

Superrefraction: $-100 < \frac{dN}{dZ} < -159.6$

Subrefraction: $\frac{dN}{dZ} \geq 0$

The number of occurrences of ducting, superrefraction and subrefraction determined from the Buffalo radiosonde data is shown in Figure 4-20. Occurrences over the months November 1974 to August 1975 of ducts at Buffalo from all radiosonde data available is 26 percent.

The number of sets of twice-daily radiosonde data reported per month, the number of sets of the total for which ducting did not occur and the monthly mean and median values of the radio a/R are given in Table 4.5.

Figure 4-21(a) shows comparison probability plots for winter and summer of the computed a/R ratios. Also shown are the probability plots from Figure 1 in Reference 17 of the a/R ratios obtained from the radiosonde data from Sola, Norway for winter and summer. It can be observed that although the separation between winter and summer Buffalo data appears to be the same in magnitude as that of the winter and summer data from Sola, Norway, the slopes of the plots are obviously not; the Buffalo data exhibit a much wider variance. Figure 4-21(b) presents comparison probability plots of the a/R ratios computed from winter and summer morning (12Z) and afternoon (0Z) Buffalo radiosonde data. The seasonal variations in the values of a/R can be seen with the summer values being greater than the winter values. A morning and afternoon variation for winter is not observed, while there appears to be distinct variation for summer.

From monthly mean and median values of a/R given in Table 4-5 and from probability plots in Figures 4-21(a) and 4-21(b), the use of the standard 4/3 earth model for theoretical evaluation or prediction of radio

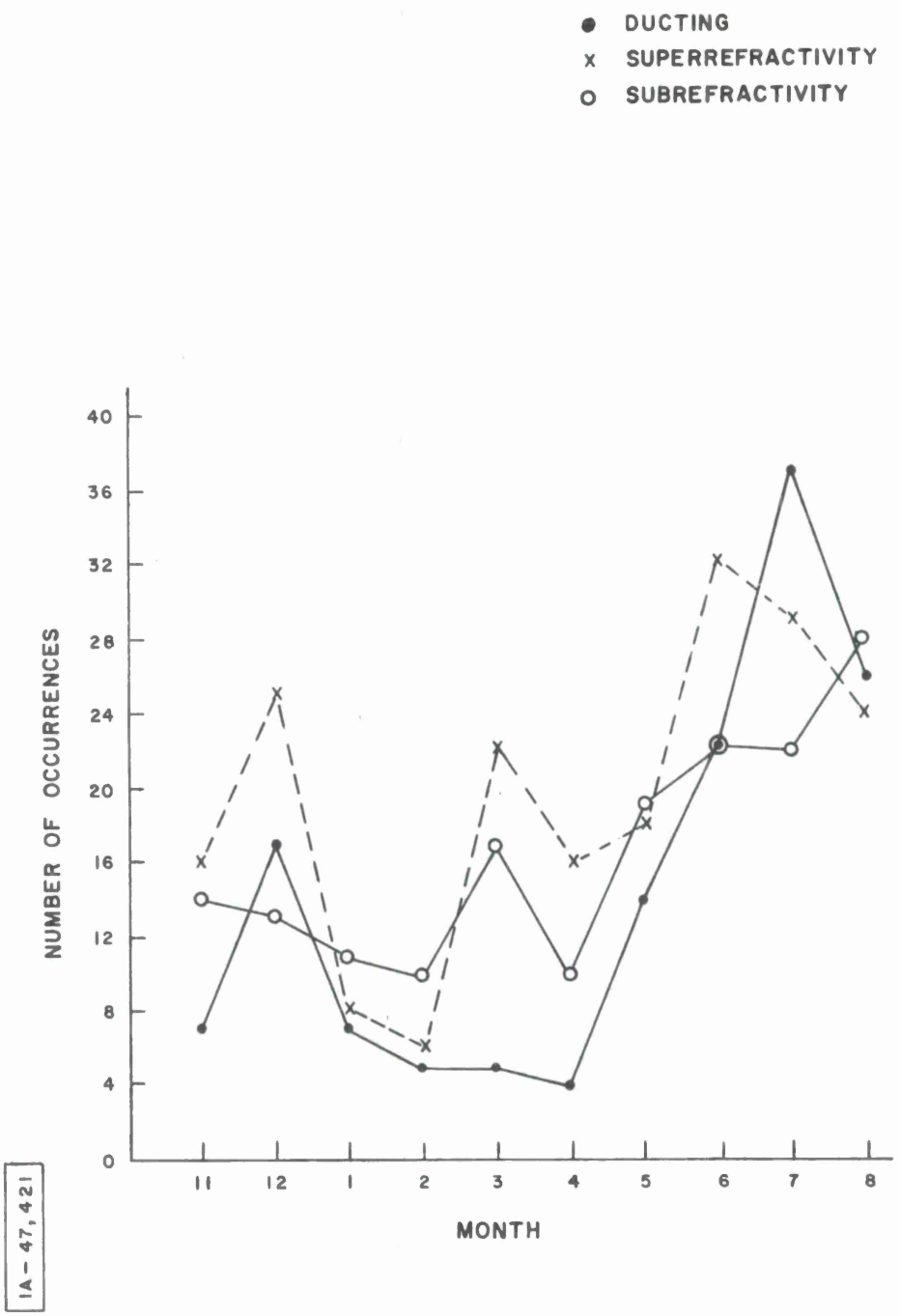

Figure 4-20. Occurrences of Ducting, Superrefraction, and Subrefraction (Buffalo)

Table 4-5

Monthly Mean and Median Values of a/R

Month	No. of 0Z and 12Z Radiosonde Data	No. of Non-ducting Sets of Data	Mean a/R	Median a/R
1974				
NOV.	56	49	1.32	1.31
DEC.	57	40	1.33	1.33
1975				
JAN.	51	44	1.31	1.30
FEB.	55	50	1.29	1.28
MAR.	60	55	1.30	1.29
APR.	55	51	1.30	1.30
MAY	54	40	1.31	1.32
JUNE	57	35	1.36	1.34
JULY	57	20	1.32	1.39
AUG.	56	30	1.36	1.34

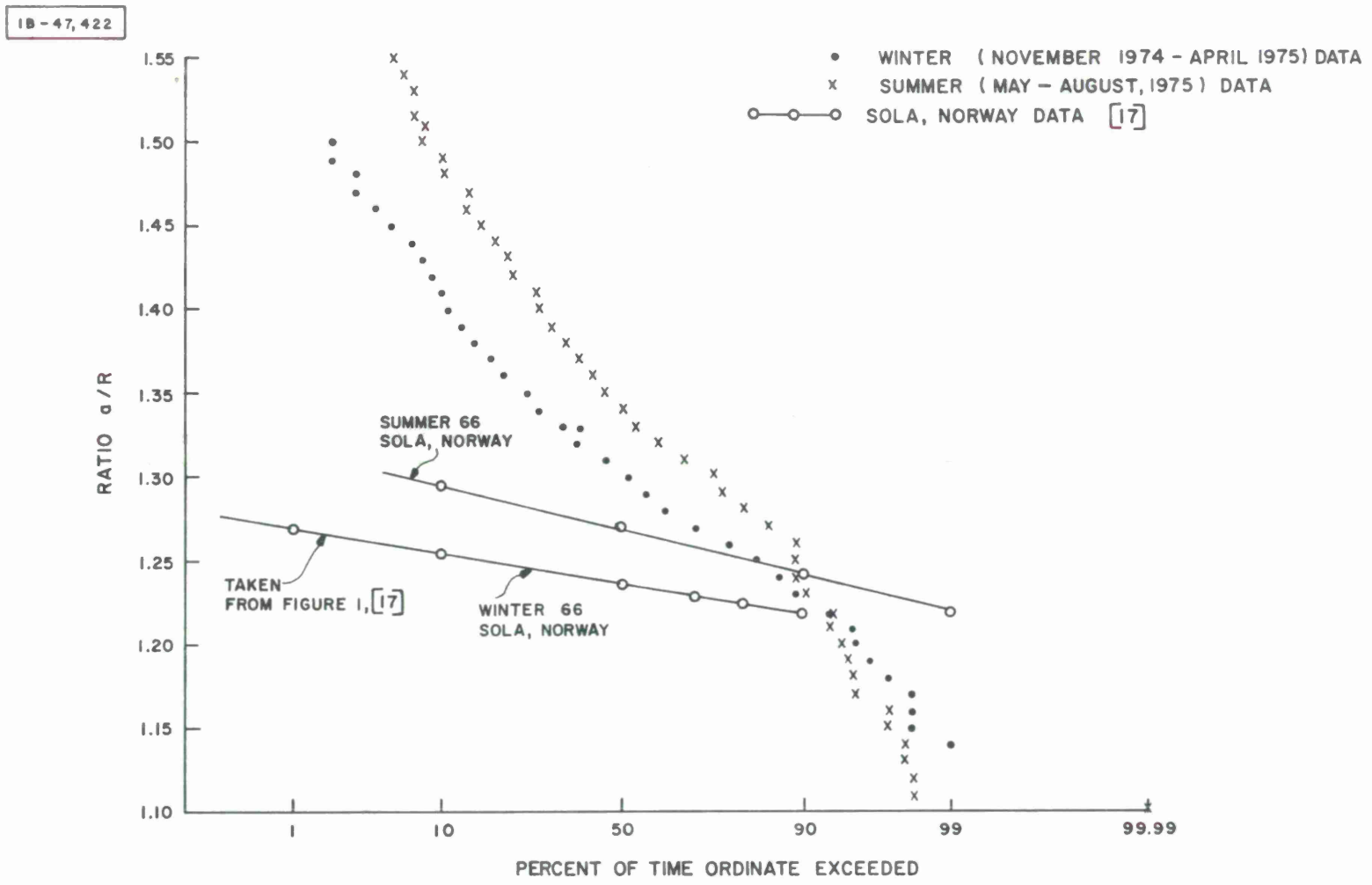

Figure 4-21(a). Ratio a/R Distributions — Winter and Summer Data (Buffalo; Sola, Norway)

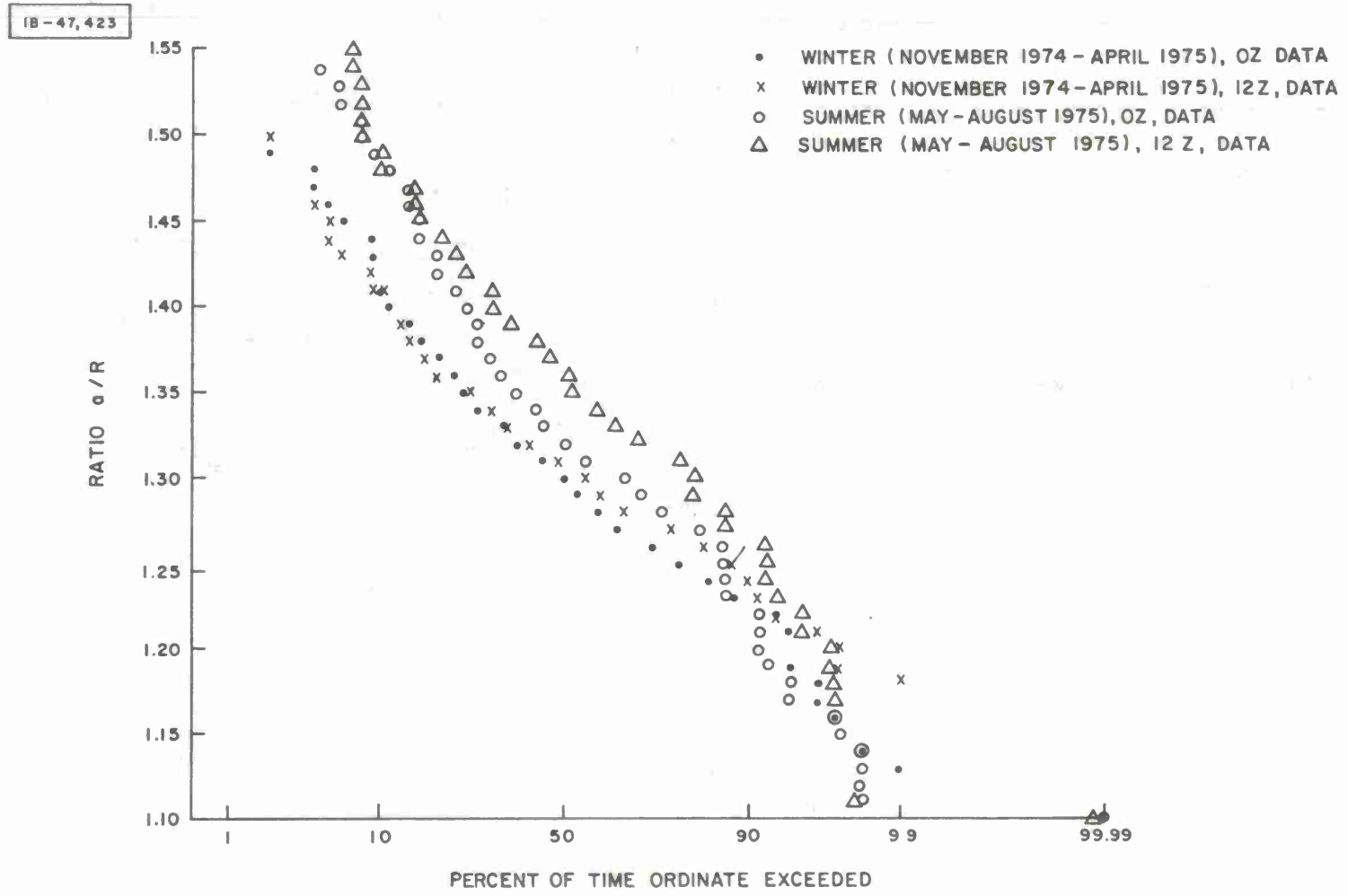

Figure 4-21(b). Ratio a/R Distributions — Winter Morning and Afternoon Data, Summer Morning and Afternoon Data (Buffalo)

parameters is appropriate for tropo radio links in the region near Buffalo and as a long-term model.

An unsuccessful attempt was made to evaluate the exponent n in the relation $\Phi(K) \sim K^{-n}$, where $\Phi(K)$ is the refractive index irregularity spectrum [17] and K, the wavenumber, is a function of wavelength λ and scatter angle θ. (This exponent n is equivalent to the scattering parameter m in the Bello model, see Section 5.3.) Following the formulation given in Reference 17, n is determined from temperature and temperature gradient profile available from radiosonde observations and a linear equation (Equation 6 in Reference 17). The values of the coefficient in the referenced equation had been obtained from experimental data collected in Norway [19]. It appears that the coefficients are not applicable to the Buffalo radiosonde data as their application resulted in unreasonable values of the exponent n.

4.6 THEORETICALLY COMPUTED VALUES OF THE MULTIPATH DELAY SPREAD

A computer program obtained from CNR, Inc., for the computation of the delay power spectra was run to obtain values of multipath delay spread. This program evaluates the delay power spectra from a double integral (Equation 67 in Reference 20) in contrast to the evaluation of the delay power spectra from a single integral (Equation 33 in Reference 1) which is usually referred to as the Bello-Channel model.

The following relevant inputs required to exercise the computer program were determined for the short Configuration I and long Configuration V path troposcatter radio links. The distance between the transmit and receive sites for the short path is 138.4 Km (86 miles), and the half power beamwidth is 1.88^{o} for both the receive and transmit antennas. The distance between the transmit and receive sites for the long path is 270.8 Km (168 miles) and the half power beamwidth is $.54^{o}$ for both the receive and transmit antennas.

Three values of the effective earth radius were used: 9556.5 Km, 8282.3 Km and 7645.2 Km. These three values correspond approximately to the a/R ratios of 1.50, 1.30 and 1.20. From Figure 4-21(a) these values correspond approximately to the .05, .50 and .95 points on the probability plot when all a/R ratios computed from the Buffalo radiosonde data are considered. Another input required for running the program is the exponent value n in the relation $\Phi(K) \sim K^{-n}$, the slope of the refractive index irregularity spectrum. From experimental data, values of n reported in the literature [17] range from 2 to 6 with the median value 11/3. Four values of n used as inputs to the program are 5.0, 3.6667, 3.0, and 2.50.

Figure 4-22(a) shows the short path geometry where the centers of the transmit and receive antenna beams are elevated 3/4 degree above horizontal at the terminal sites. The intersection of the center rays determine the low points of the common volume. It is assumed that antenna alignment for maximum RSL corresponds to the antenna bore sight's being on the radio horizon. This results in a shadow zone that corresponds to the lower half of the beam pattern. Figure 4-22(b) shows the long path geometry where the center of the transmit antenna beam is elevated 0.5 degree above horizontal and the receive antenna is at zero degree elevation.

The basic computer model includes a standard antenna beamwidth reduction factor of 0.6 (see Equation 35 in Reference 1). In addition to using the standard factor, results have also been obtained using a factor of 0.7.

Results from computer runs for the various combinations of values for a/R, n and multiplicative factors are shown in Table 4-6(a) for the short path and Table 4-6(b) for the long path. The delay spread values (in μs) tabulated are two-sigma values. From Figure 4-12(a), the two-sigma delay spread values of the test data for the short path at the .05, .50 and .95 probability points are respectively about .28, .17 and .10 μs, while for the long path at the same points from Figure 4-15(a), the two-sigma spread values are .20, .15 and .10 μs. The two-sigma median values of .17 μs for the short path and .15 μs for the long path are larger than any of the tabulated computed values; the difference between the median value and computed values is much larger for the long path.

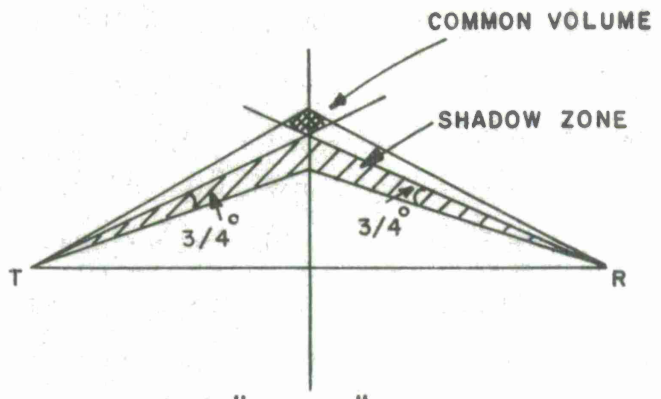

(a) "SHORT" PATH

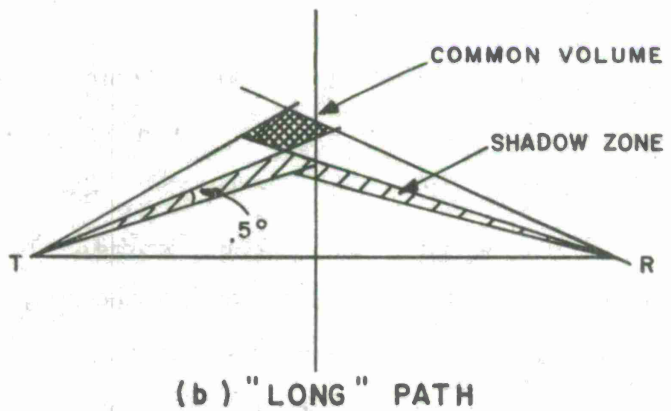

(b) "LONG" PATH

IA - 47,424

Figure 4-22. Geometries Used For Multipath Model

Table 4-6(a)

Computed Delay Power Spread (2σ), μs,
Short Path

a/R	Beamwidth Reduction Factor	Exponent =			
		5.00	3.6667	3.00	2.50
1.50	.6	.0722	.0864	.0944	.1010
	.7	.0938	.1132	.1244	.1332
1.30	.6	.0784	.0934	.1018	.1084
	.7	.1014	.1216	.1328	.1418
1.20	.6	.0818	.0968	.1054	.1122
	.7	.1054	.1256	.1370	.1462

Table 4-6(b)

Computed Delay Power Spread (2σ), μs,
Long Path

a/R	Beamwidth Reduction Factor	Exponent =			
		5.00	3.6667	3.00	2.50
1.50	.6	.0118	.0130	.0138	.0144
	.7	.0202	.0226	.0240	.0250
1.30	.6	.0154	.0170	.0178	.0184
	.7	.0254	.0280	.0296	.0306
1.20	.6	.0186	.0204	.0214	.0222
	.7	.0300	.0328	.0344	.0358

4.7 COMPARISON OF TEST DATA WITH METEOROLOGICAL DATA

In this section, various comparisons are made of the test data with meteorological data from Syracuse, Rochester and Buffalo. These comparisons are made for different time blocks--monthly, daily and hourly. Correlation values are obtained and scatter plots drawn for various time blocks of test data, surface refractivity data and the a/R ratios. Because meteorological data are obtained from locations in the relative proximity of the tropo radio test paths but not along the test paths (see Figure 2-1), correlation values, except on a long-term basis (e.g., monthly) for various time blocks, may not be representative of the true correlation.

4.7.1 Monthly Average

Monthly average path loss and RMS multipath delay data for test Configuration I, Receiver 1, were computed for the eight months that testing was performed for the configuration. Monthly average of the surface refractivity, N_s, data was also computed from surface meteorological data obtained at Syracuse.

The monthly averages for the N_s data in Figure 4-23(a) were computed as follows. Since N_s data are obtained hourly, a 1-to-1 correspondence of the path loss data with the N_s data (local time) was made with the time of the test data rounded to the closest hour, e.g., 1029 taken as 1000 local time. With this 1-to-1 correspondence, monthly averages of the path loss and N_s data were computed; the scatter plot for eight points (monthly averages) is shown in Figure 4-23(a). In Figure 4-23(b), the monthly averages of the N_s data from Syracuse include all values of N_s reported (usually 24 reports a day).

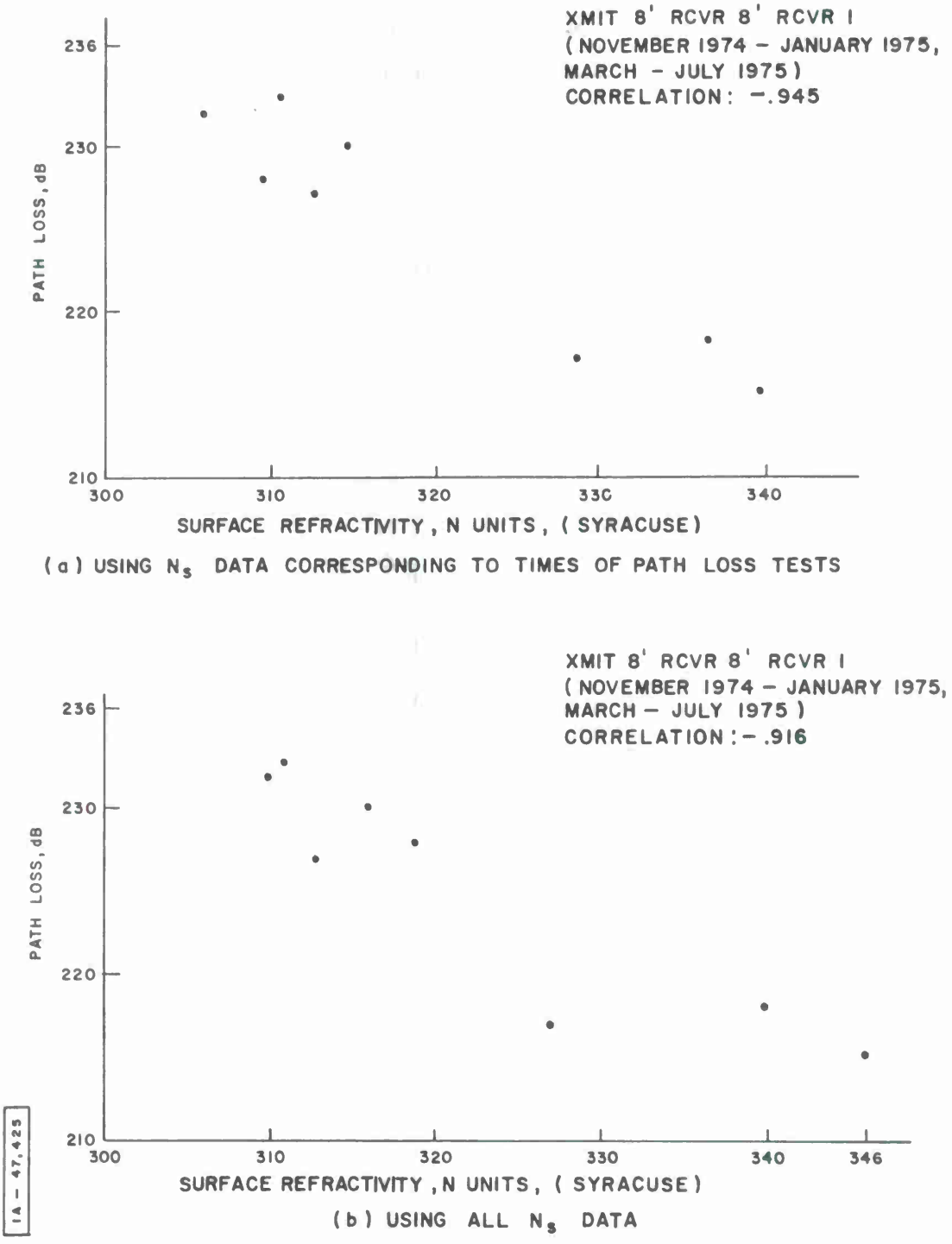

Figure 4-23. Mean Monthly Path Loss VS Mean Monthly N_s

A graph of the monthly averages (all data reported) of N_s from Buffalo, Syracuse and Rochester is presented in Figure 4-24, for the months of November 1974 - August 1975. From this graph, it can be seen that the monthly spread of N_s at these three locations is generally 3 N units, maximum spread 6 N units. Thus, on a long-term basis (monthly average) N_s reports from one station appear adequate for the entire region in upper New York.

Although the correlation values of data in the scatter plots of Figure 4-23(a) and 4-23(b) are high, it should be noted that there are only eight data points.

Figures 4-25 and 4-26 are scatter plots of the monthly averages of path loss data and a/R ratios, and of the RMS delay data and a/R ratios. Correlation values are shown on the figures. These values indicate slight correlation for path loss and little correlation for RMS delay with a/R ratios.

Correlation values between all path loss data and all RMS delay spread data obtained in a month for each of eight months were computed for test Configuration I, Receiver 1. These values along with the number of data samples per month are tabulated in Table 4-7. Although this table does not contain results of comparison of test data with meteorological data, it is included here because of the grouping of the test data by months. Comparison of values in this table with values in Table 4-4 indicates that this grouping did not greatly change the extent of correlation. High correlation value for April 1975 can be reasonably explained by the small number of test data.

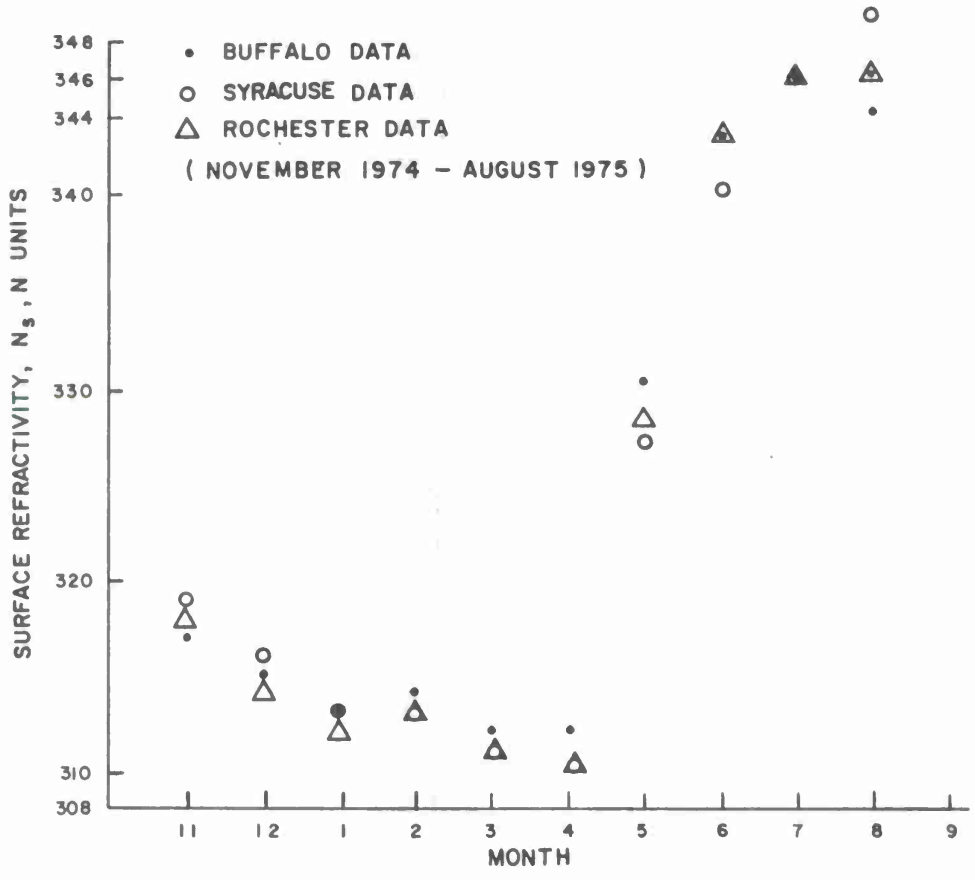

Figure 4-24. Monthly Average N_s

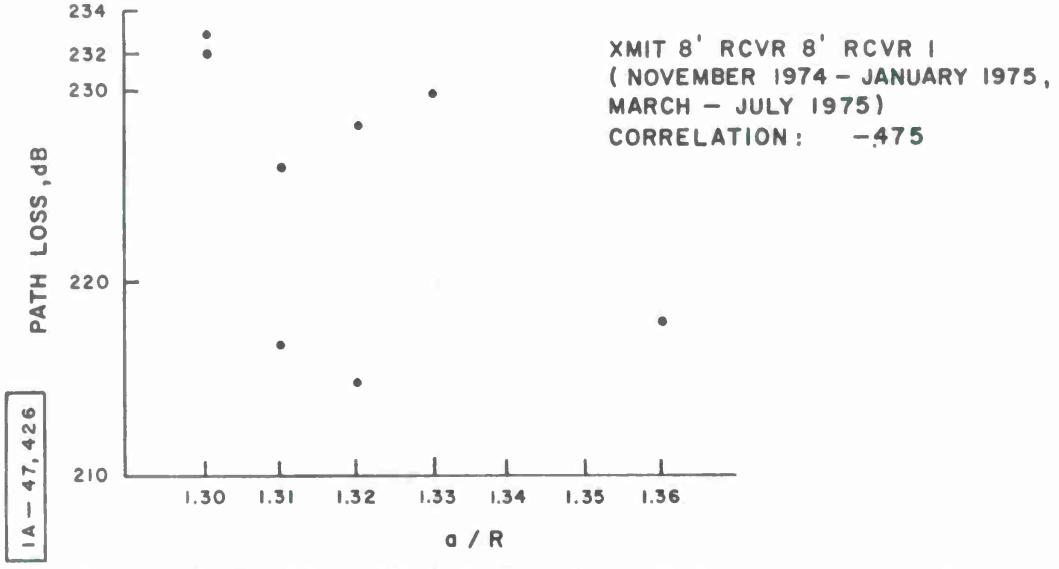

Figure 4-25. Mean Monthly Path Loss VS Mean Monthly a/R

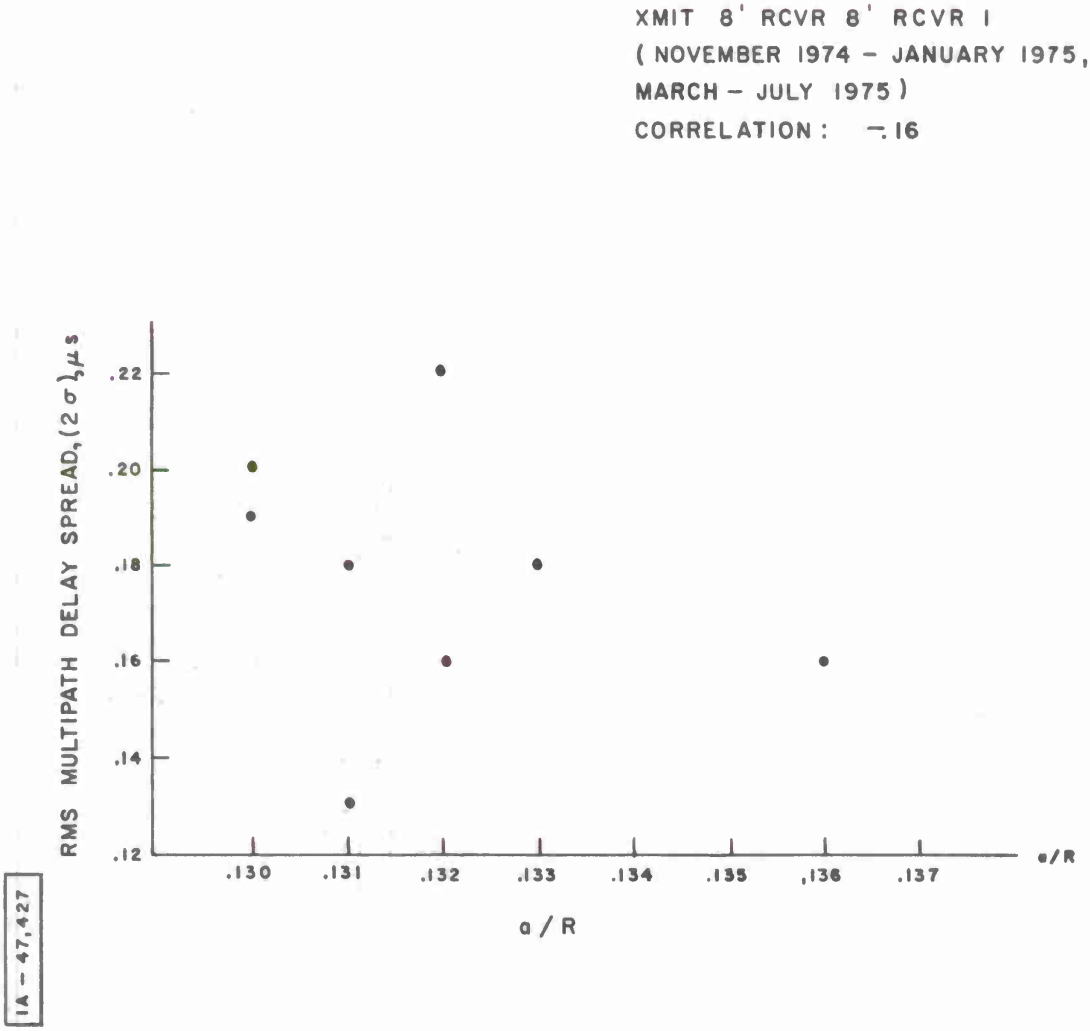

Figure 4-26. Mean Monthly RMS Delay Spread VS Mean Monthly a/R

Table 4-7

Monthly Correlation Values of Path Loss Versus RMS Delay Spread (Test Configuration I, Receiver 1)

Date	No. of Samples	Correlation Values Path Loss VS. RMS Delay
1974		
NOV.	28	.326
DEC.	81	.343
1975		
JAN.	96	-.043
MAR.	43	.355
APR.	13	.627
MAY	208	.311
JUNE	189	.359
JULY	37	.194

4.7.2 Daily Averages

Daily averages of test data for the various test configurations were computed. Daily averages of N_s were computed from meteorological (surface) data from Syracuse and Rochester. For daily averages of path loss and RMS delay spread and corresponding daily average of N_s from Syracuse, correlation values were computed for test Configurations I-IV. Daily averaged test data and N_s data from Rochester for test Configuration V were also computed. Correlation values of the daily averaged test data for test Configuration I and V, Receiver 1, were computed and the daily average of the a/R ratios computed from radiosonde data from Buffalo. These correlation values along with the number of samples (daily averages) used are tabulated in Table 4-8. The correlation value for test Configuration I, Receiver 1, is relatively large in magnitude but less than the correlation value for monthly averages (Figure 4-23b). Figure 4-27 is a scatter plot of this particular set of data.

Table 4-8

Correlation Values of Averaged Daily Path Loss, RMS Delay Spread Data vs Averaged Daily N_s, a/R

Configuration Number	Receiver Number	Correlation: Surface Refractivity Versus			Correlation: a/R Ratio Versus		
		No. of Samples	Path Loss	RMS Delay	No. of Samples	Path Loss	RMS Delay
I	1	90	-.680		81	-.296	
		86		-.068	77		-.067
V	1	19	-.682		17	-.418	
		17		-.388	15		.188
II	2	35	.022				
		33		.037			
III	1	19	-.233				
		19		.040			
IV	2	18	-.008				
		17		-.191			

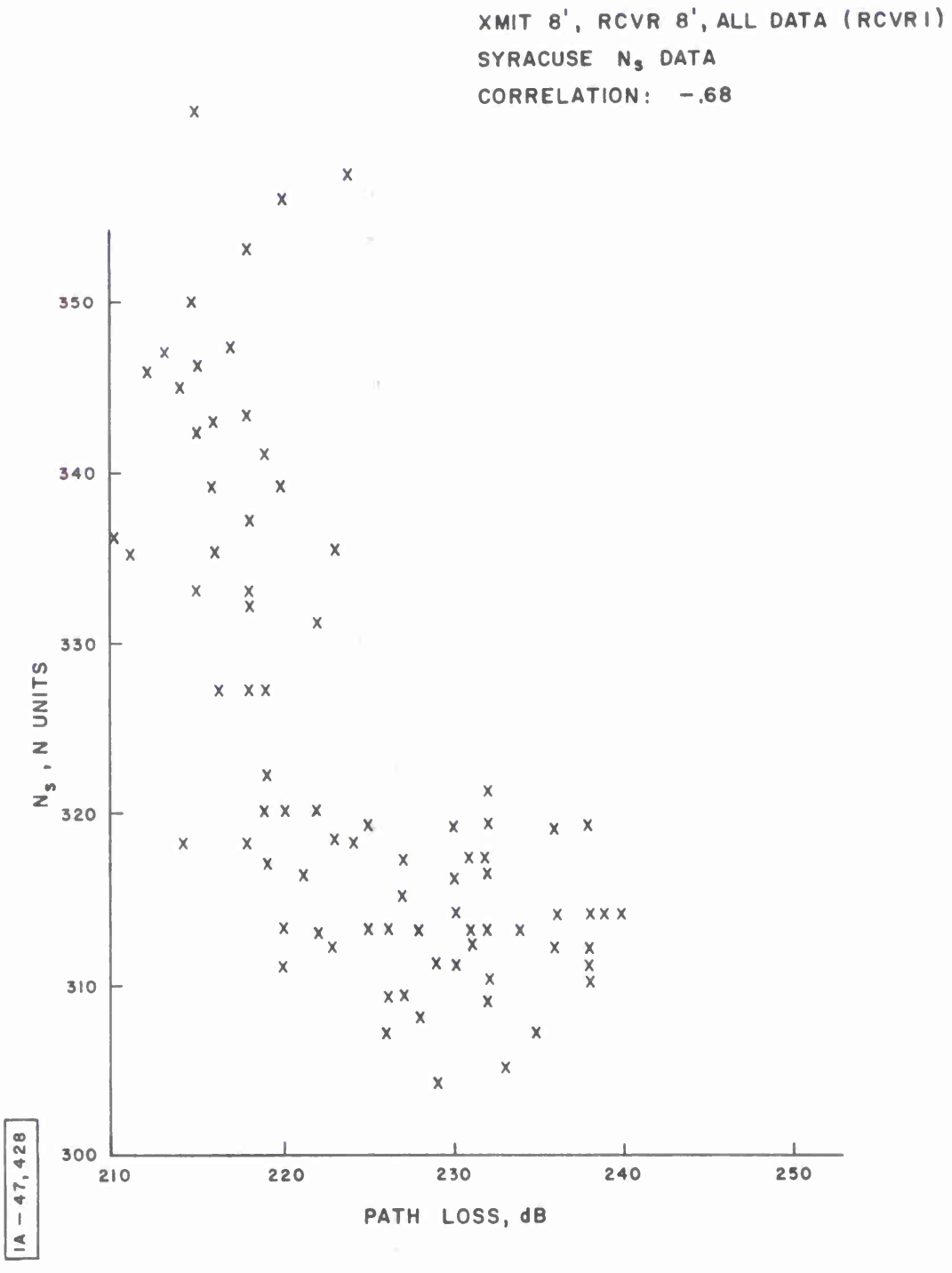

Figure 4-27. Daily Averaged Path Loss Data VS Daily Averaged N_s

4.7.3 Hourly Averages

Hourly averages of test data for test Configuration I, Receiver 1, and test Configuration V, Receiver 1, were computed. Path loss and RMS multipath spread values in the interval x - 29 minutes, x + 30 minutes, (where x is the hour) were averaged. Corresponding hourly reports (local time) of N_s from Syracuse, (test Configuration I) and from Rochester (test Configuration V) were used. Correlation values for N_s versus test data along with the number of samples are tabulated in Table 4-9. For test Configuration I, Receiver 1, a steady decrease in the magnitude of correlation between path loss and N_s can be seen for the monthly, daily and hourly averages.

Table 4-9

Correlation Values of Averaged Hourly Path Loss, RMS Delay Spread vs Hourly N_s

Configuration No.	Receiver No.	No. of Samples	Correlation: N_s Versus	
		No. of Samples	Path Loss	RMS Delay
I	1	394	-.562	
		379		.016
V	1	70	-.571	
		69		.404

Hourly averages of test data within a month for two winter months, December 1974 and January 1975, and two summer months, May and June 1975, were computed. Comparison plots of the hourly averaged median RSL data, hourly averaged RMS delay spread and the hourly averaged N_s data from Syracuse for these four months versus local time of day are shown in Figures 4-28, 4-29 and 4-30.

From Figures 4-28 and 4-29, it can be seen that tests normally were conducted between 0800 -1900 local time. In Figure 4-28, the two end points 0800 and 1700 for the month of January reflect the fact that only one test for each of the times was conducted during that month. Excluding these two end points, the variations of median RSL values between testing hours is less in the winter than in the summer months. This corresponds with Figure 4-30 where the N_s variations are less in the winter than in the summer months. From Figure 4-29, it appears that for May and June, the RMS delay spread is less in the morning than in the afternoon (for the hours when tests were conducted, 0800-1900), whereas for December and January the RMS delay spread is greater in the morning than in the afternoon. From Figure 4-30, a pronounced diurnal fluctuation of N_s can be seen for the summer months of May and June, while for the winter months of December and January, the variation is not great and appears almost flat.

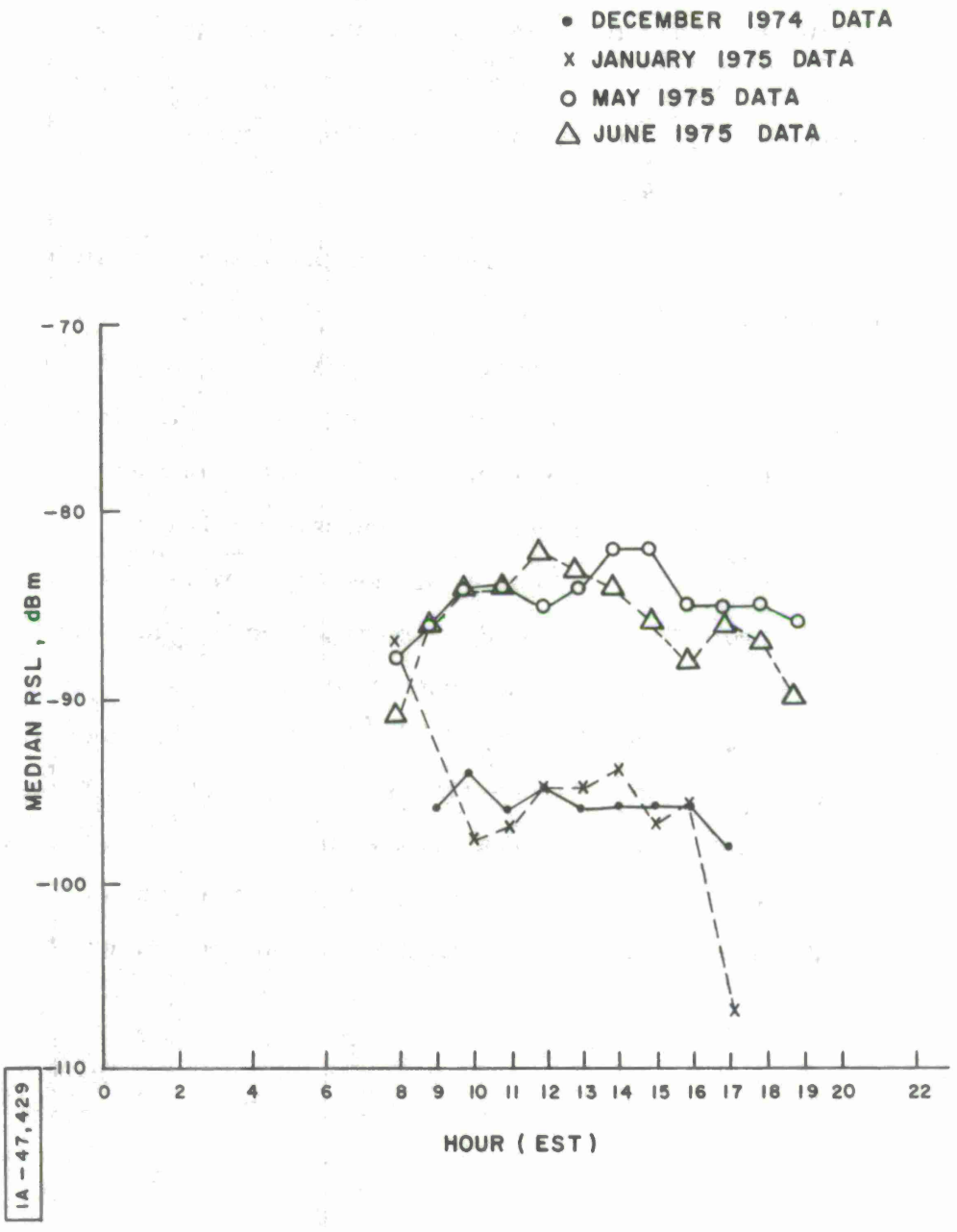

Figure 4-28. Averaged Hourly Median RSL — XMIT 8 Ft., RCVR 8 Ft., (RCVR 1)

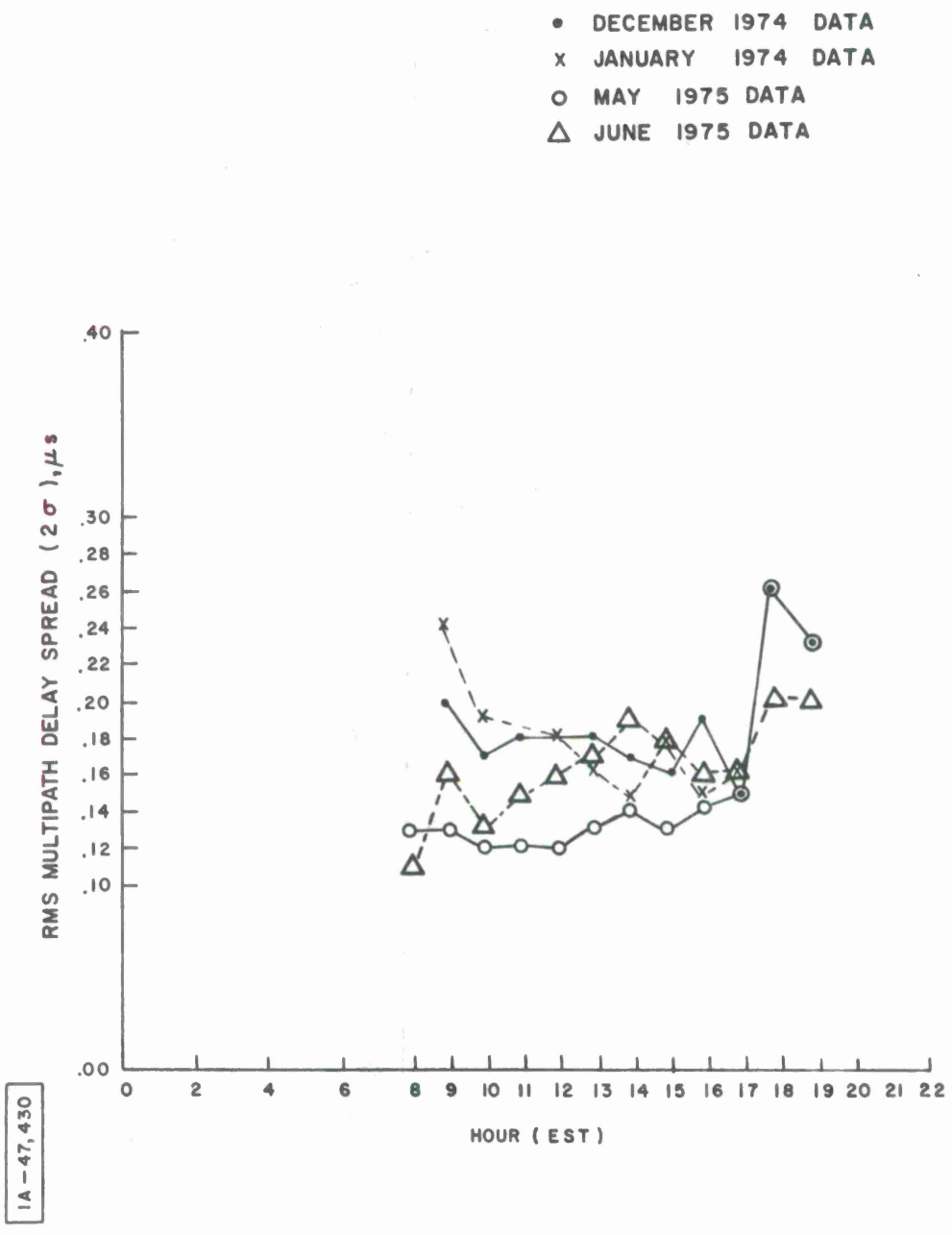

Figure 4-29. Averaged Hourly RMS Delay Spread — XMIT 8 Ft., RCVR 8 Ft., (RCVR 1)

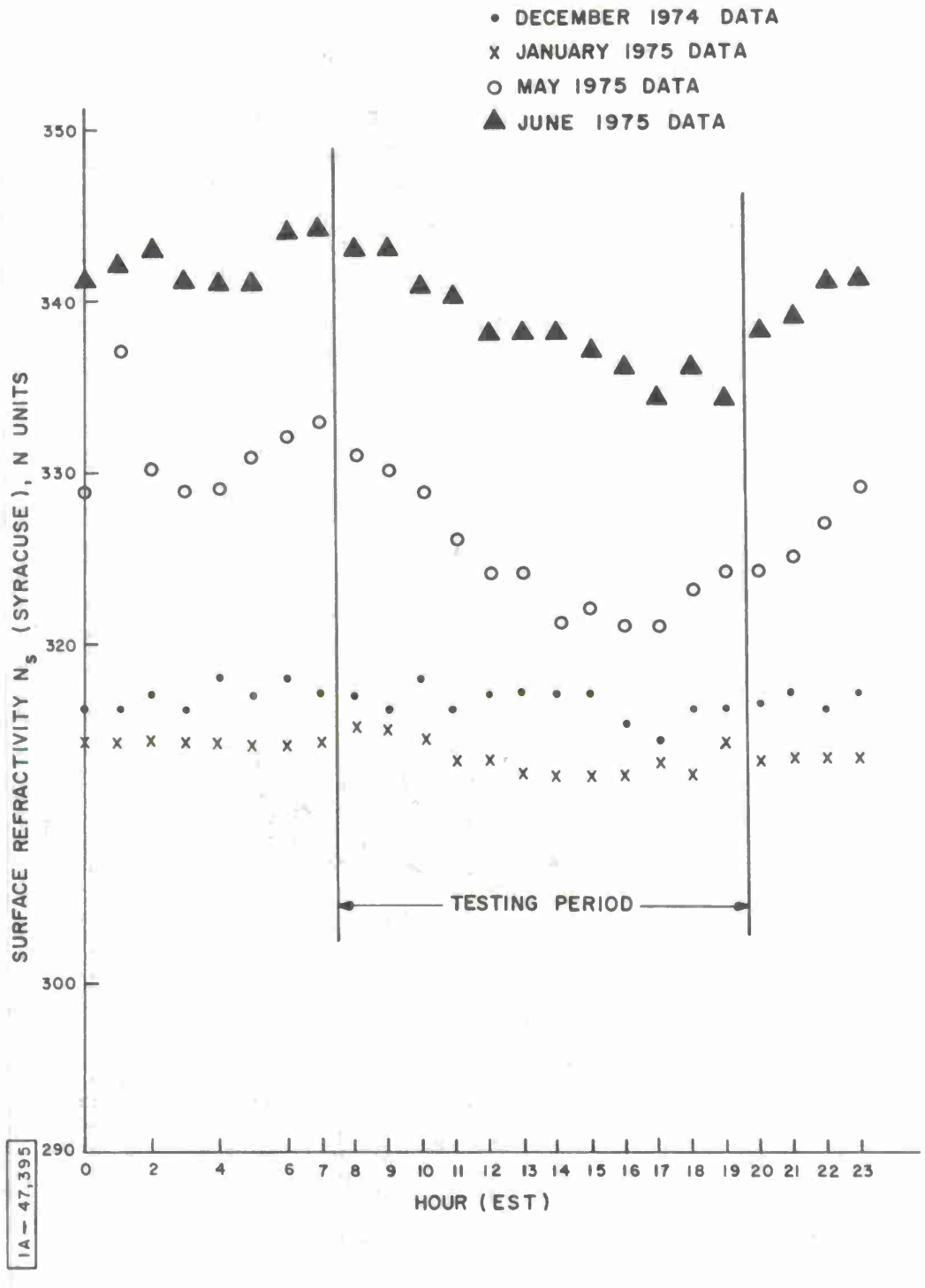

Figure 4-30. Averaged Hourly N_s

4.8 OBSERVATIONS AND SUMMARY OF DATA

Although there are limitations on the test and meteorological data, the set of data obtained from the site at Verona over the duration of the test program is one of the most extensive currently available. It should be noted that certain tests that were planned and scheduled were not performed because of equipment breakdowns or breakdowns or malfunctions of the data processing system. For example, plans for the round-the-clock, 24-hour testing at least one day a week were not carried out often enough to obtain sufficient data. There is also some question of the sufficiency of the number of test data gathered for different test configurations listed in Table 4-1. Consideration of the path loss or received signal level on an hourly ("slow" variations of the level in contrast to "fast" variations of the level) basis would require 1000 hours of testing to reliably determine a 99 percent probability point [16].

As stated in Section 3.2, meteorological data were obtained from various locations in the relative vicinity of the long and short test radio links but not in the proximity of or in the common volumes of the test links. This precludes any attempt to conjecture a meteorologically based explanation of why particular test data values were obtained. Further, results obtained from comparing the meteorological data with test data must be interpreted with the consideration that meteorological data are taken from locations near the test links.

In Table 4-10, high, low and the spread between high and low values of the RMS delay spread and median RSL test data are tabulated for various test configurations. The high and low test data values are obtained from Figures 4-15(a) and 4-15(b) and Figures 4-18(a) and 4-18(b). The spread between

Table 4-10

RMS Delay and Median RSL Variations

Test Conf.	Rec. No.	RMS Delay μs			Median RSL dBm		
		High	Low	Spread	High	Low	Spread
I	1	.37	.08	.29	-81	-107	26
	2	.28	.07	.21	-82	-107	25
II	2	.37	.05	.32	-79	-107	28
III	1	.30	.07	.23	-75	-107	32
IV	2	.26	.06	.20	-78	-107	29
V	1	.23	.08	.15	-85	-110	25
	2	.24	.08	.16	-85	-110	25

the high and low values for the RMS delay in general becomes less as the size of the antenna increases. This pattern is not evident for the spreads between the high and low values for the median RSL data. It should be noted, however, that the low values for the median RSL data are instrument cut-off values.

In Table 4-11, the .10, .50 and .90 points on the probability plots in Figures 4-15(a) and 4-15(b) and Figures 4-18(a) and 4-18(b) are tabulated. A general decrease in the RMS delay values for each of the three probability points is seen as antenna size increases for the short path. A similar statement can be made for the median RSL data for the three probability points; a general increase is seen in median RSL as antenna sizes increase for the short path. Values in Tables 4-10 and 4-11 are for test data, predominantly from the winter months.

Table 4-11

RMS Delay and Median RSL Values at
.10, .50 and .90 Probability Points

Test Conf.	Rec. No.	RMS Delay μs			Median RSL dBm		
		.10	.50	.90	.10	.50	.90
I	1	.27	.18	.12	-87	-96	-106
	2	.22	.16	.12	-88	-97	-106
II	2	.19	.13	.09	-83	-91	-99
III	1	.17	.13	.09	-84	-91	-101
IV	2	.15	.11	.09	-82	-86	- 92
V	1	.20	.15	.11	-90	-95	-102
	2	.21	.17	.11	-89	-93	-101

The procedure to calculate the effective earth radius to obtain the ratio a/R was taken directly from a paper by Gjessing and McCormick [17], in which prediction equations for a number of performance parameters of a troposcatter radio link are given. The equations are based on the evaluations of the effective earth radius and the "scattering" exponent, respectively, from the refractive index profile and temperature profile contained in the radiosonde data. As stated in Section 4.5, an attempt using Buffalo radiosonde data to calculate the "scattering" exponent was not successful. In view of the fact that the prediction equations provide values of performance parameters prior to the establishment of a troposcatter radio link, further investigation and study of the formulation cited in Reference 17 is recommended.

Theoretically computed values of the delay spread tabulated in Tables 4-6(a) and 4-6(b) show that they are less than delay spreads of test data for both paths, with the difference between the computed and test data values being much greater for the long path than the short path. Computed values of the delay spread in Tables 4-6(a) and 4-6(b) are for the link configuration and geometry given for the short and long paths. Direct comparison of the delay spread of a particular combination of input values in Table 4-6(a) or 4-6(b) with the RMS delay spread of test data is difficult. Lacking knowledge of effective earth radius along the path and the "scattering" exponent in the common volume, it is not known what combination of input values would most closely reflect the test conditions. Further effort and investigation of the modeling of the troposcatter channel used in the computer program is recommended.

A difference of opinion exists as to what radiometeorological parameter, refractive index gradient, "mean" gradient, surface refractivity or other, is the pertinent parameter to use for comparison with radio data (see References 16 and 18). In these references there is also a difference of opinion as to whether the use of surface refractivity index parameter to represent the effects of refraction is limited to only a few climatic regions, namely the temperate region. There is also a question as to whether only one radiometeorological parameter is adequate, i.e. whether the use of refractive index plus some form of a stability parameter may be the radiometeorological parameters to use for comparison with radio data. The ability to use multiple parameters is dependent, however, on understanding the phenomenon of propagation [16].

Monthly averaged surface refractivity data, N_S, for Buffalo, Syracuse and Rochester for ten months are shown in Figure 4-24; the seasonal variation of N_S is apparent. In addition, difference of the monthly average of the data from the three locations are generally 3N units, maximum 6 N-units. On a long-term basis, averaged values of N_S, say from Syracuse, would be representative of the values of N_S in the area of the short path link. This being so, one would expect a high correlation between path loss and N_S on a monthly average, which is seen in Figures 4-23(a) and 4-23(b). Correlation between monthly averaged a/R values determined from radiosonde data obtained from Buffalo and path loss/RMS delay spread is slight (Figures 4-25 and 4-26). The monthly averaged test data in these figures are for test Configuration I, Receiver 1.

For the daily averaged path loss and RMS delay test data, the number of sample data available (Table 4-8), other than for test Configuration I, is small. The correlation values other than for N_S versus path loss for test Configurations I and V are small. The drop in correlation for monthly, daily, and hourly (Table 4-9) averaged path loss data versus N_S for test Configuration I, Receiver 1 is considerable. This would indicate that prediction formula for path loss using N_S data, other than on a monthly basis, would not be valid.

SECTION V

DISCUSSION OF TEST RESULTS

Though limited in nature, the test results reported in Section 4 have application in the design and evaluation of digital modulation/detection techniques. They may also serve as an additional source of data for those attempting to model troposcatter propagation phenomena.

5.1 DIGITAL MODEM PERFORMANCE

As indicated in Section 2.1, the dispersive characteristics of the troposcatter channel can have significant impact on design and performance of digital modem techniques. These test results are consistent with earlier correlation bandwidth measurements in that the observed dispersion was of significant magnitude and subject to wide variation. Observed values of Δ (two-sided RMS multipath spread) ranged from 0.05 μs up to 0.37 μs. Assuming, again, a nominal data rate of 2 Mbps and QPSK modulation, ratios of multipath spread to symbol width (Δ/T) would range from 0.05 to 0.37. Such a range strongly suggests the use of specialized modem techniques which reduce intersymbol interference penalty and realize the available multipath (implicit) diversity. Such techniques have been tested and evaluated. Observed realizable performance has been employed as a baseline for determining appropriate performance specifications for the AN/TRC-170 family of digital troposcatter radio terminals. Performance has been specified over a range of multipath profiles which encompasses the range observed during these tests.

Of practical concern, then, is the basic question of whether or not the test paths are representative of the range of possible operational

conditions. The upper expected values of Δ are important in that any modem technique, when reduced to hardware, will have some fixed maximum value of dispersion that can be processed to advantage. While the actual cutoff may be a design variable, in general, increased multipath protection results in increased cost and complexity. Also, even if the range of Δ falls within design constraints, performance will depend on the actual values of Δ that are encountered. For users to predict link performance prior to deployment, they will need to estimate the mean and variance of Δ just as they must do with path loss. It appears that neither an adequate base of empirical data nor adequate channel models exist from which reliable estimates of Δ can be derived for a wide range of operational conditions.

5.2 COMPARISON WITH OTHER RESULTS

Most of the earlier test results for short-to-medium range paths at C band have consisted of measurements of correlation bandwidth, an indirect measurement of multipath. In order to make a comparison with this earlier data, an approximate relation has been developed which relates correlation bandwidth to multipath spread Δ.

On the assumption that, for short observation periods, a complex Gaussian wide-sense stationary uncorrelated scattering model is appropriate[†], Bello [11] has shown that the delay power spectrum $Q(\xi)$ and the complex envelope frequency correlation function $R(\Omega)$ form a Fourier transform pair. The function $R(\Omega)$ is defined as

$$R(\Omega) = E\left\{ G^*(\omega)\, G(\omega + \Omega) \right\} \qquad (5-1)$$

where $G(\omega)$ is the equivalent low pass transfer function, $E\left\{ \cdot \right\}$ is the expected value operator and * denotes complex conjugate. Unfortunately,

[†]Results of preliminary processing of magnetic tape recordings of $\hat{h}(\tau, t)$ collected during this test program support the model assumption [21].

the earlier measurements were not of $R(\Omega)$ which requires a cross-correlation of the complex envelopes of received carriers of radian frequency separation Ω. Rather, the cross-correlation was of the magnitude of the envelopes of the received carriers. The resulting normalized correlation function, denoted as $\rho_e(\Omega)$, is real as opposed to the complex $\rho(\Omega)$, which is the normalized $R(\Omega)$. The magnitude of ρ_e is related to ρ_e by an expression involving elliptic integrals and to a good approximation [22]

$$|\rho| \approx (\rho_e)^{1/2}. \tag{5-2}$$

The measurements of ρ_e can then be used to estimate $|\rho|$; however, inverse Fourier transform to obtain $Q(\xi)$ is not possible without the phase information. One could assume ρ to be real but this would be equivalent to assuming symmetry of $Q(\xi)$ around some delay ξ which is contrary to actual observations.

For purposes of obtaining gross estimates of $Q(\xi)$ from the published ρ_e data, it was assumed that $Q(\xi)$ has a simple Gamma function shape:

$$Q(\tau) \simeq b^2 \tau e^{-b\tau}. \tag{5-3}$$

This shape is a reasonably good fit to the $Q(\xi)$ predicted by the Bello model and to the $\hat{Q}(\tau)$ observed during this test program. The two-sided RMS spread is simply

$$\Delta = \frac{2\sqrt{2}}{b} \tag{5-4}$$

and the magnitude squared of the Fourier transform, using Equation 5-2, is an estimate of ρ_e:

$$\rho_e(\Omega) \simeq \frac{1}{\left(1+\Omega^2/b^2\right)^2} \quad . \tag{5-5}$$

This approximation is a reasonably good fit to the shape of the observed ρ_e; however, the actual shapes are quite variable. Most published data was in the form of the frequency separation f' in Hz for which $\rho_e = 0.4$.

Using Equations 5-4 and 5-5, Δ may be estimated as

$$\hat{\Delta} \simeq 0.343/f'. \tag{5-6}$$

Other data are presented as values of ρ_e for fixed frequency separations from which estimates of Δ may be obtained in a similar manner.

One series of tests was conducted over a 100-statute-mile overland path in Florida (Gainsville to Orlando) during the period 14 May through 15 June 1962 [23]. Tests were conducted at 4940 MHz using 12-foot and 4-foot parabolic reflectors with antenna elevation angles of approximately zero degrees. For 100 hours of testing with the 12-foot reflectors, the median value of Δ is estimated as 0.24 μs. The lower and upper percentile values of Δ are estimated as 0.14 μs and 0.41 μs. During one day, tests were alternated between the 12-foot and 4-foot reflectors with the result that the observed correlation bandwidths were essentially the same.

During the period August 1969 through February 1970, a series of correlation bandwidth tests [2, 3, 24] were conducted over 4 paths at the RADC test range. The tests were conducted at 4600 MHz using 10-foot parabolic reflectors. The path parameters and estimated values of Δ are presented in Table 5-1, which shows the mean and variance of the estimated Δ is consistent with the current test results (See Table 4-11).

Another observation was gained from simultaneous tests at 7600 MHz (X band) using the same 10-foot reflectors, resulting in a 1.07^o beamwidth as opposed to the C-band beamwidth of 1.5^o. On a test-by-test basis and

Table 5-1

Estimated Multipath Spreads From 1969-1970
Correlation Bandwidth Measurements

Path/Period Model City To:	Antenna Elevation α, deg	Distance St. Mi.	Estimated 2σ Spread μs		
			10%	50%	90%
Ontario Center	0.025; -0.124	86.9			
Summer			0.17	0.12	0.065
October			0.17	0.098	0.065
Winter			0.23	0.14	0.047
Average			N.A.*	0.11	N.A.
Whitford Field	0.049; 0.865	123.7			
Summer			0.27	0.20	0.12
November			0.26	0.18	0.087
Average			N.A.	0.19	N.A.
Point Petre†	-0.034; -0.059	101.5			
September			0.19	0.11	0.069
Winter			0.20	0.093	0.069
Average			N.A.	0.10	N.A.
Port Byron	0.049; -0.010	119	0.25	0.14	0.076
February					

*N.A. - Data Not Available
†Overwater Path (Lake Ontario)

on an average basis, the X-band correlation bandwidths were essentially the same as those observed at C band. The correlation bandwidths were slightly wider (Δ slightly narrower) for the narrower antenna beamwidth, for shorter path distances and for smaller scatter angles; however, there was a relative insensitivity to these parameters.

A series of C-band (4800 MHz) tests were conducted between Tobyhanna, Pennsylvania and Fort Monmouth, New Jersey from October 1966 through January 1967, and from February 1968 through July 1968 [25]. During the first testing segment, 15-foot parabolic reflectors were employed, 10-foot reflectors during the second period. More than 90 percent of the tests were conducted with the 10-foot reflectors. The path distance is given as 93 statute miles. Antenna elevation angles are not given; however, the scatter angle (4/3 earth corrected) was calculated to be 0.67 degrees. From Figure 17 of Reference 25, the 10%, 50% and 90% values of Δ are estimated as 0.12, 0.082 and 0.054 μs respectively. These results are based on all test data from both segments of the test program. The observed correlation bandwidths were wider (Δ narrower) than what was observed on the Florida or New York paths.

For the very limited number of "test" paths referenced above, it appears that the range of multipath spread is consistent with the range observed in the current test program. Test paths were in the 80-120 mile range with antenna reflectors varying from 8 to 15 feet. The only exception is the 168-mile path, 28-foot reflector combination employed in the current tests. All paths, except for one, were overland and most were over relatively smooth terrain. Not included in this limited data base are: data for longer paths with antenna reflectors in the 8 to 15-foot range; shorter range paths where diffraction effects predominate; paths with large scatter angles

because of terrain obstacles; obstacle gain diffraction paths; and paths in other climatic regions. That is to say that data from direct or indirect measurement of multipath do not, for the most part, exist for the types of conditions expected in an operational employment of tactical troposcatter radios.

5.3 CHANNEL MODEL CONSIDERATIONS

Existing troposcatter channel models represent an attempt to predict average dispersion based on path geometry, assumed refraction effects, and, in some cases, assumptions relative to scattering efficiency as a function of scatter angle and height. No attempt has been made, as part of this current program, to analyze in detail the various models and their underlying physical assumptions or to develop a new or modified model. There are, however, some observations that are worth mentioning.

The Bello channel model [1] is based on the turbulent scattering theory developed by Booker and Gordon [26]. The theory is based on an assumed reasonably well-mixed atmosphere (no well-defined stratification) where refractive index inhomogeneties occur in the process of turbulent mixing. An average permittivity ϵ is assumed and $\Delta\epsilon$ is defined as the departure from ϵ at a point P. The autocorrelation function of permittivity as a function of distance r between any two points P and P' is then assumed to have an exponential form:

$$R(r) \propto e^{-r/\ell}$$

where the parameter ℓ is related to the distance over which refractive index fluctuation are correlated. A uniform isotropic R(r) was assumed to exist throughout the common volume. This results in a scattering cross section σ which is a function of scatter angle θ :

$$\sigma(\theta) \propto \frac{1}{\theta^m} .$$

The problem with this theory is that R(r) is not, in general, isotropic due to stratification effects and is not, in general, independent of height because of the height dependency of temperature, humidity and pressure. Bello assumed an inverse height dependence in σ to result in a scattering cross section per differential volume of

$$\sigma(\theta) \propto \frac{dV}{h\,\theta^m} .$$

The received power scattered from such a differential volume is then assumed to be

$$dP \propto \frac{GH}{R^2\,S^2} \quad \frac{dV}{h\,\theta^m}$$

where G and H are the antenna gains at the differential volume location and where R and S are the distances from dV to each of the antennas. Estimation of the delay power spectrum $Q(\xi)$ then involves integration over all differential volumes for which the path delay is in the interval $(\xi, \xi + d\xi)$, a shell of a prolate spheroid having foci at the antenna sites. Correction for refraction effects is included by assuming an effective earth radius.

The shape of the $Q(\xi)$ predicted by the Bello model (Figure 5-1) is a good fit to the observed $\hat{Q}(\tau_k)$, that is, a sharp rise in relative power starting at the minimum path delay followed by a rather sharp peak, then a more gradual fall off. This supports the theory that the greatest scattering cross section exists in the lower portion of the common volume, near the

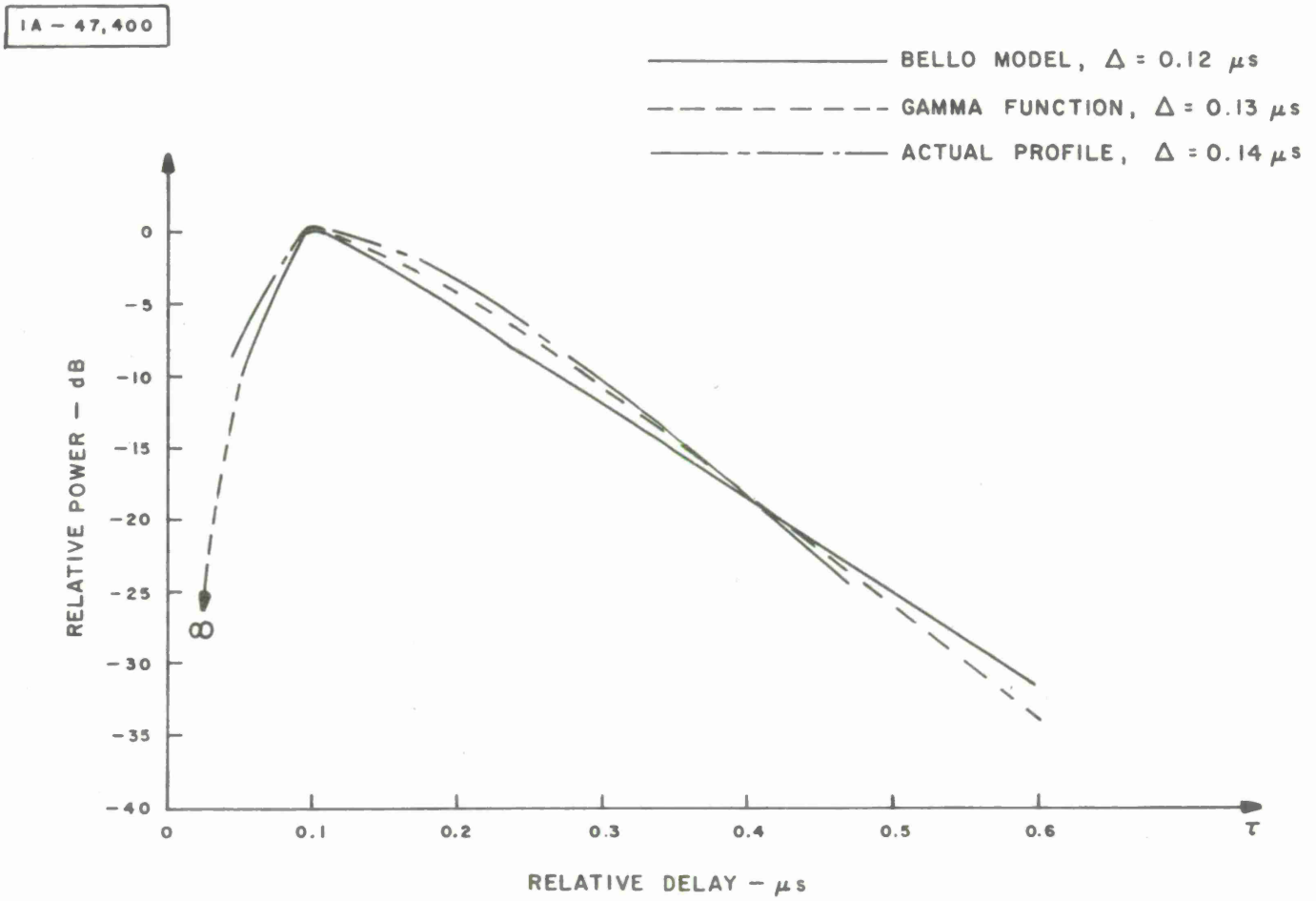

Figure 5-1. Comparison of Multipath Power Profile Shapes

great circle path. This may be due to the dependence of σ on scatter angle or height or more probably, both. This leads quite naturally to the concept of "effective" scattering volume which is less than some "potential" common volume defined in some way by intersection of antenna beam patterns (a half power beamwidth may be too restrictive). The predicted $Q(\xi)$ is a function of the assumed value of m and effective earth radius (see Table 4-6). These parameters, however, are quite dependent on local meteorological conditions and, even for a given path, can be expected to vary over a wide range. This would result in an "effective" common volume of variable size and hence a variation in Δ. If average meteorological conditions for a given area were used in the Bello model, then it may serve as a useful tool in obtaining initial gross estimates of average dispersion.

The relatively narrow multipath profiles observed at times during these tests suggest that the effective common volume may sometimes be very small relative to the "potential" size. In fact, ducting conditions may result in values of Δ which approach zero. At the other extreme, the large values of Δ may result from the effective common volume approaching the potential common volume. Also, reflections from the foregrounds of the antennas may tend to broaden their effective vertical patterns. This may give rise to a "potential" common volume larger than defined by the antenna patterns, which may then give rise to values of Δ larger than predicted.

It is also possible that one or more elevated layers result in large values of Δ; this was observed on two occasions during the current tests when an inversion layer was present at an altitude of about 5,000 feet. In addition to the standard shape multipath power profile due to normal scattering, a second peak of near-equal magnitude was observed about 0.6 μs later in delay. The second peak was observed in one case over a four-hour period during which it varied in relative magnitude and delay. The possible

existence of such high level "reflecting" layers make a half-power beamwidth definition of "potential" common volume restrictive, as the relatively high scattering efficiency may compensate for fall-off in antenna gain.

A troposcatter multipath model proposed by Sunde [27] assumes a rectangular-shaped multipath power profile of width $2\Delta'$. Sunde defined Δ' as the maximum departure from the mean path delay using geometric ray tracing (corrected for refraction) and half-power beamwidths. An approximate expression for Δ' for a symmetric path is

$$\Delta' \approx \frac{d}{c}\left(\frac{\gamma + \beta}{2}\right)\left(\theta + \frac{\gamma + \beta}{2}\right)$$

where: d = path distance in Km

c = velocity of light

γ = 1/2 of 3 dB antenna beamwidth in radians

β = antenna elevation angle in radians

θ = d/2RK

R = earth radius, 6373 Km

K = 4/3.

Using data for the Ontario center to Verona path with 8-foot parabolic reflectors, $2\Delta'$ is calculated to be 0.36 μs. The two sigma spread for this rectangular profile would be 0.21 μs, which is slightly wider than the median value of 0.18 μs observed during these tests. Values of Δ as high as 0.37 μs and profiles which extended over 1 μs in significant width were observed during these tests. This tends to suggest that the "potential" common volume is of an extent somewhat larger than that defined by half-power beamwidths. An approach similar to that used by Sunde may,

however, have some value in estimating the extreme values of Δ, provided that a somewhat more liberal value of antenna beamwidth is employed.

5.4 CORRELATION RESULTS

The observed correlations between path loss and multipath spread (Tables 4-4 and 4-7) were generally weak. Over long periods of time, the correlation coefficient was usually in the range of 0.2 to 0.4; however, for shorter periods (several weeks), values in the 0.5 to 0.6 range were observed. This, of course, may be due to the smaller number of samples used to generate the statistic. The weak long-term correlation is consistent with earlier results where path loss was correlated with correlation bandwidth [24]. It is clear from comparing Figures 4-12(a) and 4-16(a) that any long-term correlation should be weak. Essentially the same values of multipath spread were observed during winter and summer, while path loss was strongly influenced by season. The higher correlation over shorter observation periods may not be due entirely to variations in path loss because received signal level (RSL) was measured rather than direct measurements of path loss. Path loss was computed as

$$L_P = P_T + G_T + G_R - L_C - RSL$$

where

P_T = XMIT Power in dBm

G_T, G_R = Antenna gains in dB

L_C = Aperture - Medium Coupling loss in dB

RSL = Received Signal Level in dBm.

The value of L_C was assumed to be a constant and was calculated using the C.C.I.R. formula:

$$L_C = 0.07 \exp \left[0.055 \, (G_T + G_R) \right] .$$

The loss L_C over free-space antenna gain is usually attributed to the fact that the free-space gain assumes a point source and a plane wave front over the antenna aperture. For troposcatter propagation a very large number of sources are dispersed over an effective common volume which results in phase incoherence over the antenna aperture. As the aperture size (and free-space gain) is increased, this effect is more pronounced and L_C is greater. In fact, it is this phase incoherence as a function of spatial separation that allows the realization of conventional space diversity operation with two or more antennas. For a given path geometry and antenna apertures, L_C is a variable rather than a fixed parameter where existing formulas for estimation of L_C attempt to predict average values. It is suggested that the variation of L_C may be related to the variation in extent of the effective common volume, of which multipath spread Δ is a measure. If this is true, then the correlation between path loss, as measured here, and Δ may actually reflect some degree of correlation between L_C and Δ.

No apparent correlation was observed between RSL and fade rate; however, as explained in Section 4.4, this may be due in part to the crude measurement of fade rate.

Correlation of path loss with meteorological data resulted in the expected high correlation between path loss and surface refractivity N_s. No significant correlation was observed between N_s and Δ which is then consistent with the weak correlation between path loss and Δ. The effective earth radius is usually highly correlated with N_s. This effects the amount

of refraction and, hence, the mean scatter angle and mean path loss. Multipath spread, however, is not dependent on absolute scattering efficiency but on the relative scattering efficiency as a function of height and scatter angle, which does not appear to be strongly influenced by surface refractivity.

5.5 PERFORMANCE PREDICTIONS

The quality of performance of a high-speed digital troposcatter circuit currently can be satisfactorily assessed only after the circuit has been operational. Predictions of its future performance can be made only after channel data previously collected have been analyzed. The predictions so obtained are basically relevant only to the operational radio circuit. The ability to generalize parameters of performance of an operational circuit to predict performance of a different circuit at a different geographic location has not been reliably established. NBS Technical Note No. 101 [14] provides reliable techniques for predicting path loss for a wide range of configurations and for several climatic regions. It is based on a large amount of empirical data collected over numerous paths around the world. As digital troposcatter circuits begin to replace analog circuits, it may be appropriate to supplement Technical Note No. 101 with prediction techniques for multipath spread and fade rate. Such a supplement would require a systematic collection and analysis of channel and meteorological data.

Many results have been published where statistical parameters were obtained by comparing channel data with meteorological data and parameters computed from meteorological data. Descriptions of some of these results are in Reference 16 and 20; more recent results are in a series of papers — References 17, 18, 28, 29, and 30. At present there is no common agreement on which meteorological parameter(s) is the most relevant for a troposcatter circuit or on which parameter(s) should be used for statistical analysis with channel data.

REFERENCES

1. P.A. Bello, "A Troposcatter Channel Model," IEEE Trans. Comm. Technology, Vol. COM-17, pp. 130-137, April 1969.

2. R. Branham et al, "Correlation Bandwidth Measurements over Troposcatter Paths," Technical Report ECOM-0251-F (AD 871200L), June 1970.

3. D.J. Kennedy, "A Comparison of Measured and Calculated Frequency Correlation Functions over 4.6 and 7.6 GHz Troposcatter Paths," IEEE Trans. Comm., Vol. COM-20, pp. 173-178, April 1972.

4. P.A. Bello, L. Ehrman and D.S. Arnstein, "Modeling and Data Analysis - Short and Medium Range Digital Troposcatter Tests," Technical Report RADC-TR-69-233 (AD 862236), October 1969.

5. R. Price and P.E. Green, Jr., "A Communication Technique for Multipath Channels," Proc. IRE, Vol. 46, pp. 555-570, March 1958.

6. M.M. Goutmann, "Intersymbol Interference as a Natural Code," IEEE Trans. Comm., Vol. COM-20, pp. 1033-1038, October 1972.

7. P. Monsen, "Feedback Equalization for Fading Dispersive Channels," IEEE Trans. on Information Theory, Vol. IT-17, pp. 56-64, January 1971.

8. M. Schwartz, W.R. Bennett and S. Stein, Communication Systems and Techniques, New York, McGraw-Hill, Chapter 11, 1966.

9. R. Gallant, "Troposcatter Multipath Analyzer," Technical Report RADC-TR-70-155 (AD 712415), August 1970.

10. B.B. Barrow, et al, "Indirect Atmospheric Measurements Utilizing Rake Tropospheric Scatter Techniques," Proc. IEEE, Vol. 57, pp. 537-551, April 1969.

11. P.A. Bello, L. Ehrman and T.H. Crystal, "Tropo-Scatter Multichannel Digital Systems Study," Technical Report RADC-TR-67-218 (AD 817211), May 1967.

12. R. Gallant, op. cit., Appendix A.

13. "Quad Diversity Dynamic Channel Simulator Model S-139B - Operating and Maintenance Manual," Signatron, Inc.

14. P.L. Rice, et al, "Transmission Loss Predictions for Troposcatter Communications Circuits," NBS Technical Note 101 (Revised), 1967.

15. P. Beckman and A. Spizzichino, The Scattering of Electromagnetic Waves from Rough Surfaces, MacMillan, New York, 1963.

16. F. duCastel, Tropospheric Radiowave Propagation Beyond the Horizon, Permagon Press, New York, 1966.

17. D.T. Gjessing and K.S. McCormick, "On the Prediction of the Characteristic Parameters of Long Distance Tropospheric Communication Links," IEEE Trans. Comm., Vol. COM-22, pp. 1325-1331, September 1974.

18. B.R. Bean and E.J. Dutton, "Radio Meteorology," National Bureau of Standards Monograph 92, 1966.

19. D.T. Gjessing and A.G. Kjellas, "Spectral Measurement and Atmospheric Stability," Journal of Atmospheric Sciences, Vol. 26, pp. 462-468, May 1969.

20. P.A. Bello, P. Alexander and S. Ahmed Meer, "Investigation of Atmospheric Parameters with Forward Scatter Probing," Technical Report AFCRL-70-0397, (AD 712088), June 1970.

21. G.E. Eller, "Rake Tropospheric Scatter Channel Prober Data: Reduction and Analysis," RADC Technical Report to be published.

22. M. Schwartz, W.R. Bennett and S. Stein, op. cit., p. 479.

23. W.S. Patrick and M.J. Wiggins, "Experimental Studies of the Tropospheric Scatter Medium at Five Gigacycles," IEEE Trans. Aerosp. Navig. Electronics, Vol. ANE-10, pp. 133-137, June 1963.

24. R.A. Branham, "Experimental Observations of Correlation Bandwidth Over Troposcatter Paths," Proc. ICC, June 1961.

25. W.A. Olsen, "Comparison Between Computer-Controlled Troposcatter Simulation and an Actual Link," Research and Development Technical Report ECOM-3423 (AD 728102), May 1971.

26. H.G. Booker and W.E. Gordon, "A Theory of Radio Scattering in the Troposphere," Proc. IRE, Vol. 38, pp. 401-412, April 1950.

27. E.D. Sunde, "Digital Troposcatter Transmission and Modulation Theory," BSTJ, Vol. 43, pp. 144-214, January 1964.

28. D.T. Gjessing, H. Jeske and N.K. Hansen, "An Investigation of the Tropospheric Fine Scale Properties Using Radio, Radar and Direct Methods," Journal of Atmospheric and Terrestrial Physics, Vol. 31, pp. 1157-1182, 1969.

29. D.T. Gjessing, "Atmospheric Structure Deduced From Forward-Scatter Wave Propagation Experiment," Radio Science, Vol. 4, No. 12, pp. 1195-1210, December 1969.

30. J.A. Børensen and D.T. Gjessing, "Homogeneity of the Tropospheric Refractive - Index Structure," Radio Science, Vol. 4, No. 12, pp. 1235-1239, December 1969.